# A High-throughput Microfluidic Platform for Profiling Photosensitizer Efficacy in Cancer Therapeutic Applications

**by**

**Xia Lou**

**A dissertation submitted in partial fulfillment**
**of the requirements for the degree of**
**Doctor of Philosophy**
**(Electrical Engineering)**
**in The University of Michigan**
**2013**

**Doctroral Committee:**

**Professor Euisik Yoon, Chair**
**Professor Yogesh B. Gianchandani**
**Professor Raoul Kopelman**
**Assistant Professor Mina Raieszadeh**
**Professor Kensall D. Wise**

***This work is dedicated to my family.***

***"Scientists investigate that which already is;***
***Engineers create that which has never been."***

***Albert Einstein***

## ACKNOWLEGEMENTS

This dissertation is far beyond a brief summary of my research work I am been devoting to during my Ph.D. period in Michigan. But also it would be my life-long memory here of mentorship, friendship, family relationship, and my youth in laughter and tears.

I would first like to thanks my advisor Professor Euisik Yoon, who has been setting up such a model of mentoring in both academia and personal life. Thanks for his continuous support over these more than five years, without which it would be impossible for me realizing all the accomplishments and coming to this final stage of my pursuit of Ph.D. From the first time meeting with him discussing what I want to do, every time's talk he has been bringing in inspiration, profundity, optimism, confidence and unstoppable passion to start working right away. I can hardly image a better experience than that you can learn, make accomplishment, get connected with other professionals and also enjoy your research. I consider it a high privilege to have been part of IML (Integrated Microsystem Laboratory) and I look forward to the opportunities working with him and his group in the future.

I also would like to thank my dissertation committee, for their continuous support, thoughtful feedbacks and encouragement. Professor Ken Wise has been such a splendid leader in EECS department, who however in the other side is so easy going when you talk to him. A special thank goes to Professor Raoul Kopelman for the pleasant long time

collaboration relationship with his group. Professor Yogesh B. Gianchandani is one of the first faculties I met here and warmly welcomed me to Michigan. Professor Mina Rais-Zadeh teaches fabulous classes from which I benefited a lot, and also she is so close in age with me that we feel like more to share joy together.

I would also like to thank my collaborators on this project, Dr. Yong-Eun Lee Koo, Dr. Gwangseong Kim and Hung Ki Yoon. It has been great pleasure to be able to work with them and thanks to that I have been able to learn a lot outside of my own expertise. Also I would like to thank some of my colleagues here, Yipei Wang, Thant Zhu, Jin Zhang, Luqia Hou, Angela Dixon, Geeta Mehta and Arlyne Simon who have been providing various helps in biological samples, standard operation protocols, testing instruments and productive discussions. And a special thank go to Professor Shuichi Takayama, who always gives rapid response when I ask for help and kindly allows me to use the cell storage facilities in his lab.

I would like to thank both past and current members in Yoon group, Il-Joo Cho, Hyung-Kew Lee, Khaled Al-Ashmouny, Sun-Il Chang, Jaehyuk Choi, Jaehoon Chung, Seong-Jin Kim, Young-Ji Kim, Mithun Shenoi, Patrick Ingram, Yu-Chih Chen, Kyunghwan Na, Seok-Jun Park, Sung-Yun Park, Fan Wu, Tom Bersano, Maesoon Im, Hwa Sung Shin, Mike McCormick, Roberto Miguez, Dr. Ji Yoon Kang, Dr. Songjun Lee, Dr. Bo Yang and Dr. Ararta Nakajima. Thanks for making our group so pleasant and thanks for spending time with me in the lab. And also I would like to thank the help and support from staff of Lurie Nanofabrication Facility making my projects going smoothly. And thanks to the faculty, staff and students here in EECS making our department a best and most attractive over the world.

Finally, I want to give my thanks to my family. Thanks to my father, Lin Lou, who is always encouraging me to purchase whatever I want. Thanks to my mother, Baoxiang Fang, who never ask what I have achieved but only cares whether I am happy or not. Thanks to my wife, Xiaoyu Su, for always being my side and close to my heart. Thank you for the constant encouragement, unfailing support and boundless love.

## TABLE OF CONTENTS

## LIST OF FIGURES

## LIST OF APPENDICES

## ABSTRACT

In this work a high-throughput microfluidic platform has been developed for evaluating efficacy of photodynamic therapy (PDT) and investigating its dependence on various therapeutic factors. PDT is receiving increasing attention in cancer treatment due to its minimal side effects, precise cancer-targeting, non-invasion and low cost. It utilizes a specific group of anti-cancer drugs (called photosensitizers), which can be only activated under a certain wavelength light illumination and kills cancer cells. Evaluating PDT efficacy in vitro is essential in both photosensitizer development (how powerful the drug candidate is) and PDT treatment protocol setup (how to reach desired efficacy). However, it has been extraordinarily challenging compared to evaluating other anti-cancer drugs due to its extra reliance on light illumination and local oxygen existence, leading to an increased number of therapeutic factors that need to be included during the test process.

The proposed microfluidic platform exclusively added the microenvironment control of oxygen and light for PDT efficacy evaluation. It provides the capability of comprehensive PDT efficacy response test over various therapeutic factors including photosensitizer concentration, oxygen level, illumination dose (fluence), incubation time and shear stress. The microfluidic platform is composed of three PDMS microfluidic layers, each of which provides the dynamic controls of different therapeutic factors. The first cell layer contains cancer cells and controls the delivering drug concentration,

incubation time with cancer cells, and shear stress of flow during drug delivery. The second gas layer generates a gas mixture with required oxygen concentration, which is then readily imposed on to cancer cells in the first cell layer by diffusion through the 70um thick PDMS membrane between these two layers. The third filter layer works as a grayscale mask, modulates illumination from an external light source, and applies a given illumination intensity to the cancer cells during PDT treatment.

A gradient of each therapeutic factor is generated on the chip and by combining these gradients together we can realize a high-throughput efficacy test with various PDT conditions in parallel. In this work PDT efficacy tests under 1,296 different conditions have been evaluated within an active area of 5mm×5mm of one chip in one test run. Further expansion of throughput over 10,000 or even 100,000 would be straightforward since the minimum segment of each test condition occupies an area of 80um×80um. Oxygen gradient distribution is monitored through oxygen quenching fluorescence dye tris(2,2'-bipyridyl)dichloro-ruthenium(II) hexahydrate (RTDP) solution in cell culture channels. Illumination intensity distribution is measured through the illumination pattern after passing through the grayscale filter. The gradient of each therapeutic factor is confined within a physiologically meaningful range like photosensitizer type1 (Methylene blue) concentration (0~10uM), photosensitizer type2 (functionalized nanoparticles) concentration (0~1mg/ml), incubation time (0~75minutes), oxygen level (1.4%~19.1%), illumination dose (0~42.8mJ/cm$^2$) and shear stress (0.75~14.1dyn/cm2).

The complete experiment cycle, including both cell culturing in the chip and PDT efficacy test, is restricted within one day providing rapid feedback of test results. PDT efficacy evaluation on the chip has been tested with five cell lines (C6, 9L, MCF-7, DI

TNC1 and Skov3) and two photosensitizers (Methylene blue and functionalized nanoparticles). This ultra-rapid, high-throughput capable microfluidic platform should enable rapid developments of novel photosensitizers, expanding PDT applications in cancer treatments, and optimizing clinical PDT protocols. It not only overcomes many limitations of previous technologies for PDT efficacy test, but also can be extensively applied to other anti-cancer drug screening which requires similar investigation on relevant therapeutic factors.

# CHAPTER 1 INSTRUCTION AND BACKGROUND

## 1.1 Photodynamic therapy for cancer

Photodynamic therapy (PDT) is a light assisted therapeutic strategy used for a wide range of medical conditions. It involves three essential elements during the treatment: a drug, which is usually called a photosensitizer (PS); a light source; and local oxygen. Under light illumination of a certain wavelength, the photosensitizer can be excited to an unstable singlet state, which then in turn transfers an oxygen molecule in proximity into a reactive oxygen species (ROS), mostly an oxygen singlet, by energy transfer. These aggressive oxygen species rapidly react with nearby cells, leading to cell apoptosis or necrosis [1, 2]. In PDT for cancer treatment, there are mainly three methods that lead to tumor destruction. First is direct cancer cell killing, in which cancer cells are directly killed by the active oxygen species generated during PDT process. Second is vascular damage, in which tumor related vessels are damaged and stopped carrying nutrients to tumor leading to its destruction. Third is immune response, in which inflammatory reaction of PDT contributes to local accumulation of lymphocytes, leukocytes, macrophages against tumor cells, especially surviving cells after the bulk tumor is destroyed by direct PDT effects [1, 3].

Cancer has been a disease existing throughout human history. As early as in 3000 BC, Egyptians recorded a case of breast cancer as a grave disease with no treatment for it [4]. Since 1971, the United States has invested over 200 billion dollars in the “War on Cancer”; however, the general cancer death rate only decreased by around five percent

[5]. Within the last decade one of the most important findings in cancer research is that people realized cancer should be identified as a series of chronic diseases, and the World Health Organization (WHO) has proposed that a comprehensive treatment strategy could be the best way to increase survival rate and improve life quality, especially for advanced cancer patients [6]. Currently surgery, chemotherapy and radiation therapy are the three major choices in practice for cancer management, along with immunotherapy, monoclonal antibody therapy and a number of other experimental cancer treatments [7].

PDT, sometimes considered as a special form of chemotherapy, can be either adopted as a palliative therapy or a primary therapy for cancer. It possesses its own specific advantages compared to conventional radiotherapy, chemotherapy and surgical operations [1, 2, 8]. First, PDT is considered minimally invasive and minimally toxic. Second, PDT is highly selective and localized in several ways. A photosensitizer can be only excited by a certain wavelength so the treatment is restricted within the illumination area especially when using a waveguide laser light source. On the other side, photosensitizers also can be locally applied at specific treatment sites. Some photosensitizers tend to accumulate at tumor sites and have a higher affinity for vascular endothelial cells, and this kind of selectivity can be further improved by conjugating photosensitizers with antibodies targeting specific tumor cells. Third, PDT can be repeatedly applied to extensive malignancies until reaching a final cure like cryotherapy. Fourth, PDT is always a much cheaper alternative treatment, which makes it especially popular in developing countries. Fifth, PDT is a gentle treatment, having a short recovery period in terms of days or even hours, rather than weeks.

Since ancient time people have found that light could be employed in some disease treatments. However, only around 100 years ago a first related mechanism of cell death was reported and the concept of PDT started to be widely accepted [9, 10]. In the past 30 years, PDT experienced extensive development in medical applications. In 1993, the first PDT agent, Photofrin, was approved by the Food and Drug Administration (FDA) in clinical use for cancer. And currently 9 photosensitizers are commercially available for clinical use, with much more under different steps of development [11, 12]. In addition to development of various new photosensitizers, which can provide higher efficiency generation of oxygen singlet, better selectivity on targeting tumor cells and better matching exciting wavelength with deeply penetrating lights like infrared light or X ray, two other areas are currently focused on in PDT research. One is different stages of clinical trials under way to expanding PDT's application to more cancer types and optimizing clinical protocols. The other is improving PDT equipments especially the specific light sources for the activating light delivery [13].

### 1.2 In vitro photosensitizer efficacy assay

Similar to anti cancer drug development for chemotherapy, newly developed photosensitizers are routinely evaluated for their efficacy with cancer cell line models in vitro first before moving to the next step of animal testing or clinical trials, avoiding the high cost of later stage failures [14, 15]. As the simplest and still most common method, this kind of test is carried out with a petri dish or microwell plate [16, 17]. First the target cell line is fed and cultured in a petri dish with culture media. Then for the PDT test, the media is replaced with the photosensitizer solution followed with or without certain period of continued culture. After being equilibrated with a certain concentration of

oxygen, the dish is irradiated with a certain dose of light, from LED or laser light source. Cell viability relative to untreated controls can be determined by vital dye staining, MTT assay or other cytotoxicity measuring methods. Finally the survival curves can be generated based on the results of different photosensitizer doses, oxygen concentrations, illumination doses and incubation times.

However, compared to chemotherapy drugs, even further challenges of high-throughput screening are present for photosensitizers, considering not only the huge number of combinations of drug candidates and cancer cell lines but also various PDT factors. While the same methods applied in chemotherapy drug high-throughput screening, like microwell plates, robotic sample handling and microfluidic devices, can be readily adopted in photosensitizer screening, new features are required because of PDT's more complicated mechanism involving light illumination and further emphasis on other factors including oxygen concentration and incubation time [18-20]. Considering related technology is lagging far behind, researchers have been making efforts to face this challenge as we will discuss in the rest of this section.

A first method in facing these challenges is providing a different guided illumination for each well of a microwell plate using a combinational light source like arc xenon lamp plus a bundle of fibers [21]. The light radiation from the lamp is restricted within a specific wavelength range after passing through several filters. After being focused by an elliptical reflector, the light beam is aligned to fiber distal and collected by the bundle of 60 fibers. Each fiber leads to one of the microwells of the plate, and since the nonuniformity at the light collection ends, each fiber delivers a different light intensity

providing a variation of PDT illumination dose during each 96 well plate test, as shown in Figure 1.1.

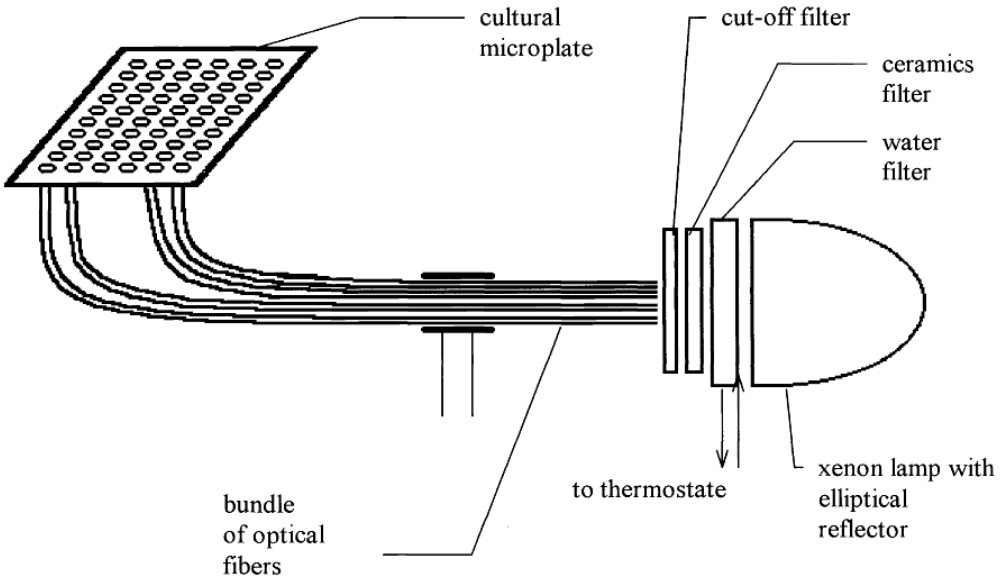


Figure 1.1 The scheme of the light source setup for studying of photodynamic action on monolayers of cells in 96-well cultural plate. 60 different levels of light power are delivered to 60 microwells [21].

As we might notice here this is a method fits a 96 well plate and increasing to higher number of wells in each plate will require more numbers of fibers bundled together and a more complicated setup. One major limitation here is that it is difficult to control the coupling between the fiber and lamp. As a result, the illumination intensity gradient among the wells is unpredictable with many wells having similar illumination. Also, this coupling is vulnerable to vibrations and residual light from the lamp, which needs to be kept away from the test microwell plate during the PDT test.

Another method used by researchers is to use a LED array as a illumination light source with one LED for each well of a 96-well plate [22]. As shown in Figure 1.2, the light source is set up by inserting an individual LED into each well to make the same 8 by 12 array as a standard 96-well plate. The diver box beneath LED array provides power

supply and air cooling. As the LEDs are placed inside a black frame, the emitted lights are somehow collimated and spaced apart from each other.

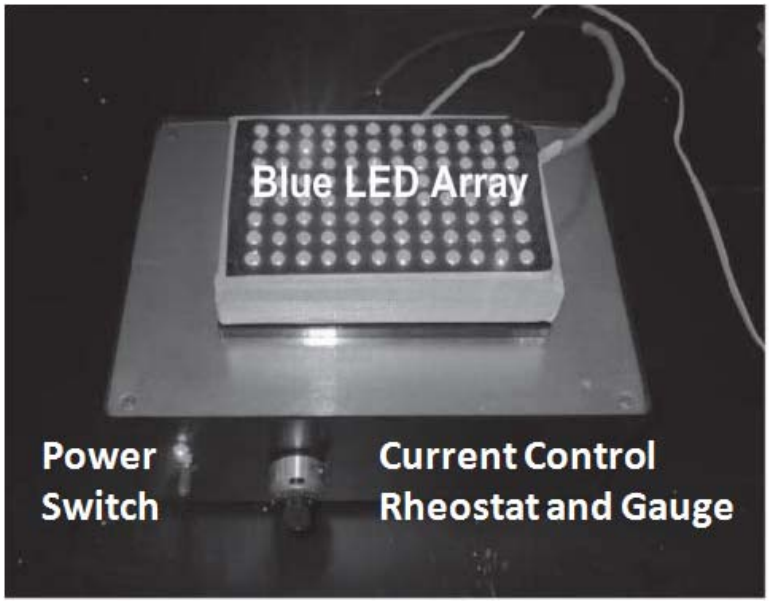


Figure 1.2 A representative operational blue LED array and the driver beneath. During the PDT test, the tested 96-well plate would be set right on top of the LED array and each well is illuminated with preset intensity (partial adjusted by the current control) for the same time period [22].

This platform provides a more flexible illumination method by incorporating LEDs of different wavelengths (colors) into the same array, fitting the requirement of different photosensitizers with different light absorption peaks. The major limitation here is that the light source tends to be power consuming, and the capability of further expansion would be limited because of the minimal LED size, the increasing effort needed for assembly and the increasing power intensity.

A third reported method, which is more innovative than traditional methods, utilizes microfluidic droplet generation and continuous flow screening [23]. As shown in Figure 1.3, the whole efficacy assay process from cell preparation to viability detection is

finished within the chip in the way of continuous flow. Droplets of the cell-photosensitizer mixture are generated by cross-flow shear method, which potentially can provide a variety of photosensitizer concentrations by changing the flow rate ratio of cell suspension and reagent solution inputs. Then, depending on the flow rate in the main channel, cells are incubated with the photosensitizer for a certain time period and receive a certain illumination dose. Then the droplets after PDT treatment are merged with live/dead staining solution for viability assay and evaluated at the detection zone after another time period of incubation in the chip.

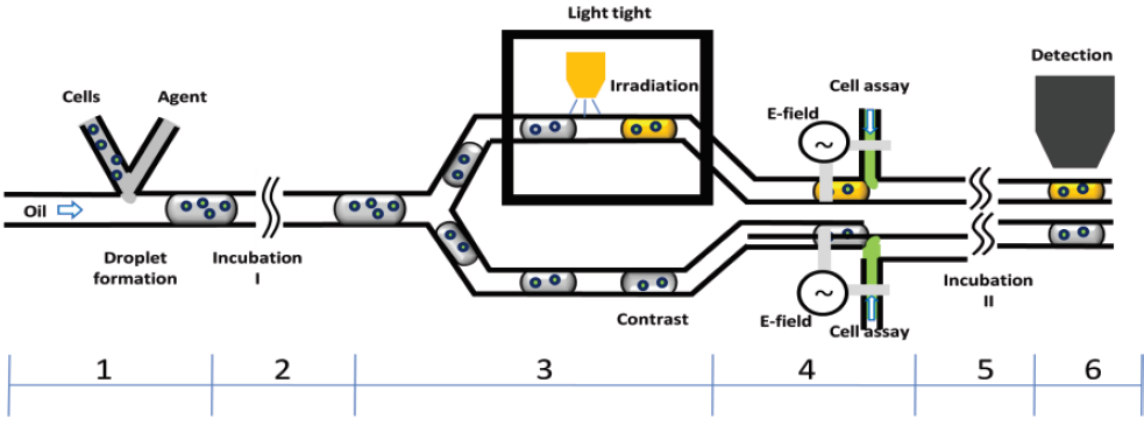


Figure 1.3 Schematic of the chip design for continuous flow PDT efficacy test. It is divided into six parts as labeled: 1. Droplet formation for mixing cells and photosensitizer; 2. Incubation I for photosensitizer uptaken by cells; 3. PDT illumination with a white LED; 4. Electrical field induced addition of cell assay solution; 5. Incubation II; 6. Cell viability detection [23].

This method demonstrates the great potential of microfluidic technology in high-throughput photosensitizer screening, with a complete PDT efficacy test process integrated on the chip. However, since there is only one report on this method so far, there is limited information regarding the many challenges this kind of continuous flow scheme might face with. For example, this study only tested cell samples suspended in

solution. It might be difficult to use other cell samples, which need to attach to solid culture substrate to maintain normal cell behavior or even survive. It is not clear yet possible method to incorporate the oxygen level control. Also, it is very challenging to provide dynamic controls for each part in order to evaluate PDT efficacy with different photosensitizer concentrations, incubation times before illumination, illumination doses, etc. In this scheme, two factors are usually correlated, such as incubation time and illumination dose-a reduction in the main channel flow rate would increase both of them in the same way.

### 1.3 High-throughput microfluidic drug screening

Typical anti-cancer drug efficacy assays are carried out in multi-well plates. Cells are cultured to confluence, incubated with drug for a certain period of time, and have their viability evaluated. Large-number microwell plates and automated liquid-handling robotics provide the capabilities for high-throughput drug screening. However, even these tools cannot meet the needed number of tests [15]. Additionally, high cost restricts their usage to only a few biggest companies and core research facilities. Besides, often these in-plate models are too simple to predict the actual drug efficacy and toxicity in vivo [24-26]. First, despite their size and cost, automated plate assays only provide control of drug dose and treatment time. They lack dynamic control of other therapeutic factors such as oxygen level, pH value, mechanical stimulations like shear stress, and illumination dose. Second, cell culture conditions in plate differ greatly from their native environment. Most cancer cell samples are separated cell lines and lacking interactions among different cell types. Also cells are cultured as monolayers in the final tests. This 2D environment lacks

complex ECM structures and 3D cell organizations, which directly changes chemical transportations and mechanical supports.

Microfluidic technology can be leveraged to solve these challenges. With its intrinsic capability for manipulating tiny volumes of fluids (nl, pl, fl), microfluidics helps save lab space and reagent and power consumption [27, 28]. More importantly, it provides more powerful drug screening platforms with dynamic control of various therapeutic factors and new cancer models closer mimicking in vivo conditions [29]. People have developed numerous microfluidic platforms for drug screening, and the following section provides an overview of the new capabilities that they have enabled.

**Microfluidic Multiplexing**

Microfluidic multiplexing provides the capability for automated combinations of different therapeutic factors and parallel drug efficacy assays. The most common multiplexing application is screening various drug candidates with multiple cell line models [30, 31]. As shown in Figure 1.4, usually cell loading channels and drug loading channels are orthogonal to each other. Each channel intersection serves as a cell culture chamber. These chambers mimick the layout of microwells in a conventional plate. Controlling the two pairs of elastomeric valves around the chamber enables switching the chamber between open to either cell loading or drug exposure. Although all different drug candidates and cell lines still need to be fed into corresponding chip inlets individually, efficacy tests of their combinations are automatically realized in chip. In conventional microwell plates, “A (number of drug candidates) x B (number of cell lines)” times of pipetting are required for sample loading. Instead, microfluidic handling enables sample loading in an “A+B” manner. It is a major labor reduction considering the around

10,000 chemical compounds for screening per year and standard cell line models of 60 kinds (NCI 60) or even 1,200 kinds (CMT1000) [15]. Multiplexing, together with multistep biochemical processing, parallelization strategies, and economics of scale, sets up the fundamentals of large-scale integration for high-throughput microfluidic platforms.

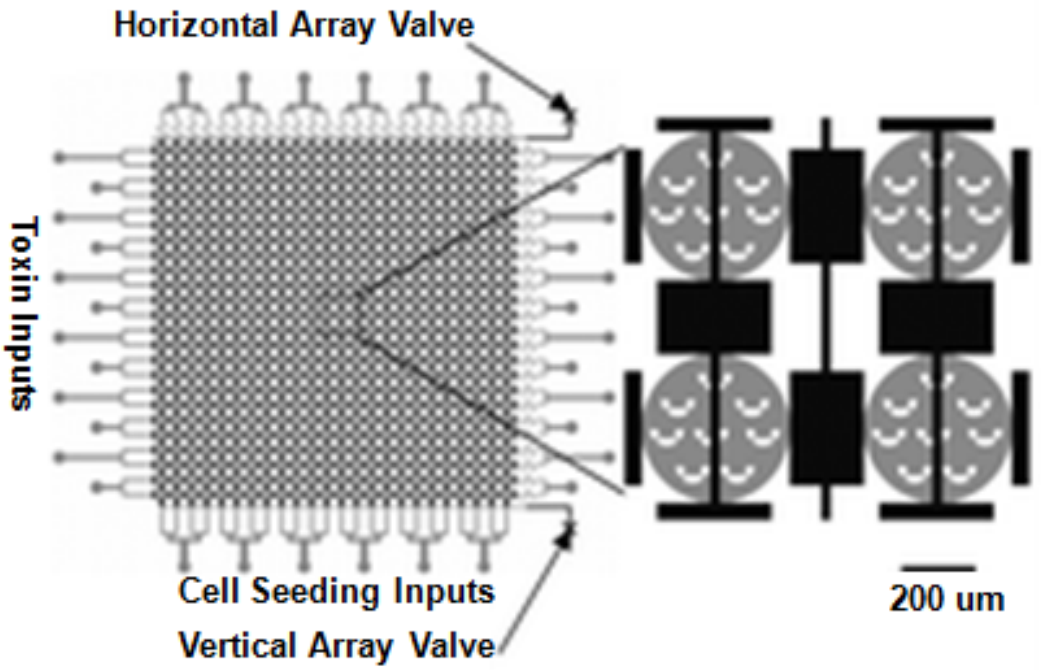


Figure 1.4 Schematic of the 24 x 24 chambers array chip for cytotoxicity study, with 6 inlets for different cell lines loading and 12 inlets for different toxins feeding. Each chamber is surrounded by two pairs of elastomeric valves, while lateral pair controls its open/close to toxin exposure and vertical pair controls its open/close to cell loading[31].

**Drug concentration gradient**

The dose response curve describes the anti-cancer drug efficacy change in target cells caused by differing levels of dose after certain exposure times. In experimental models, usually it includes a range of steep and linear relationship between cell viability and drug dose [32, 33]. Exploiting the difference between dose response curves of normal cells and cancer cells is central for determining an optimized drug dose, which provides targeted

therapy and minimal side effects. Preparing different drug concentrations is an important step in drug efficacy assays for getting the dose response curve, and microfluidics can provide the capability of automatic drug concentration gradient generation on chip [34-36].

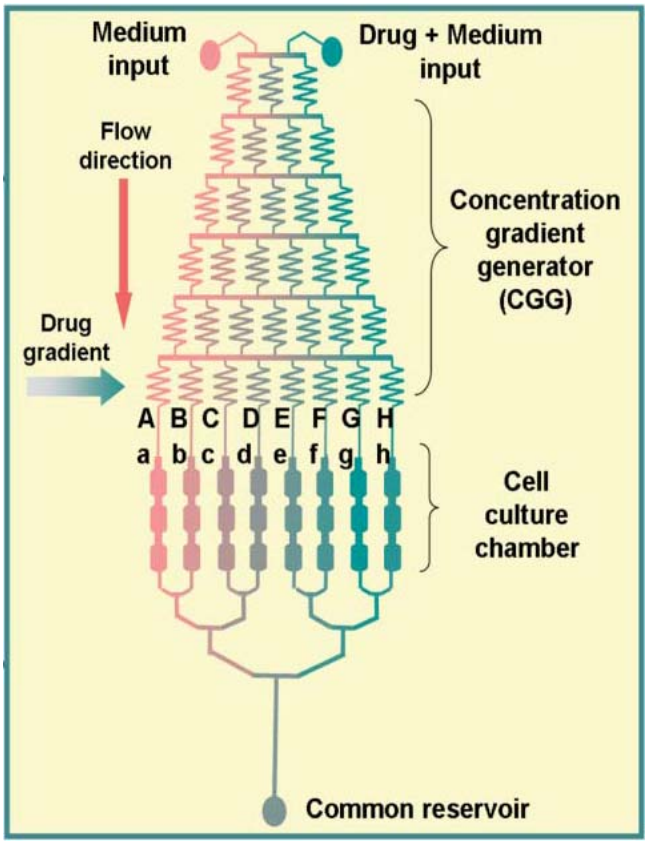


Figure 1.5 Schematic of the high-throughput drug screening chip with an upstream concentration gradient generator (CGG) and downstream parallel cell culture chambers [36].

One example of microfluidic drug screening chips with this integrated capability is shown in Figure 1.5. A pure culture medium (0% drug concentration, red color) and another medium with the drug of interest are introduced into the concentration gradient generator (CGG) part through two separate inlets. Within this part, flows with different concentrations are mixed to make a flow of a new concentration between the mixed levels. This process of flow split, mixing, and recombination repeat each stage with an

increasing number of drug concentrations, and final output of the CGG is a series of drug different concentrations (ranging from 0% to starting drug concentration, in which the color change from red to green indicates the drug concentration increasing), which are fed into following parallel cell culture chambers for drug treatment on cells.

**Oxygen gradient generation**

While most in vitro cell culture and drug efficacy tests are carried out under atmosphere condition of around 21% oxygen, in vivo cells experience a wide range of oxygen tensions, which affects their behaviors. Hypoxia, a condition of reduced oxygen level, presents in a variety of solid tumors. Its many effects on tumor biology include selection of favoring genotype survival, gene expression changes, enhancement of metastasis, and immune response suppression. These in turn implicate drug resistance changes. While most reported evidence reflects compromised therapy efficiency under hypoxia conditions, some exceptions show that hypoxic cells result in increased drug sensitivity [37, 38]. In any case, it emphasizes the necessity of including the oxygen concentration as an important therapeutic factor in preclinical drug screening. Conventional methods for providing a controlled oxygen concentration for cell culture such as using direct bubbling require complicated instruments, large volume of gas supply, and lack the capability of high throughput drug screening. Microfluidics provides a convenient way of generating various oxygen concentrations on chip and controllable oxygen distribution over the cell culturing area inside [39, 40].

Figure 1.6 shows an example of controllable oxygen gradient generation in chip for anti-cancer drug screening. The middle wide channel is for cancer cell culturing and the two side channels provide constant boundary conditions of fixed oxygen concentrations.

One of the side channels is having a mixture of Pyrogallol and NaOH flowing through, which is having an oxygen scavenging reaction and provides the boundary condition of low oxygen concentration. The other side channel is having a mixture of $H_2O_2$ and NaOCl flowing through, which is having an oxygen generation reaction and provides the boundary condition of high oxygen concentration. The PDMS walls between the central channel and side channels are less than 50um thick and it is easy for gas (oxygen) to diffuse, equilibrate and form a gradient within the cell culture channel. Various oxygen gradient profiles in the cell culture channel can be generated by adjusting the chemical reaction rates within the side channels. Also as an alternative way, gas mixture flows with certain oxygen concentrations can be directly feed through the side channels providing a same effect of boundary condition constraints.

**Flow shear stress**

Cancer cells cultured or treated with anti-cancer drugs in a microwell plate are surrounded with static culture media, in which all the external mechanic stimulus is absent. However, in vivo cancer cells are exposed to all types of mechanic stimulus like tension, compression, and shear stress, all of which affect cells' behavior and viability. Tumor-cell adhesion intrinsically depends on characteristics of tumor cells, endothelial cells (EC) and extracellular matrix (ECM), and is also proved shear rate dependent [41, 42]. Invasive positional of different cell lines are demonstrated to be altered differently by shearing forces [43, 44]. Flow shear stress could also modulate cell cycle distribution and inhibit cell differentiation as a natural regulator [45]. Marked changes of cancer cells' signal transduction, gene expression, and proliferation as results of exposure to shear

stress are also reported [46]. All of these suggest cancer cell responses to mechanical stimulus like fluid shear stress should be considered for the disease management.

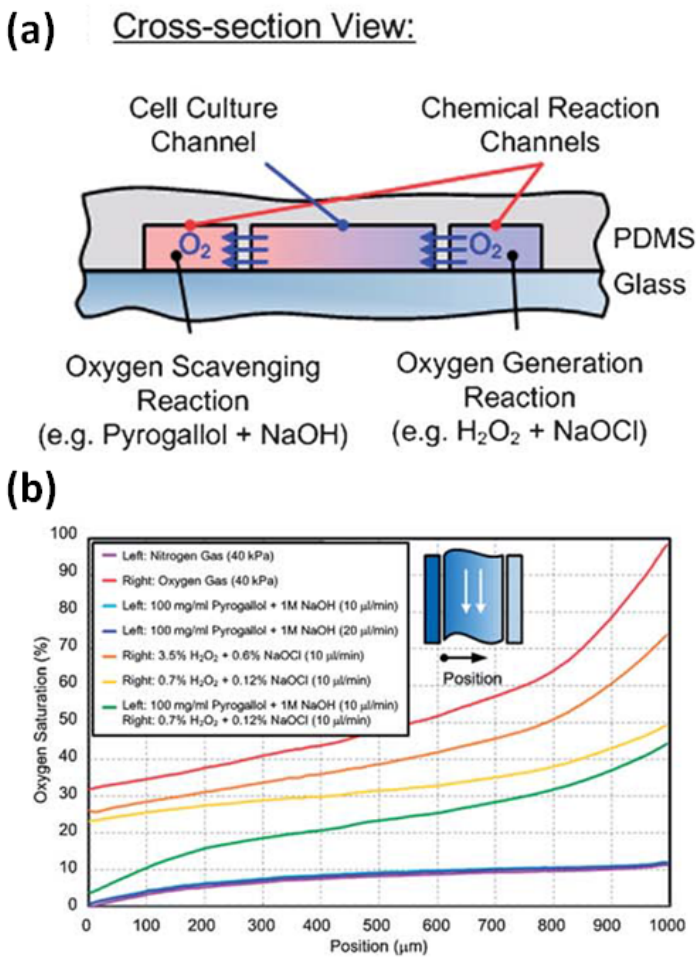


Figure 1.6 (a) Cross-section view of the device showing the working principle of oxygen gradient generation. (b) Measured oxygen gradient profiles under different chemical reaction combinations, different solution flow rates, and different gas flow rates [39].

Microfluidics, with its intrinsic capability of dynamic fluidic flow control, provides an ideal way to look into shear stress's influence on cancer cells. Figure 1.7 shows an example of microfluidic system for studying the interactions between nanoparticle drugs and cancer cells under different flow shear stresses. The drug containing nanoparticles are having aptamers conjugated on surface for recognizing the transmembrane prostate-

specific membrane antigen (PSMA) and helping them target and attach to prostate cancer cells. During the test, a narrow strip of cells is patterned first on the substrate. Then the microfluidic channel is aligned onto the cells and bonded to the substrate. Nanoparticle solutions are introduced into the microfluidic channel under a certain flow rate, resulting in a specific shear stress during the nanoparticles' delivery to the cancer cells. Observed results show under static culturing or a low shear stress, this kind of nanoparticles could selectively adhere to PSMA expressing cells. But if the shear stress goes too high, nanoparticles could not attach to any kind of cells, even the PSMA expressing cancer cells they have been designed to target.

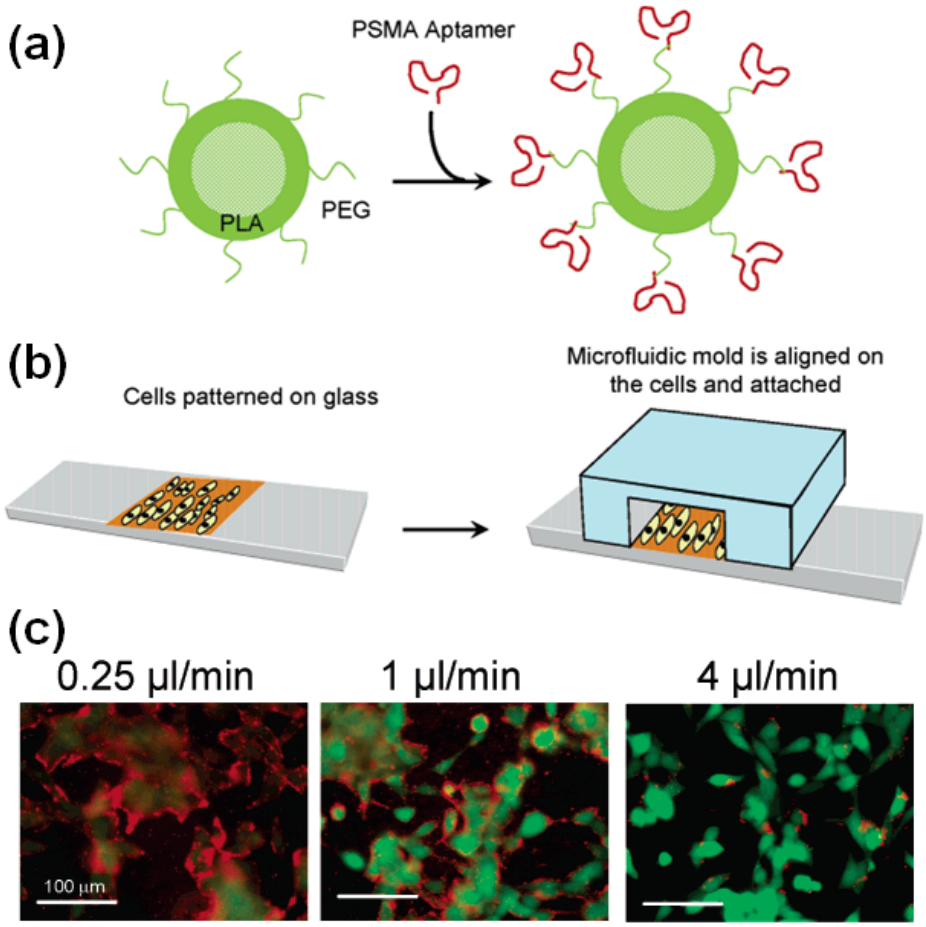


Figure 1.7 (a) Schematic diagram of the nanoparticle with surface covalently conjugated with aptamers recognizing PSMA protein. (b) Cancer cell lines are patterned

on glass substrate and then the microfluidic channel is aligned and bonded on top. (c) Fluorescent images of rhodamine labeled nanoparticles (red) binding to cancer cells (green) under different shear stresses[47].

**3D cancer model**

3D cancer cell models, like spheroid culture or polymer scaffolds, better reflect in vivo tumor tissues and potential drug efficacies than conventional 2D monolayer cell culture or single cell suspension culture. Heterologous cell-cell interactions and cell-ECM interactions can be established in 3D cell culture [48]. Also the heterogeneity of cellular microenvironments in tumor severely limits drug efficacy, and 3D tumor models incorporating multiple microenvironment gradients will enable more precise analysis of the effective working cancer drugs in vivo [49].

Microfluidics acts as the favorable method for drug efficacy assay with 3D cancer models, which usually include different size samples ranging from tens to hundreds of microns. Also microfluidics' benefits for 2D cell model applications could be retained. Not only it is still high-throughput, low cost, but also it is keeping the additional features like flow shear stress control, dynamic nutrition/drug delivery and waste removal [50, 51]. Figure 1.8 shows an example of microfluidic chip utilizing hydrodynamic cell trapping and accumulation to form large scale 3D spheroid arrays. Each cell culture chamber contains multiple U-shape traps with a designable volume capable of containing a certain number of cancer cells. The 2um wide gap between the trap and substrate allows a significant flow passing through before the trap is fulfilled with cells. After the cells are trapped inside, continuous by-pass flows help maintain them in a compact group, make them adhere to each other and gradually form a firm spheroid. After the spheroid formation, the continuous flow passing besides the trap exchanges nutrition/drugs and

waste with the spheroid by diffusion. This is mimicking the function of blood vessels in tumor, which is a major cause of heterogeneity microenvironment in vivo.

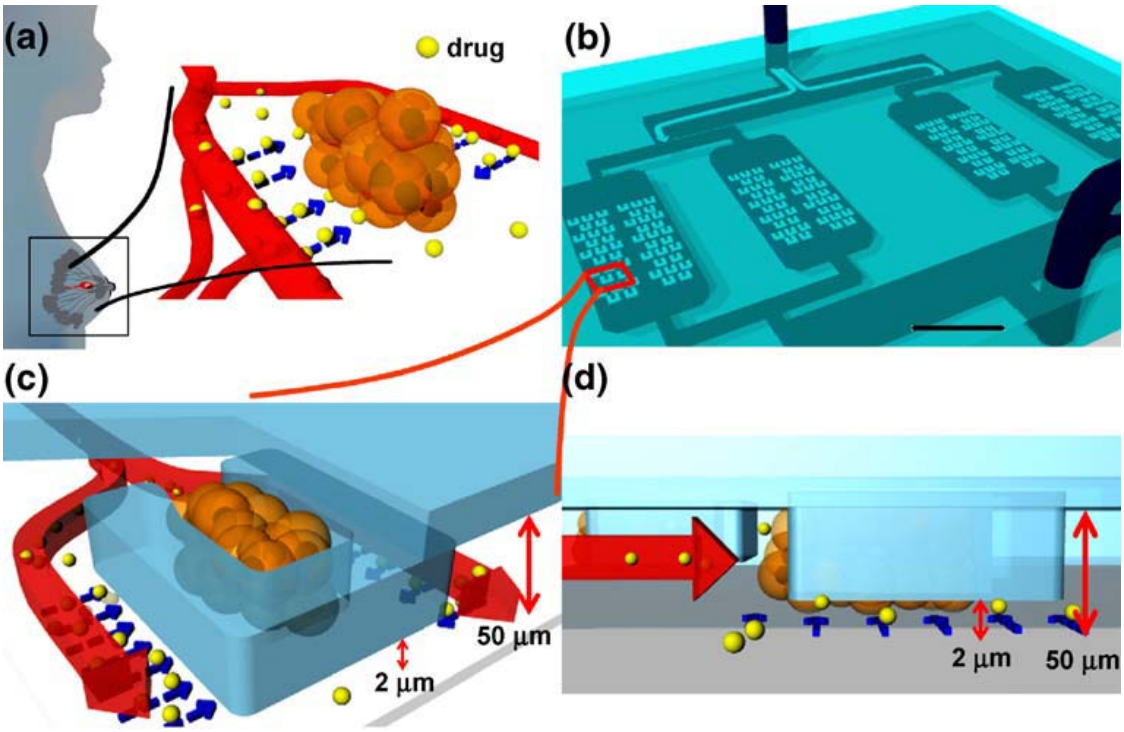


Figure 1.8 (a) Schematic of the in vivo tumor spheroid with blood vessels around delivering nutrients and removing wastes. (b) Diagram of the microfluidic device constituted of parallel cell culture chambers, each of which contains a high density of U-shape traps for cell trapping and spheroids formation. (c) Perspective view of a single U-shape trap. Continuous flow passing beside provides molecule exchanges with the spheroid which mimics the in vivo situation. (d) Side view of the trap [51].

3D cancer cell culturing usually provides coexisting gradients of multiple therapeutic factors including chemical signals, mechanical stress, nutrition, anti-cancer drugs, metabolic wastes, oxygen, pH level and etc. It is providing an ideal model closer to in vivo conditions for optimum drug screening. However that does not mean it is replacing conventional methods like 2D monolayer models. Even utilizing microfluidic technology, 3D cell culturing is still comparatively more complex and time-consuming. Also, it is

necessary to have some other cell models with independent single therapeutic factors for deconvolving cancer complexity and looking into relevant biological mechanisms [52].

### 1.4 Motivation and research goals

As presented in the section above, researchers have started to look into high-throughput screening for photosensitizers but current technologies are still lagging far behind to meet the demands of new drugs discovering and clinical protocols optimization. Existing solutions for high-throughput photosensitizer screening all have their limitations, which could be overcome by developing a new generation of platforms with higher screening capability and more powerful control over therapeutic factors.

Compared to photosensitizer screening, chemotherapy drug screening utilizing microfluidic platforms has been more widely investigated. Some of these platforms can be adapted and used for photosensitizer screening too. But other unique features of PDT are usually not included or lacking looking into including oxygen level, illumination intensity and time, and drug incubation time. Besides, since these platforms are developed in different research groups, usually they only focus on one or two therapeutic factors and are different from each other in design, fabrication, and test protocols.

Thus, it is desirable to develop a new microfluidic platform for high-throughput photosensitizer efficacy screening, as described in the following chapter. This platform is capable of performing parallel efficacy tests of hundreds of or even more than a thousand PDT conditions during a single test on one chip. Also it provides the capability of PDT efficacy evaluation on various therapeutic factors including drug concentration, incubation time, oxygen concentration, illumination intensity and time, as well as flow shear stress. Depending on the research focus, different combinations of these therapeutic

factors can be incorporated together in different versions of microfluidic chips. A same PDT illumination setup is used and these therapeutic factors' effects on PDT efficacy can be evaluated following similar test protocols. As described in the 4th chapter, PDT efficacy tests using this platform are demonstrated with multiple cell types (C6, DI TNC1, 9L, MCF7, Skov3), two in vitro cell models (2D monolayers and 3D multicellular spheroids), and two distinctive generations of photosensitizers (Methylene Blue free molecules and functionalized nanoparticles (NPs).

To be specific, contributions of this work include:

- ✧ Establishment of a microfluidic platform for photosensitizer screening with therapeutic factors of drug concentration, incubation time, oxygen concentration, illumination intensity, illumination time, and flow shear stress
- ✧ Demonstration of microfluidic gradient generations of drug concentration, incubation time, oxygen concentration, illumination intensity, and flow shear stress for relevant PDT efficacy tests
- ✧ Demonstration of the on-chip PDT efficacy evaluations using different cell lines and photosensitizers
- ✧ Demonstration of the parallel evaluation of PDT efficacy response to multiple therapeutic factors
- ✧ Establishment of the 3D cancer cellular model for high-throughput PDT efficacy screening on chip

## Chapter 1 References


[1] D. E. J. G. J. Dolmans, *et al.*, "Photodynamic therapy for cancer," *Nat Rev Cancer,* vol. 3, pp. 380-387, 2003.

[2] M. Triesscheijn, *et al.*, "Photodynamic Therapy in Oncology," *The Oncologist,* vol. 11, pp. 1034-1044, October 1, 2006 2006.

[3] A. P. Castano, *et al.*, "Photodynamic therapy and anti-tumour immunity," *Nat Rev Cancer,* vol. 6, pp. 535-545, 2006.

[4] S. I. Hajdu, "A note from history: landmarks in history of cancer, part 1," *Cancer,* vol. 117, pp. 1097-102, Mar 1 2011.

[5] G. Kolata, "Advances Elusive in the Drive to Cure Cancer," in *The New York Times*, ed. New York, 2009, p. A1.

[6] Y. Cao, *et al.*, "Cancer research: past, present and future," *Nat Rev Cancer,* vol. 11, pp. 749-754, 2011.

[7] J. Herndon. (2009). *The most common treatments for cancer*. Available: http://www.livestrong.com/article/68492-common-treatments-cancer/

[8] S. B. Brown, *et al.*, "The present and future role of photodynamic therapy in cancer treatment," *The Lancet Oncology,* vol. 5, pp. 497-508, 2004.

[9] R. Ackroyd, *et al.*, "The history of photodetection and photodynamic therapy," *Photochem Photobiol,* vol. 74, pp. 656-69, Nov 2001.

[10] J. Moan and Q. Peng, "An outline of the hundred-year history of PDT," *Anticancer Res,* vol. 23, pp. 3591-600, Sep-Oct 2003.

[11] R. R. Allison, *et al.*, "Photosensitizers in clinical PDT," *Photodiagnosis and photodynamic therapy,* vol. 1, pp. 27-42, 2004.

[12] N. Kudinova and T. Berezov, "Photodynamic therapy of cancer: Search for ideal photosensitizer," *Biochemistry (Moscow) Supplemental Series B: Biomedical Chemistry,* vol. 4, pp. 95-103, 2010.

[13] *Photodynamic therapy for cancer*. Available: http://www.cancer.gov/cancertopics/factsheet/Therapy/photodynamic

[14] S. V. Sharma, *et al.*, "Cell line-based platforms to evaluate the therapeutic efficacy of candidate anticancer agents," *Nat Rev Cancer,* vol. 10, pp. 241-253, 2010.

[15] R. H. Shoemaker, "The NCI60 human tumour cell line anticancer drug screen," *Nat Rev Cancer,* vol. 6, pp. 813-823, 2006.

[16] S. H. Lim, *et al.*, "A new naturally derived photosensitizer and its phototoxicity on head and neck cancer cells," *Photochem Photobiol,* vol. 87, pp. 1152-8, Sep-Oct 2011.

[17] Y. Lu, *et al.*, "Methylene blue-mediated photodynamic therapy induces mitochondria-dependent apoptosis in HeLa cell," *J Cell Biochem,* vol. 105, pp. 1451-60, Dec 15 2008.

[18] J. D. Chapman, *et al.*, "Oxygen Dependency of Tumor Cell Killing in Vitro by Light-Activated Photofrin II," *Radiation Research,* vol. 126, pp. 73-79, 1991.

[19] A. Paul, *et al.*, "Comparative Study of the Photosensitization of Jurkat Cells in vitro by Pheophorbide-a and a Pheophorbide-a Diaminobutane Poly-Propylene-Imine Dendrimer Complex," *Laser Physics,* vol. 13, pp. 22-29, 2003.

[20] E. O. Serebrovskaya, *et al.*, "Targeting cancer cells by using an antireceptor antibody-photosensitizer fusion protein," *Proceedings of the National Academy of Sciences,* May 20, 2009 2009.
[21] I. G. Meerovich, *et al.*, "High-throughput screening system for the study of phototoxicity of photosensitizers in vitro," *Proc. SPIE 4952, Optical Methods for Tumor Treatment and Detection: Mechanisms and Techniques in Photodynamic Therapy XII,* San Jose, CA, USA, 2003, pp. 203-208.
[22] M. C. Butler, *et al.*, "A high-throughput biophotonics instrument to screen for novel ocular photosensitizing therapeutic agents," *Invest Ophthalmol Vis Sci,* vol. 51, pp. 2705-20, May 2010.
[23] X. N. Robert Jarvis, Andrew J. de Mello, Mark Wainwright, Robert C.R. Wootton, "A microfluidic flow system for activity screening of Photo-Dynamic Therapy agents," in *International Conference on Miniaturized Systems for Chemistry and Life Sciences*, 2009, pp. 603-605.
[24] J.-P. Gillet, *et al.*, "Redefining the relevance of established cancer cell lines to the study of mechanisms of clinical anti-cancer drug resistance," *Proceedings of the National Academy of Sciences,* vol. 108, pp. 18708-18713, November 15, 2011 2011.
[25] T. Voskoglou-Nomikos, *et al.*, "Clinical predictive value of the in vitro cell line, human xenograft, and mouse allograft preclinical cancer models," *Clin Cancer Res,* vol. 9, pp. 4227-39, Sep 15 2003.
[26] D. Zips, *et al.*, "New anticancer agents: in vitro and in vivo evaluation," *In Vivo,* vol. 19, pp. 1-7, Jan-Feb 2005.
[27] C. D. Chin, *et al.*, "Commercialization of microfluidic point-of-care diagnostic devices," *Lab on a Chip,* vol. 12, pp. 2118-2134, 2012.
[28] S. D. Minteer, *Microfluidic Techniques: Reviews and Protocols*: Springer, 2006.
[29] M. Baker, "Tissue models: A living system on a chip," *Nature,* vol. 471, pp. 661-665, 2011.
[30] Y.-J. K. Jaehoon Chung, Il-Joo Cho, Euisik Yoon, "Highly efficient single cell capturing in microwell array using hydrodynamic guiding structures," presented at the International Conference on Miniaturized Systems for Chemistry and Life Sciences, 2008.
[31] Z. Wang, *et al.*, "High-density microfluidic arrays for cell cytotoxicity analysis," *Lab Chip,* vol. 7, pp. 740-5, Jun 2007.
[32] D. L. L. Bruce A. Chabner, *Cancer Chemotherapy and Biotherapy: Principles and Practice*: Lippincott Williams & Wilkins, 2010.
[33] W. B. Pratt, *The Anticancer Drugs*: Oxford University Press, 1994.
[34] B. G. Chung and J. Choo, "Microfluidic gradient platforms for controlling cellular behavior," *ELECTROPHORESIS,* vol. 31, pp. 3014-3027, 2010.
[35] A. Tirella, *et al.*, "A microfluidic gradient maker for toxicity testing of bupivacaine and lidocaine," *Toxicol In Vitro,* vol. 22, pp. 1957-64, Dec 2008.
[36] N. Ye, *et al.*, "Cell-based high content screening using an integrated microfluidic device," *Lab Chip,* vol. 7, pp. 1696-704, Dec 2007.
[37] J. A. Bertout, *et al.*, "The impact of O2 availability on human cancer," *Nat Rev Cancer,* vol. 8, pp. 967-975, 2008.

[38] W. R. Wilson and M. P. Hay, "Targeting hypoxia in cancer therapy," *Nat Rev Cancer,* vol. 11, pp. 393-410, 2011.
[39] Y.-A. Chen*, et al.*, "Generation of oxygen gradients in microfluidic devices for cell culture using spatially confined chemical reactions," *Lab on a Chip,* vol. 11, pp. 3626-3633, 2011.
[40] M. Polinkovsky*, et al.*, "Fine temporal control of the medium gas content and acidity and on-chip generation of series of oxygen concentrations for cell cultures," *Lab Chip,* vol. 9, pp. 1073-84, Apr 21 2009.
[41] E. Bastida*, et al.*, "Influence of shear stress on tumor-cell adhesion to endothelial-cell extracellular matrix and its modulation by fibronectin," *Int J Cancer,* vol. 43, pp. 1174-8, Jun 15 1989.
[42] C. Luthur Siu-Lun*, et al.*, "Adhesion dynamics of circulating tumor cells under shear flow in a bio-functionalized microchannel," *Journal of Micromechanics and Microengineering,* vol. 21, p. 054033, 2011.
[43] K. Lawler*, et al.*, "Mobility and invasiveness of metastatic esophageal cancer are potentiated by shear stress in a ROCK- and Ras-dependent manner," *Am J Physiol Cell Physiol,* vol. 291, pp. C668-77, Oct 2006.
[44] H. Qazi*, et al.*, "Fluid Shear Stress Regulates the Invasive Potential of Glioma Cells via Modulation of Migratory Activity and Matrix Metalloproteinase Expression," *PLoS ONE,* vol. 6, p. e20348, 2011.
[45] S.-F. Chang*, et al.*, "Tumor cell cycle arrest induced by shear stress: Roles of integrins and Smad," *Proceedings of the National Academy of Sciences,* vol. 105, pp. 3927-3932, March 11, 2008 2008.
[46] C. L. Avvisato*, et al.*, "Mechanical force modulates global gene expression and beta-catenin signaling in colon cancer cells," *J Cell Sci,* vol. 120, pp. 2672-82, Aug 1 2007.
[47] O. C. Farokhzad*, et al.*, "Microfluidic System for Studying the Interaction of Nanoparticles and Microparticles with Cells," *Analytical Chemistry,* vol. 77, pp. 5453-5459, 2005/09/01 2005.
[48] J. Friedrich*, et al.*, "Experimental anti-tumor therapy in 3-D: spheroids--old hat or new challenge?," *Int J Radiat Biol,* vol. 83, pp. 849-71, Nov-Dec 2007.
[49] C. L. Walsh*, et al.*, "A multipurpose microfluidic device designed to mimic microenvironment gradients and develop targeted cancer therapeutics," *Lab on a Chip,* vol. 9, pp. 545-554, 2009.
[50] Y. C. Tung*, et al.*, "High-throughput 3D spheroid culture and drug testing using a 384 hanging drop array," *Analyst,* vol. 136, pp. 473-8, Feb 7 2011.
[51] L. Y. Wu*, et al.*, "Microfluidic self-assembly of tumor spheroids for anticancer drug discovery," *Biomed Microdevices,* vol. 10, pp. 197-202, Apr 2008.
[52] M. Håkanson*, et al.*, "Controlled Breast Cancer Microarrays for the Deconvolution of Cellular Multilayering and Density Effects upon Drug Responses," *PLoS ONE,* vol. 7, p. e40141, 2012.

# CHAPTER 2 HIGH-THROUGHPUT MICROFLUIDIC PLATFORM FOR PDT EFFICACY: CONCEPT AND DESIGN

## 2.1 Device overview

As described in Chapter 1, high-throughput technology for photosensitizer screening is underdeveloped. Although some microfluidic platforms for chemo drug screening can be utilized for photosensitizer screening, they are only capable of characterizing drug dose response instead of including also other therapeutic factors like incubation time, oxygen level, illumination dose and shear stress. Usually these factors' influences on drug efficacy have been ignored in these platforms, which could make the efficacy test results greatly different from each other or from the actual efficacy in clinical treatment. The microfluidic platform being presented in this chapter overcomes such limitations. Specifically, it is providing the following features of:

- ✧ High-throughput of 1,296 parallel-running PDT efficacy tests in one chip
- ✧ A minimum test sample area of 80um×80um for each PDT condition
- ✧ A maximum number of therapeutic factors, including photosensitizer concentration, incubation time, oxygen level, illumination dose and flow shear stress
- ✧ Compatibility with different generations of photosensitizers (free molecule dyes and multi-functional nanoparticles) and different in vitro models (2D cell monolayers and 3D multicellular spheroids)

- ✧ LEGO-like microfluidic modules, which are subjected to be reconfigured to fit specific requirements of different in vitro cell models, photosensitizers and focusing therapeutic factors
- ✧ Automatic data collection and analysis enabled by self-written Matlab programs

This platform is based on microfluidic array technology for drug screening, and the central chip is fabricated using widely accepted multi-layer polydimethylsiloxane (PDMS) soft lithography [1-3]. Basic conceptual elements are shown in Figure 2.1. The chip is composed of three layers. The first, essential cell layer is for sample cells culturing and drug delivery. It also controls therapeutic factors including drug concentration, drug-incubation time and flow shear stress. This layer includes accesses to sample drug solution and control media, both of which are driven by either gravity flow or syringe pumping. The second, optional gas layer controls therapeutic factor of oxygen level. Its inlets are individually connected to compressed gas supplies of either nitrogen or oxygen, which are then mixed in the gas layer forming a series of oxygen levels. The third, optional filter layer controls the therapeutic factor of PDT illumination intensity (dose). Light absorption dye solution is filled into the filter layer. During the PDT test, this solution absorbs some portion of the illumination light before it reaches the sample cells, thus provides a capability of modifying the illumination intensity on cells. A brief PDT test procedure using this platform is as follows. First, sample cells are cultured inside the chip until they reach a status ready for PDT test, e.g. forming either a 2D monolayer or 3D spheroids of desired sizes. Then, therapeutic factors within the chip are equilibrated to stable levels, and the whole chip is illuminated with a red LED light source for PDT treatment for a certain time period. After that, PDT efficacy is evaluated based on the

resulting cell viability displayed by live/dead fluorescence staining. The fluorescence images are recorded for calculating the viable cell ratio using ImageJ software and custom written Matlab programs.

Here, all three basic elements in PDT are under control in a single microfluidic chip. Each of them is controlled by one microfluidic layer, and all three layers are bonded together to provide a comprehensive microenvironment control during the PDT efficacy test. Figure 2.2 shows a single such unit for PDT efficacy test. Top gas layer is filled with an oxygen/nitrogen mixture with certain oxygen concentration. Due to gas permeability of PDMS, the same oxygen concentration is rightly imposed onto the cells in the below cell layer. In the cell layer, desired drug concentration solution is fed to the cancer cells under a dynamic way for a desired incubation time. Glass substrate between cell layer and filter layer provides the mechanical support for the whole chip and cell culture. The filter layer modulates illumination intensity before the PDT light reaches the cells. Depending on the concentration of light absorption dye solution filled in the filter layer and filter thickness (microfluidic channel height), the actual illumination intensity at the cancer cell is attenuated to a desired level. And by turning on/off the LED light source, the total illumination duration can be adjusted in another way too, which also modifies the final illumination dose on cancer cells.

To provide the capability of high-throughput PDT efficacy screening, it is desirable to expand such basic test unit with microenvironment controls into the format of large scale array. First, cells are cultured into monolayer covering the whole testing area, which can be further divided into identical smaller segments for different test conditions. Secondly, therapeutic factor gradients are generated on chip. Third, these gradients can be

multiplexed and recombined into different PDT conditions. Following part we are showing how it is realized with the typical configuration of each layer.

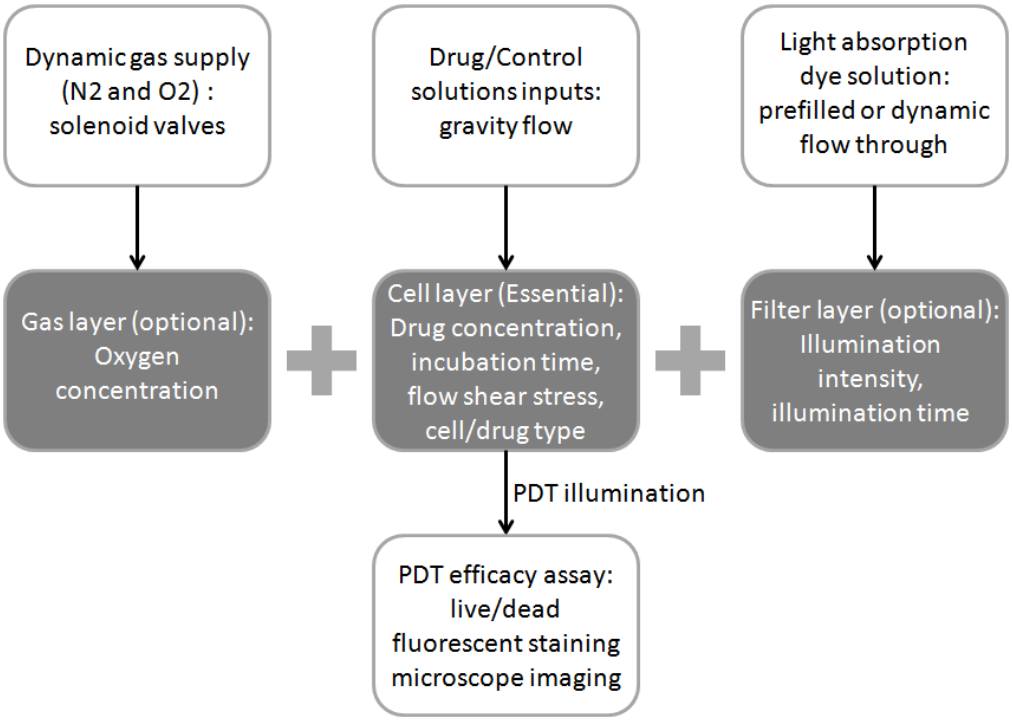


Figure 2.1 Diagram of related methodology elements of microfluidic high-throughput PDT efficacy platform.

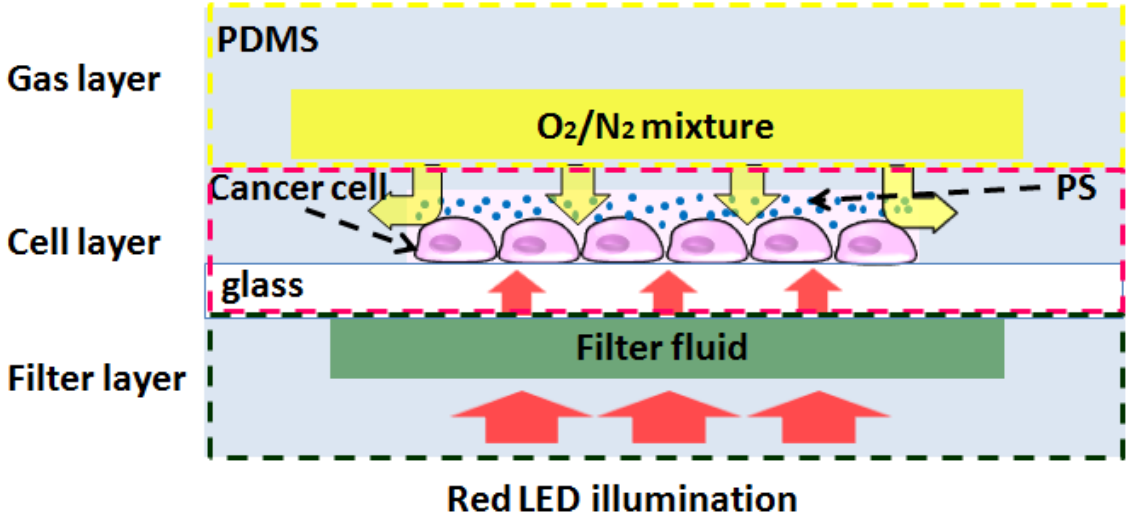


Figure 2.2 Schematic diagram of the on-chip cell microenvironment control of oxygen concentration, drug concentration, illumination intensity for PDT efficacy assay.

As shown in Figure 2.3, typical cell layer is composed of four parts: two inlets, the gradient generator, cell culture channels, and the outlet reservoir. During the cell loading process, outlet reservoir is filled with cell suspension and then a negative pressure is applied to the inlets to suck in the cells into the cell culture channels. Cell culture channels are identically 320um wide in parallel. During the drug feeding or PDT illuminating process, sample photosensitizer solution and control media are respectively introduced through two inlets. A microfluidic gradient generator based on repeatedly splitting and remixing solution samples is adopted for drug gradient generation [4]. The original two samples are turned into a series of different concentration drug solutions, and fed into each cell culture channel with one specific drug concentration. Drug feeding process is drive by gravity flow, which derives from the pressure difference between inlets and outlet [5-7].

Gas layer shares a very similar configuration with cell layer for gradient generation and distribution as shown in Figure 2.4. Instead of solutions with different photosensitizer concentrations, gas diffusion channels are having gas mixtures of different oxygen concentrations flowing through each channel, and, this series of oxygen concentrations are imposed on the corresponding positions' cell layer solutions beneath by diffusion [8-10]. A similar gradient generator but with modified channel dimensions considering the viscosity change of gas mixture is adopted [8]. Gas mixtures flowing through the gas layer are driven by a pressure difference between inlets and the outlet. The two inlets are individually connected to the gas supplies of either compressed air or compressed nitrogen, both of which are regulated at 5psi. The outlet is set open to atmosphere.

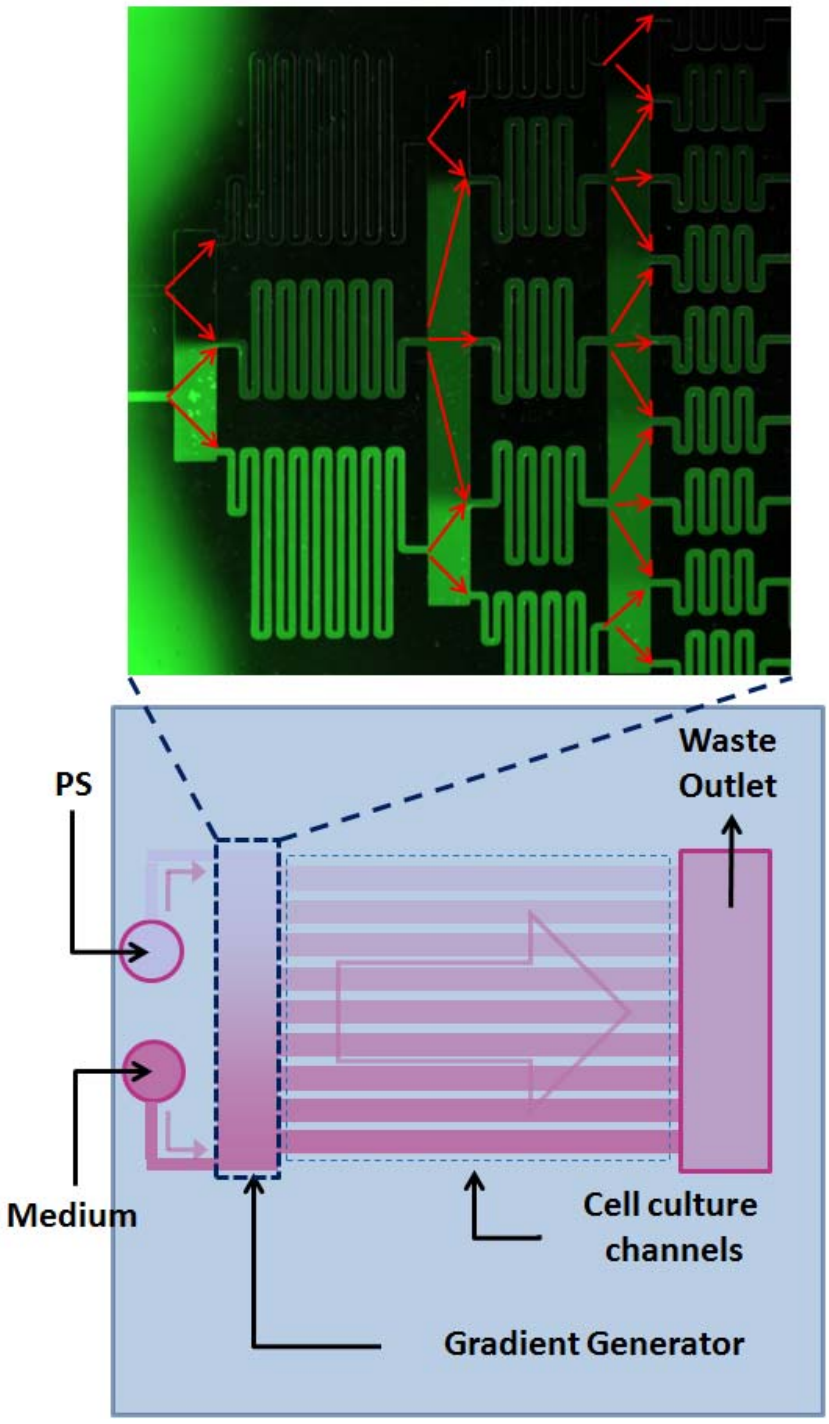


Figure 2.3 Schematic diagram of a typical cell layer for high-throughput screening. The enlarged part shows the microfluidic channel network within the gradient generator. Different concentrations are demonstrated with green fluorescent dye FITC. Arrows indicate the flow directions of splitting and remixing.

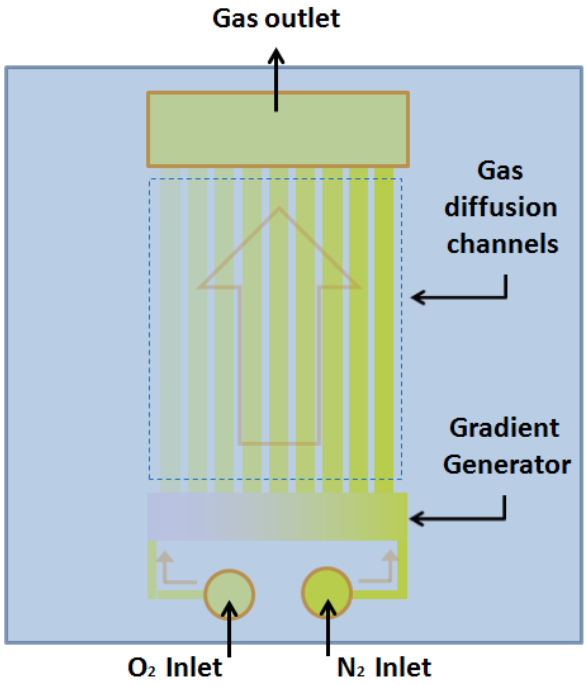


Figure 2.4 Schematic diagram of a typical gas layer for high-throughput screening.

The working principle for the filter layer is utilizing absorption dye solution in microfluidic structures to modulate final illumination intensity [11]. As shown in Figure 2.5, the central part of the filter layer is a gray scale liquid filter with repeated 4x4 grid patterns, which fit the scheme of repeated cell sample array for PDT efficacy test. This kind of 4x4 grid pattern is resulted from two orthogonally overlapped liquid filter layers. As shown in the enlarged part, each layer has four channel heights: 0um, 13um, 28um, 43um, which result in 4 different levels of transparency when filled with a same concentration dye solution. With a uniform illumination from the bottom, illumination intensity divides into 4 levels after passing the first filter layer and further divides into 16 levels after passing the second filter layer. Each of these 4x4 grid patterns covers an area of 320x320um, of which each grid unit is 80x80um. Absorption dye solutions in the filter layers can be refreshed through the inlet and outlet using a syringe pump. Also a different

gray scale can be realized by using dye solutions with different concentration combinations.

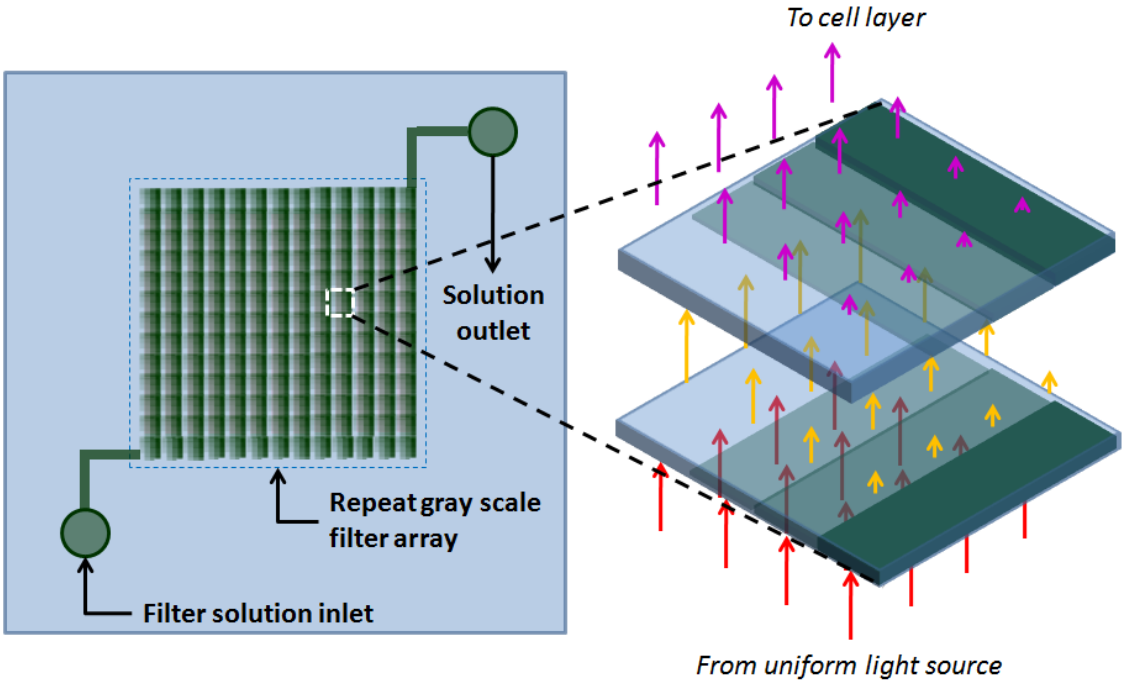


Figure 2.5 Schematic diagram of a typical filter layer for high-throughput screening. Enlarge part demonstrate the gray scale pattern generation mechanism with a single 4x4 grid unit in perspective view.

Further high-throughput integration can be realized by properly combining gradients of different therapeutic factors all together in a single chip and one PDT test. Figure 2.6 shows an example of combining the gradients of drug concentration, oxygen concentration and illumination intensity. Gas diffusion channels in gas layer and cell culture channels in cell layer are overlapped in an orthogonal way to realize a complete combination of these two gradients. In other words, each cell culture channel with one photosensitizer concentration would have divided sessions for all different oxygen concentrations, and vice verse. Furthermore, by adding the filter layer, each previous segment of certain drug concentration and oxygen concentration combination would be

covered by a same 4x4 grid grayscale pattern of the filter layer. In this case, final number of PDT test conditions would be: 9 (number of oxygen concentrations) x9 (number of drug concentrations) x16(number of illumination intensities) =1296 for one chip and one PDT test.

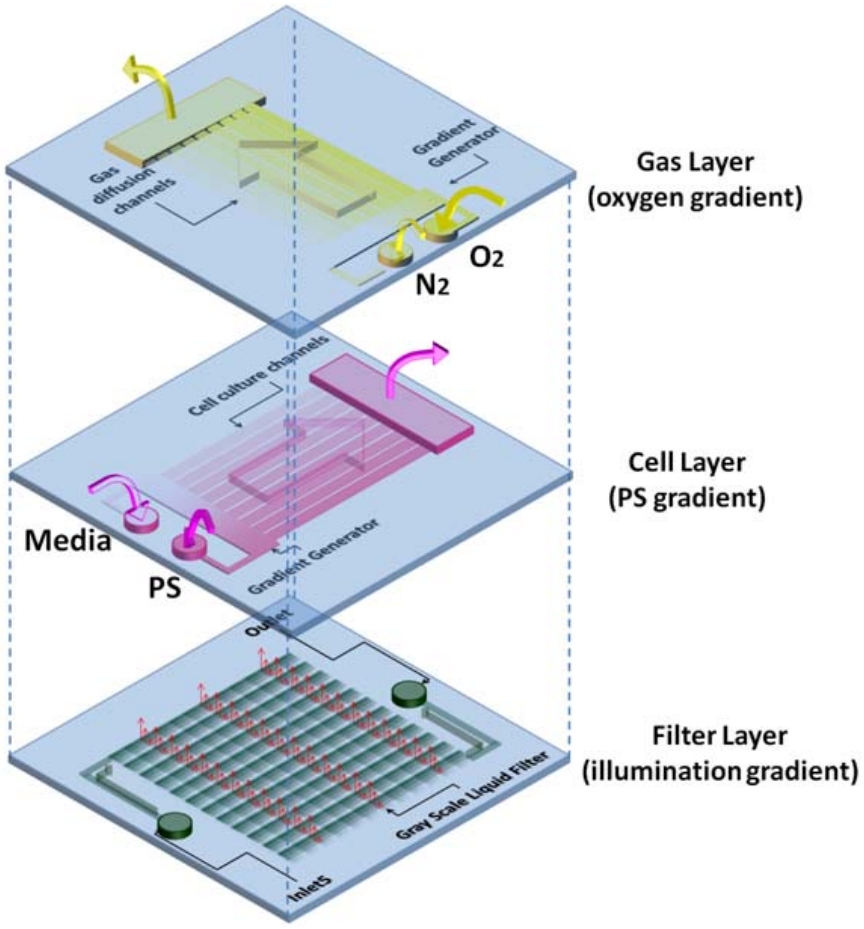


Figure 2.6 Schematic diagram of high-throughput screening scheme combining gradients of oxygen, drug and illumination intensity.

## 2.2 Adaptable configurations for different therapeutic factors and combinations

Besides the high-throughput PDT efficacy screening capability, another important feature of this platform is its adaptable configuration based on the customers' specific screening interests. First, it is possible to include more therapeutic factors within the

microfluidic platform for PDT efficacy test. Besides photosensitizer concentration, oxygen level and illumination intensity, adding temporal microfluidic controls could also modify the cell incubation time with photosensitizer, the oxygen supply duration, and the illumination duration [12-14]. To mimic the complicated shear stress conditions during drug delivery process in vivo, a microfluidic channel with varying channel widths could generate a shear stress gradient within the physiological dynamic range [15]. Second, while gradients of all various therapeutic factors can be combined together in one chip and one test to maximize the throughput; simpler version chips, for example including only one or two PDMS layers and focusing only on one or two therapeutic factor, could simplify test protocols but still provide required PDT efficiency results. Third, while maintaining the basic principle of each microfluidic layer controls one of the three basic PDT elements (drug, oxygen and light), actual microfluidic channel designs could be modified to fit the requirements of different in vitro cell models (2D monolayers or 3D spheroids) and photosensitizer types. In other words, such microfluidic platforms can be adapted in chip design and operation protocol to fit the requirement of different PDT efficacy evaluations.

Figure 2.7 shows several simplified versions of our microfluidic chips with different major configuration rearrangements emphasizing on different therapeutic factors:

(a) Shows the basic single layer scheme for PDT efficacy test with photosensitizer concentration gradient, incubation time gradient or the combination of both. A photosensitizer concentration gradient is generated through the gradient generator and fed into individual cell culture channels. The incubation time gradient is generated through a controlled slow feeding of the photosensitizer samples from

the inlets. As the drug solution is gradually filling the cell culture channel, it reaches the cells in upstream area (closer to inlets) earlier than cells in the downstream area (further to inlets). Two kinds of photosensitizers have been tested here: Methylene blue free dye and functionalized nanoparticles. For the test with nanoparticles, total flow resistance through the chip is increased to around 2 times larger than that for free dye test, in order to help decrease the flow rate and ensure a sufficient NP mixing in the gradient generator. For the test with incubation time gradient, total volume of the cell culture channels is increased around 4 times to allow for a step-by-step slow flow through the channels. Microfluidic chips of this scheme are exposed to same atmosphere (21% oxygen) condition and uniform illumination intensity during the PDT test.

(b) Shows the basic double layer scheme for the PDT efficacy test with oxygen concentration gradient, or the combination of oxygen and photosensitizer concentration gradients. Microfluidic chips of this scheme are exposed to same illumination intensity over the whole chip during the PDT test.

(c) Shows the basic double layer scheme for the PDT efficacy test with illumination intensity gradient. Instead of cell culture channel, cell layer is made with a 6mm diameter open chamber, facilitating cell loading and culture. Microfluidic chips of this scheme are e exposed to a same atmosphere (21% oxygen) condition and photosensitizer concentration over the whole chip.

(d) Shows the basic single layer scheme for the parallel PDT efficacy tests with different cell types. Different cell lines are cultured in individual culture channels with its own kind of cell culture media. And during the PDT test, a same

photosensitizer solution is added to all cell lines. A same microfluidic chip can be used for parallel PDT efficacy tests with different photosensitizers on a same cell line too, for which case all channels would be fed with a same type of cell line but different photosensitizers during the PDT test.

While in Figure 2.7 we only show some chip schemes we have used during the development of this platform, other chip schemes depending on other interesting therapeutic factor combinations are also feasible. For example, the multiple cell type screening scheme can be combined with the oxygen gradient generator or gray scale filter. Also photosensitizer gradient screening scheme can be expanded to multiple cell types. Both of them could provide more detailed comparisons of PDT efficacy profile changes among different cancer types based on a single test run of one microfluidic chip.

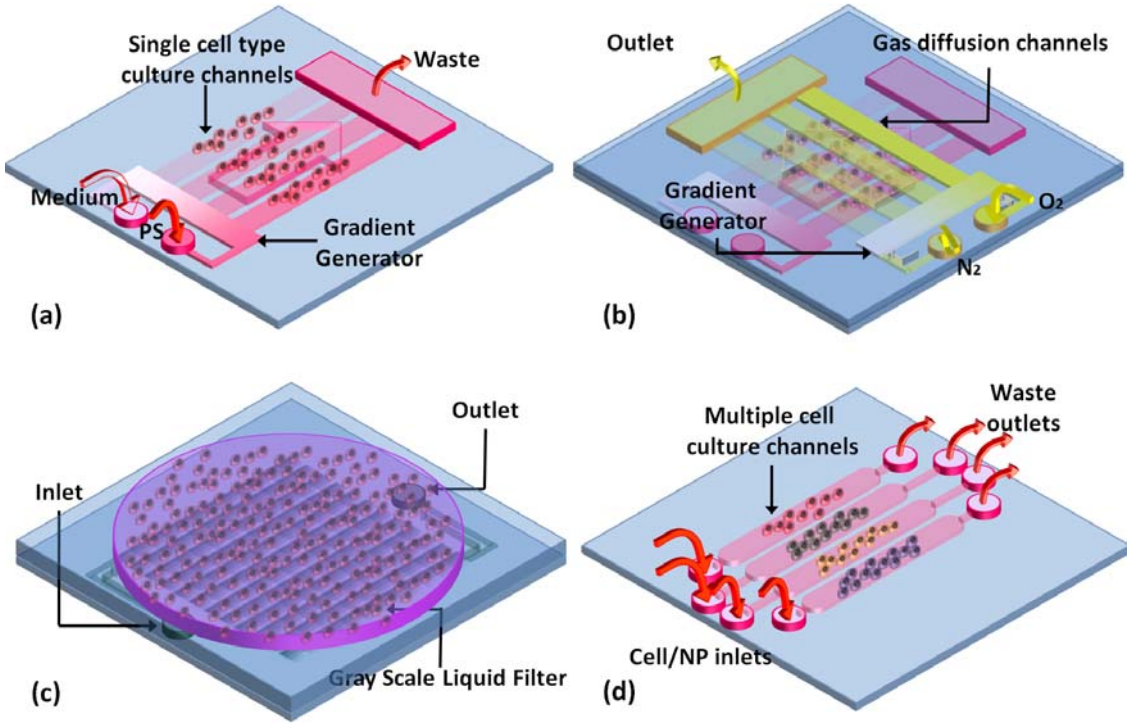


Figure 2.7 Schematic diagrams of microfluidic chip configurations for different therapeutic factors including (a) photosensitizer concentration, incubation time, (b) oxygen concentration, (c) illumination intensity, (d) cell types.

Besides major configuration changes, structural modification of the minimum cell culture unit could expand our capability of evaluating new therapeutic factors or in vitro cell models too. Figure 2.8 shows the comparison among an original basic culture chamber, a chamber with shear stress gradient, and a chamber for 3D cancer spheroid formation. While all units are having a cubic outer shape suitable for large array expansion and assembly with gas layer and filter layer, their interior structures vary a bit. The original cell culture chamber is a simple segment of rectangle microfluidic channel for uniform cell loading and photosensitizer delivery. The culture chamber with shear stress gradient is having a progressively increasing channel width, which in result generates a decreasing flow velocity and shear stress on bottom substrate's cells. The culture chamber for 3D spheroid formation includes a cell culture well beneath the cell loading channel and allows cells to settle down and aggregate into a spheroid [16-18]. The original glass substrate is blocked from the cells with a thin layer of PDMS, which can effectively avoid cell attachment during cell culturing.

Such modified cell culture units are compatible with our major platform scheme for array expansion and triple layers stacking to include multiple therapeutic factors controls. Figure 2.9 shows an example of microfluidic chip development from a single culture chamber unit prototype to a final triple layer chip with dynamic control of 6 therapeutic factors. The starting unit chamber provides self-generation of shear stress gradient via a changing channel width, which in turn a changing flow resistance. First, the basic cell culture unit in (a) is expanded into a 9 by 9 array. With added gradient generator and controlled photosensitizer feeding, two more therapeutic factors of photosensitizer concentration and incubation time can be included within a same single cell layer scheme

as shown in (b). Then a second gas layer is added on top, imposing oxygen concentration gradient as shown in (c). A final filter layer brings in the illumination intensity and time gradients as shown in (d). Each time adding a new therapeutic factor control with its gradient, the previous chip is expanded with additional identical duplicates. Apparently, same high-throughput expansion strategy can be applied to a 3D spheroid culture chamber unit, too.

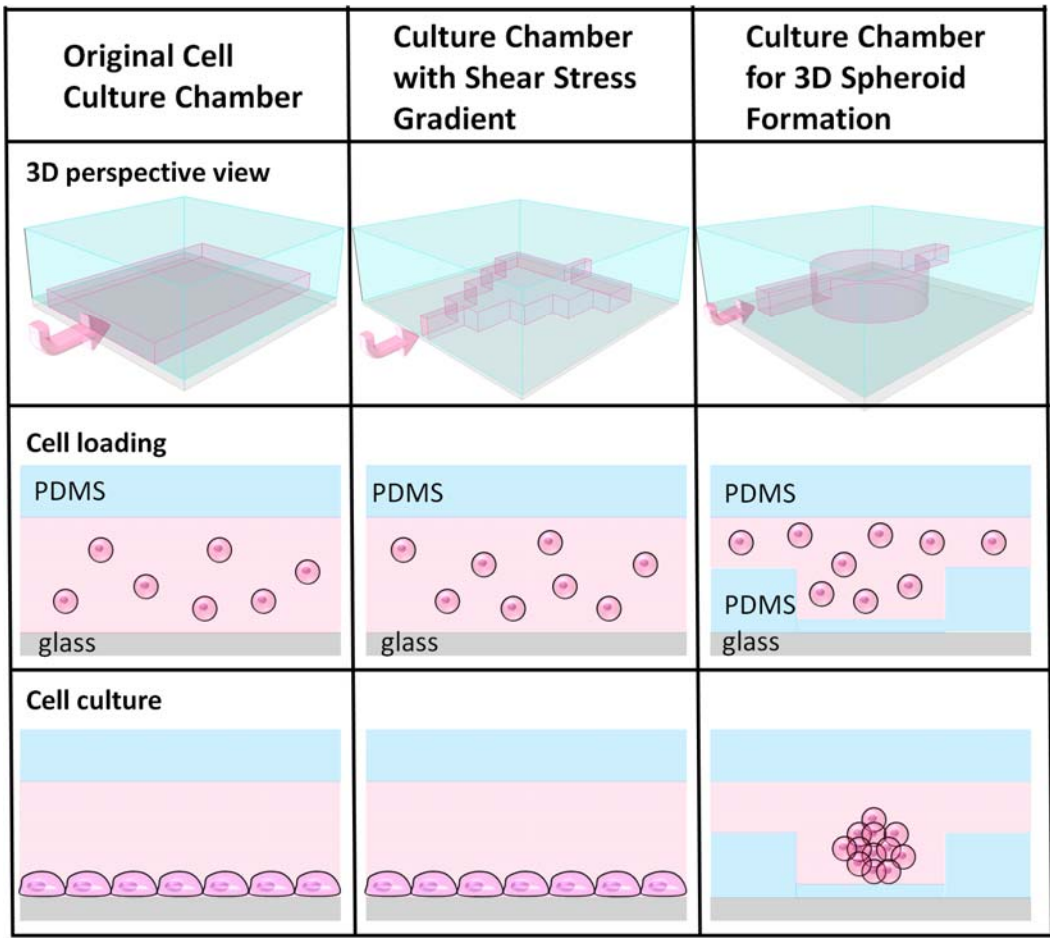


Figure 2.8 Schematic comparison among different versions of cell culture unit. The first row shows the 3D perspective view of each cell culture chamber. Arrows indicate the flow direction for sample loading. The second row shows the cross-section view of each unit and the cell distribution right after sample loading. The third row shows the cell distribution after cells are cultured for a certain period, forming either a monolayer attached to the substrate or a suspending spheroid.

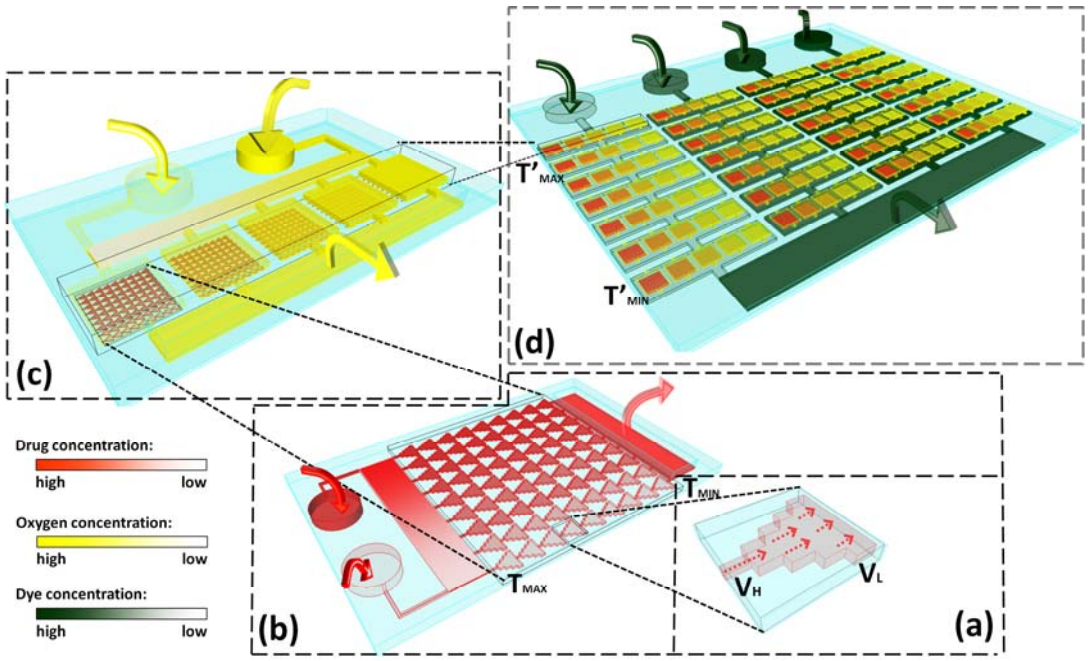


Figure 2.9 Schematic diagram of microfluidic chip development from a single cell culture unit to a final triple layer chip. (a) A single microfluidic channel with expanding width and reducing flow rate/shear stress. (b) A single-layer PDMS chip providing gradients of three therapeutic factors: drug concentration, flow rate, and incubation time (T). (c) A gas layer is added on top of the previous micro chamber array to provide an oxygen gradient (yellow) in the orthogonal direction. (d) A filter layer is added below the previous microfluidic prototype to provide a light intensity gradient and an exposure time (T') gradient. As a result, at the final stage there would be six therapeutic factors involved in a full combination for the high-throughput PDT efficacy screening.

## 2.3 Device fabrication

In our design we use PDMS as the structural material and a glass cover as the major substrate. Different thicknesses of SU8 (Microchem) are fabricated as replication molds for each layer. For gas layer, a single thickness of 33um SU8 2010 is used. For cell layer, the cell culture channel area is having a thickness of around 110um fabricated with SU8 2050, and the rest area is having a thickness of 33um fabricated with SU8 2010. For filter layer, using triple spin coatings, SU8 2010 patterns with three thicknesses of 13, 28,

43um are fabricated. Before PDMS replication, each mold is first coated with a thin layer of Trichloro(1H,1H,2H,2H-perfluorooctyl)silane (Sigma-Aldrich) facilitating PDMS peeling off.

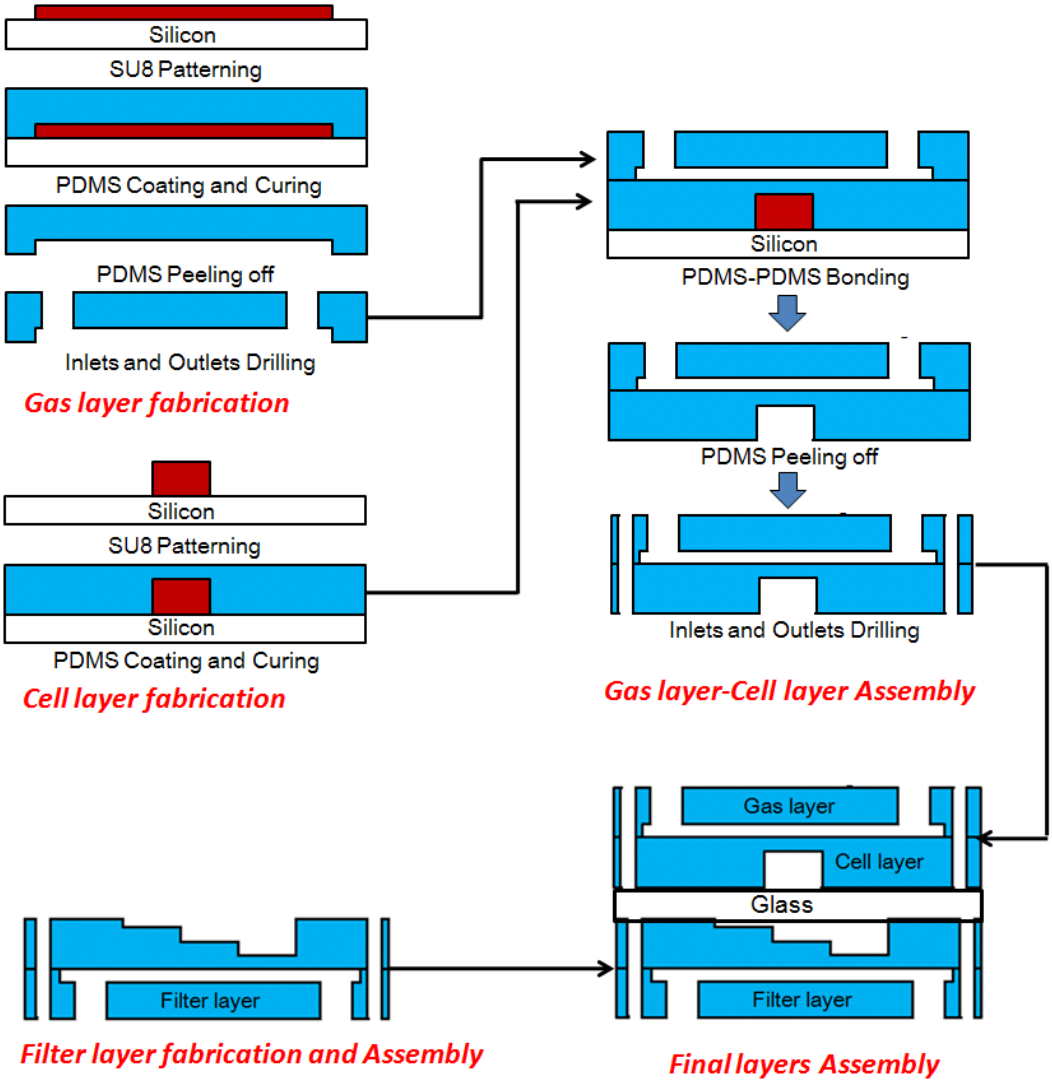


Figure 2.10 Fabrication process of the proposed triple layer PDMS microfluidic chip for PDT efficacy screening.

Figure 2.10 shows the detailed process of PDMS layers' assembly. Before each bonding process, PDMS/glass surface is cleaned with IPA and DI water, and pretreated with oxygen plasma (200 torr, 50W, 30s). After each bonding, the bonded structure is further baked at 95℃ for 30min to enhance the bonding strength. For the whole assembly

process, first, the gas layer (~3mm thick) is peeled off and has inlet/outlet drilled with a needle or biopsy punch. Then it is aligned and bonded to the cell layer, which is spin-coated on the SU8 mold with 1500rpm and cured reaching a membrane thickness around 70um. Then the two layers are peeled off together and have cell layer connections drilled. The filter layer is composed of two PDMS layers fabricated in a same way. After that, all the three layers are bonded to a 100um thick glass cover back and front, realizing the final assembly.

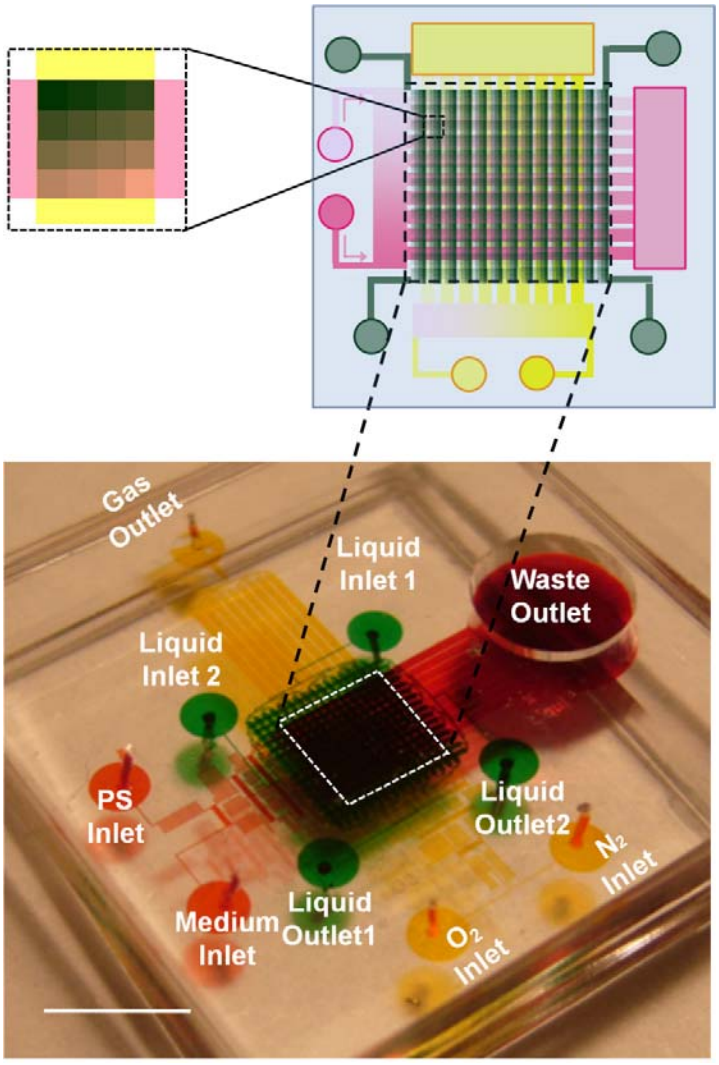


Figure 2.11 Image of a fabricated triple-layer PDT chip and the corresponding schematic showing the overlapping of the three layers from the top. For both, each layer

is labeled with different colors (yellow for the gas layer, red for the cell layer and green for the filter layer). Scale bar: 5mm.

Figure 2.11 demonstrates a typical fabricated triple layer chip filled with different color of food dyes in each layer (yellow for the gas layer, red for the cell layer and green for the filter layer). The central overlapping area of all three layers is the active PDT efficacy test region (encircled with white dash lines), which is around 5mm by 5mm. The schematic drawing on the upper part of Figure 2.11 provides a top view of the device showing how the three layers are aligned and overlapped, with a same specific color for each layer as in the image below. The enlarged section shows one overlapping section of a specific photosensitizer concentration and a specific oxygen level. For each of such sections, the liquid filter generates a same gray-scale illumination pattern of 16 levels, as we described earlier in this chapter.

While fabrication processes of different version chips are all based on multi-layer soft-lithography, their details may slightly vary with each other, including the number of assembling PDMS layers, microfluidic channel heights, PDMS thicknesses, or bonding sequences. One example with distinctive difference is the cell culture layer for 3D spheroids culturing, which is having two PDMS sub-layers instead of one for 2D monolayer culturing as show in Figure 2.12. The SU8 mold is fabricated via two times' photolithography, with one thickness of 50um for cell loading channels and another thickness of 300um for the microwells culturing the cell spheroids inside. Top PDMS is of no microfluidic pattern and around 3mm thick. Bottom PDMS layer is replicated from the SU8 mold and around 1mm thick. Two PDMS layers are bonded together face-to-face

and punched through holes as the inlet and the outlet. After that, it is bonded to a 100um thick glass slide as a rigid substrate support.

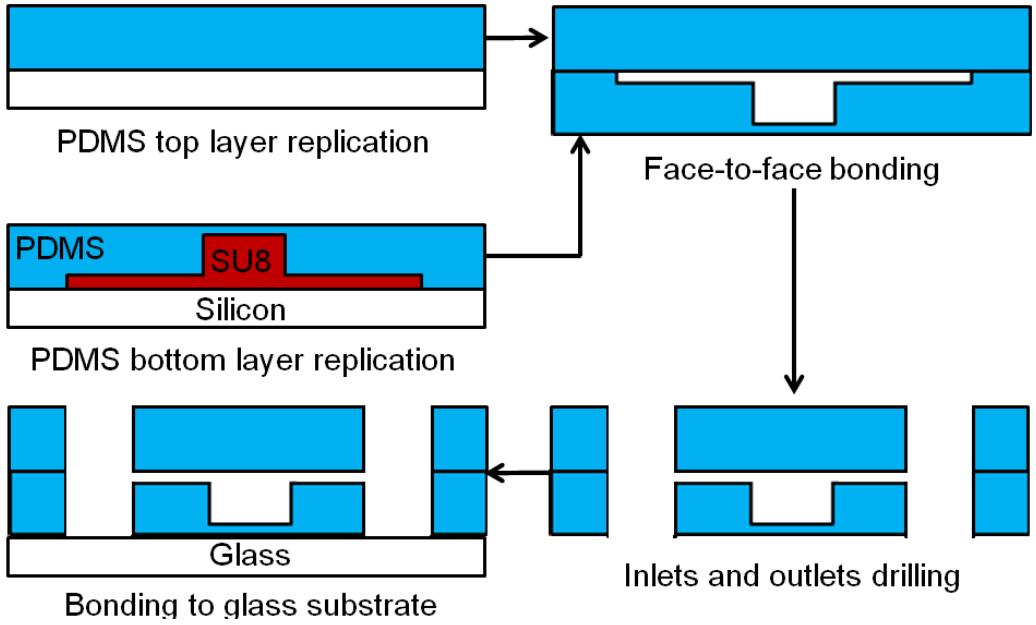


Figure 2.12 Fabrication process of the cell layer for 3D spheroids culturing in PDT efficacy test.

As we mentioned previously, this kind of 3D spheroid culturing unit is totally compatible for high-throughput expansion. Figure 2.13 shows an example of microfluidic chip with the expanded spheroid culture array for high-throughput PDT test. This is a single cell layer chip including an eight by eight chamber array for spheroids culture. This scheme with eight parallel cell culture channels is compatible with our previous photosensitizer gradient generator, which means each channel could have a distinctive photosensitizer concentration. Along each cell culture channel, there are eight microwells with different diameters ranging from 160 to 440um. With these varying sizes of cell culture microwells one extra therapeutic factor of 3D spheroid size is brought in, which is a basic parameter for 3D Multicellular Spheroid (MCS) model and directly affects PDT efficacy [19]. The final size of spheroid formed in each chamber is determined by the

microwell size (the maximum number of cells it can contain) and the cell loading protocol (the initial number of cells in it), both of which are discussed in more details in the 4th chapter.

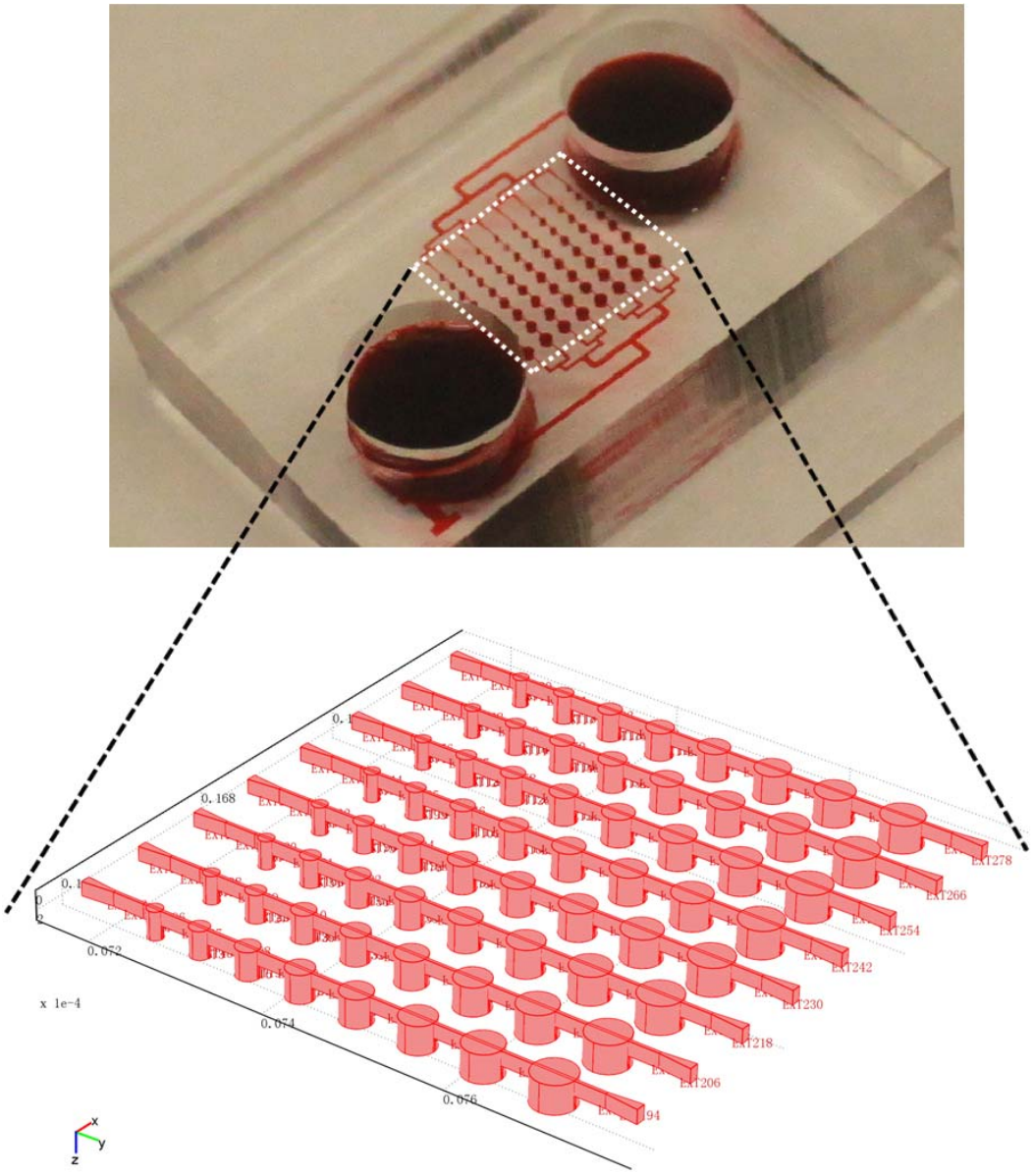


Figure 2.13 Image of a red dye filled single layer chip for high throughput PDT efficacy assay using multicellular spheroids. The enlarged part shows the scheme of microwell array.

## Chapter 2 References


[1] L. Hyung-Kew, *et al.*, "A Flexible Polymer Tactile Sensor: Fabrication and Modular Expandability for Large Area Deployment," *Microelectromechanical Systems, Journal of,* vol. 15, pp. 1681-1686, 2006.

[2] M. A. Unger, *et al.*, "Monolithic Microfabricated Valves and Pumps by Multilayer Soft Lithography," *Science,* vol. 288, pp. 113-116, April 7, 2000 2000.

[3] M. L. Sin, *et al.*, "System Integration - A Major Step toward Lab on a Chip," *J Biol Eng,* vol. 5, p. 6, 2011.

[4] K. Campbell and A. Groisman, "Generation of complex concentration profiles in microchannels in a logarithmically small number of steps," *Lab on a Chip,* vol. 7, pp. 264-272, 2007.

[5] J. Chung, *et al.*, "Clonal Culture and Chemodrug Assay of Heterogeneous Cells (PC3 Prostate Carcinoma Cells) Using Microfluidic Single Cell Array Chips," presented at the International Conference on Miniaturized Systems for Chemistry and Life Sciences (μTAS'09), 2009.

[6] W. B. Du, *et al.*, "High-throughput nanoliter sample introduction microfluidic chip-based flow injection analysis system with gravity-driven flows," *Anal Chem,* vol. 77, pp. 1330-7, Mar 1 2005.

[7] P. J. Lee, *et al.*, "Microfluidic System for Automated Cell-Based Assays," *Journal of the Association for Laboratory Automation,* vol. 12, pp. 363-367, December 1, 2007 2007.

[8] M. Polinkovsky, *et al.*, "Fine temporal control of the medium gas content and acidity and on-chip generation of series of oxygen concentrations for cell cultures," *Lab Chip,* vol. 9, pp. 1073-84, Apr 21 2009.

[9] Y.-A. Chen, *et al.*, "Generation of oxygen gradients in microfluidic devices for cell culture using spatially confined chemical reactions," *Lab on a Chip,* vol. 11, pp. 3626-3633, 2011.

[10] M. Adler, *et al.*, "Generation of oxygen gradients with arbitrary shapes in a microfluidic device," *Lab Chip,* vol. 10, pp. 388-91, Feb 7 2010.

[11] C. Chen, *et al.*, "Gray-scale photolithography using microfluidic photomasks," *Proceedings of the National Academy of Sciences,* vol. 100, pp. 1499-1504, February 18, 2003 2003.

[12] J. Melin and S. R. Quake, "Microfluidic large-scale integration: the evolution of design rules for biological automation," *Annu Rev Biophys Biomol Struct,* vol. 36, pp. 213-31, 2007.

[13] A. R. Wheeler, *et al.*, "Microfluidic Device for Single-Cell Analysis," *Analytical Chemistry,* vol. 75, pp. 3581-3586, 2003/07/01 2003.

[14] B. G. Chung and J. Choo, "Microfluidic gradient platforms for controlling cellular behavior," *ELECTROPHORESIS,* vol. 31, pp. 3014-3027, 2010.

[15] L. Wang, *et al.*, "Patterning cells and shear flow conditions: Convenient observation of endothelial cell remoulding, enhanced production of angiogenesis factors and drug response," *Lab on a Chip,* vol. 11, pp. 4235-4240, 2011.

[16] S. Agastin, *et al.*, "Continuously perfused microbubble array for 3D tumor spheroid model," *Biomicrofluidics,* vol. 5, Jun 2011.

[17] C. Kim, *et al.*, "3-Dimensional cell culture for on-chip differentiation of stem cells in embryoid body," *Lab Chip,* vol. 11, pp. 874-82, Mar 7 2011.
[18] Y. C. Xu, *et al.*, "Rapid fabrication of a microdevice with concave microwells and its application in embryoid body formation," *Biomicrofluidics,* vol. 6, Mar 2012.
[19] C. M. West, "Size-dependent resistance of human tumour spheroids to photodynamic treatment," *Br J Cancer,* vol. 4, pp. 510-514, 1989.

# CHAPTER 3 THEAPEUTIC FACTORS CONTROL AND MEASUREMENT ON CHIP

As described in previous chapters, our platform features in the capability of controlling various therapeutic factors including photosensitizer concentration, oxygen concentration, illumination intensity/dose, incubation time, and flow shear stress. Combining that with PDT efficacy test on chip, we are able to get the cell viability response of all these therapeutic factors. One essential step before doing actual PDT efficacy tests on chip is to characterize our platform first in terms of these therapeutic factors' gradient generations and distributions in chip. In this way, not only we can verify the capability of gradient generation of different therapeutic factors, but also it saves us time in future PDT tests, during which this kind of therapeutic factor level measurement would be either time consuming or even impossible to carry out. In particular, it is necessary to:

- ✧ Estimate therapeutic factor levels and distributions using mathematical modeling and numerical simulations during the microfluidic chip design (described in this chapter)
- ✧ Directly measure the therapeutic factor levels in microfluidic chips in um scale , which fits the dimension of cell microenvironment (described in this chapter)
- ✧ Discuss the principle of each therapeutic factor's gradient generation and its potential in expanding the dynamic range and improving the resolution (described in this chapter)

- ✧ Develop PDT efficacy test protocols which can reliably inherit the measured therapeutic factor levels during this pre-characterization (described in next chapter)

This chapter describes the principles, methodologies and results of on-chip gradient generations of different therapeutic factors.

### 3.1 Photosensitizer gradient generation and measurement

Two types of photosensitizers have been adopted for PDT efficacy tests using this platform. One is Methylene Blue (MB) free dye and the other is functionalized nanoparticles (NPs). Fluorescein isothiocyanate (FITC, Sigma-Aldrich) solution is used to estimate the Methylene Blue concentration distribution within the microfluidic chip. FITC is having a similar molecular mass (389) with Methylene Blue (320) and thus could properly anticipate MB's behavior in gradient generator [1, 2]. For the nanoparticles, FITC is incorporated inside to make them fluorescence-visible. The local concentration of FITC/nanoparticles within the microfluidic chip is evaluated by measuring the local fluorescence intensity. Within a low concentration range, fluorophore's fluorescence intensity increases proportionally with its concentration [2]. We verified this assumption with FITC (up to 1000ppm) solution and NP (up to 1mg/ml) solution within the microfluidic chip. Pre-known FITC/NP concentration solutions are prepared by serial dilution and loaded into same 33um-high microfluidic channels, and the measured fluorescence intensities shows a proportional increase with the concentration.

Fluorescence images are taken with an inverted fluorescence microscope (Nikon ECLIPSE TE2000-U) equipped with a cooled digital CCD camera (Photometrics, CoolSNAP ES), and the corresponding filter set (FITC HYQ). The microfluidic chip is

mounted on the microscope stage and focused on the microfluidic channels containing the FITC/NP solutions. To avoid saturation on CCD sensor, image acquiring time is restricted so that the maximum gray value of the fluorescence image is below 2500. Fluorescence images are preprocessed in two steps before adopted for measuring the fluorescence intensity values. First, the background corresponding to no fluorescence emission is subtracted from the image. Second, the image is normalized with a standard image of a uniformly fluorescent background, which helps compensate for non-uniformity of excitation illumination and emission imaging on CCD sensor. The gray values of the fluorescent image are measured and plotted with ImageJ software.

Photosensitizer gradient generation and measurement are carried out with a single cell layer chip, which is having the same configuration as part of a triple layer chip. One chip with 9 cell culture channels (9 levels of concentrations) is used for FITC gradient generation test, and another with 13 cell culture channels (13 levels of concentrations) is used for NP gradient generation test. Chips are necessarily prefilled with DMEM (Gibco) to remove any residual gas within the chip before fed with the fluorescent samples. First, chips are left in a desiccator and vacuumed for 1h. Then, the chip's outlet reservoir is filled with DMEM. Using a syringe, a negative pressure is applied at the inlet to suck in the DMEM and fill it the whole chip. After removing the negative pressure, the chip is left in atmosphere for 10mins allowing the residual bubbles within the chip varnish and make it ready for test. For the FITC gradient generation test, 1000ppm FITC in DMEM and pure DMEM are simultaneously introduced into the chip using syringe pumps at a same injection rate of 1ul/min. Fluorescence images are taken after 10minutes when FITC concentration distribution reaches stabilization within the whole chip. For the NP

gradient generation test, 1mg/ml PAA NPs in DMEM and pure DMEM are introduced into the chip using the gravity flow setup, as shown in Figure 3.1. Two identical needles filled with test samples are inserted into the inlets, providing two elevated reservoirs. A pressure difference of around 200Pa drives in-chip flows from inlets towards the outlet. Fluorescence images are taken after a same 10min which is sufficient for reaching a stable concentration profile within the gradient generator and the starting part of cell culture channels.

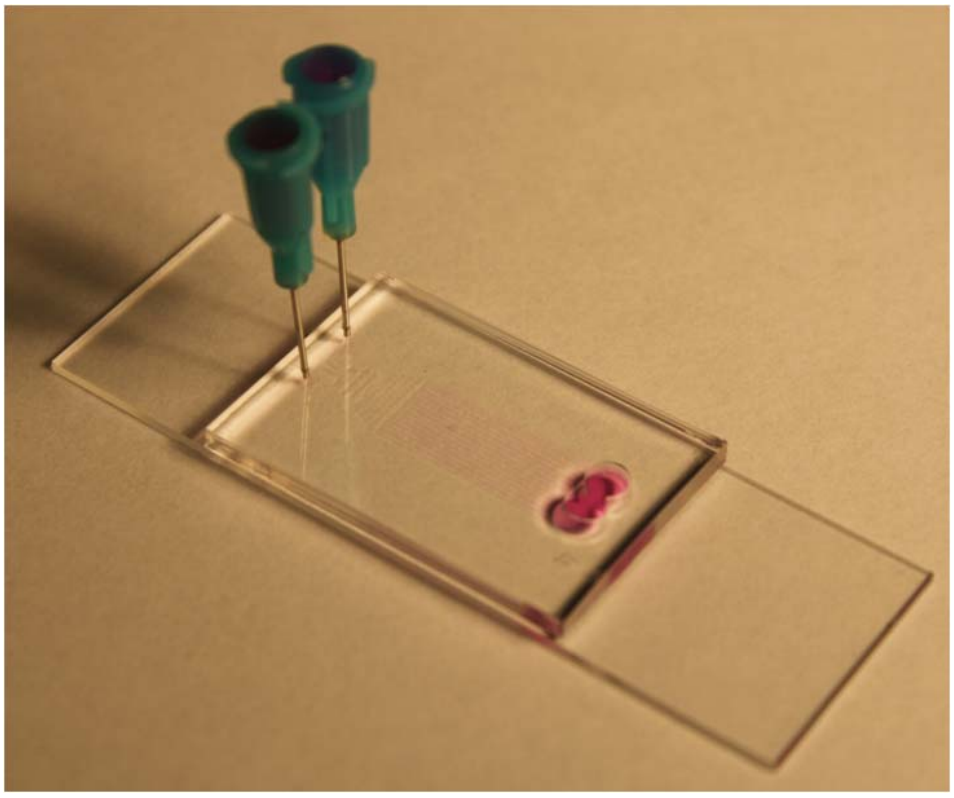

Figure 3.1 The gravity flow setup provides a 200 Pa pressure difference between inlets and the outlet.

Figure 3.2 shows the fluorescence image of FITC gradient generation in chip covering the area of gradient generator and starting part of cell culture channels. Based on the gray scale patterns displayed by the image, FITC solution flow with one concentration splits in the vertical channel, rejoins, and mixes with another concentration

flow in the serpentine channel. This kind of process repeats in each stage of the gradient generator and contributes to the final output of 9 levels of FITC concentration. The actual grayscale values indicating FITC concentration are measured along the dash line and plotted in Figure 3.2(b). Within each channel, FITC maintains a constant concentration but among the 9 channels, FITC concentrations are different and showing an overall linearly increasing profile as designed.

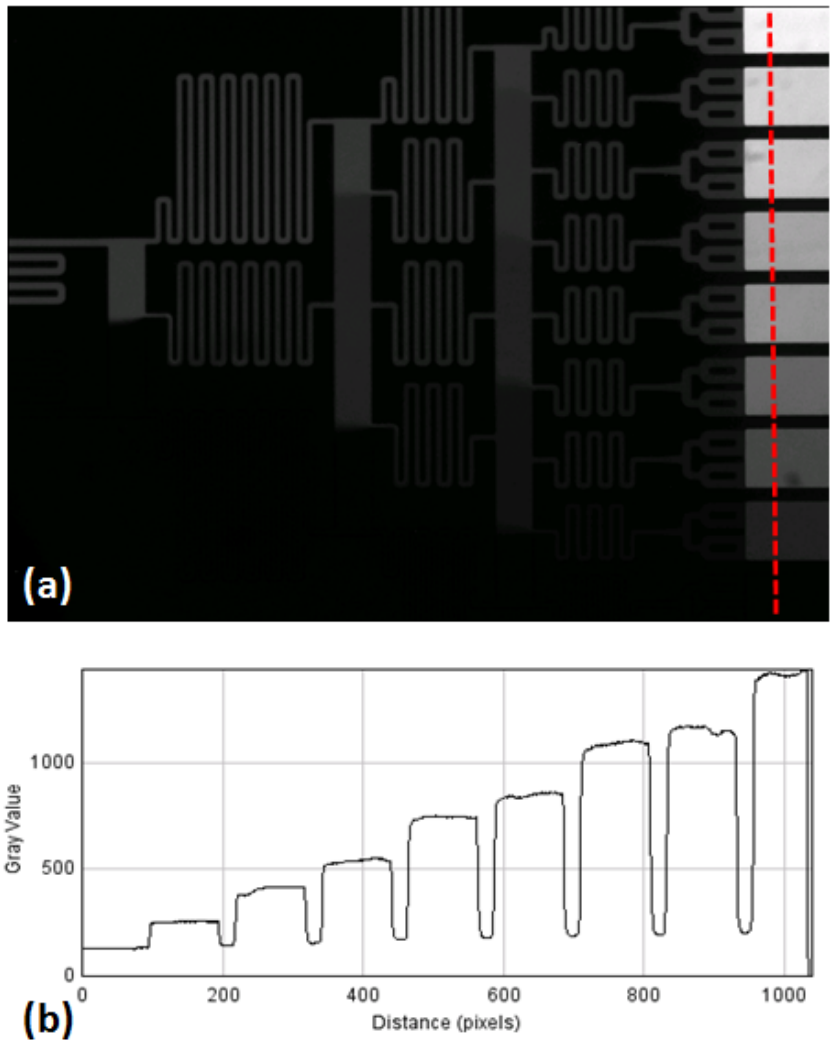


Figure 3.2 (a) Fluorescence image of the gradient generator providing 9 levels of FITC concentrations for the 9 cell culture channels. (b) Fluorescence intensity profile measured along the red dash line.

Figure 3.3 shows the fluorescence image of NP gradient generation in chip covering the latter part of the gradient generator and the starting area of cell culture channels. Photosensitizer concentration levels are increased from 9 to 13 by adding more microfluidic stages in gradient generator. NP concentrations are measured along the white dash line and showing a similar linear profile with previousb FITC result.

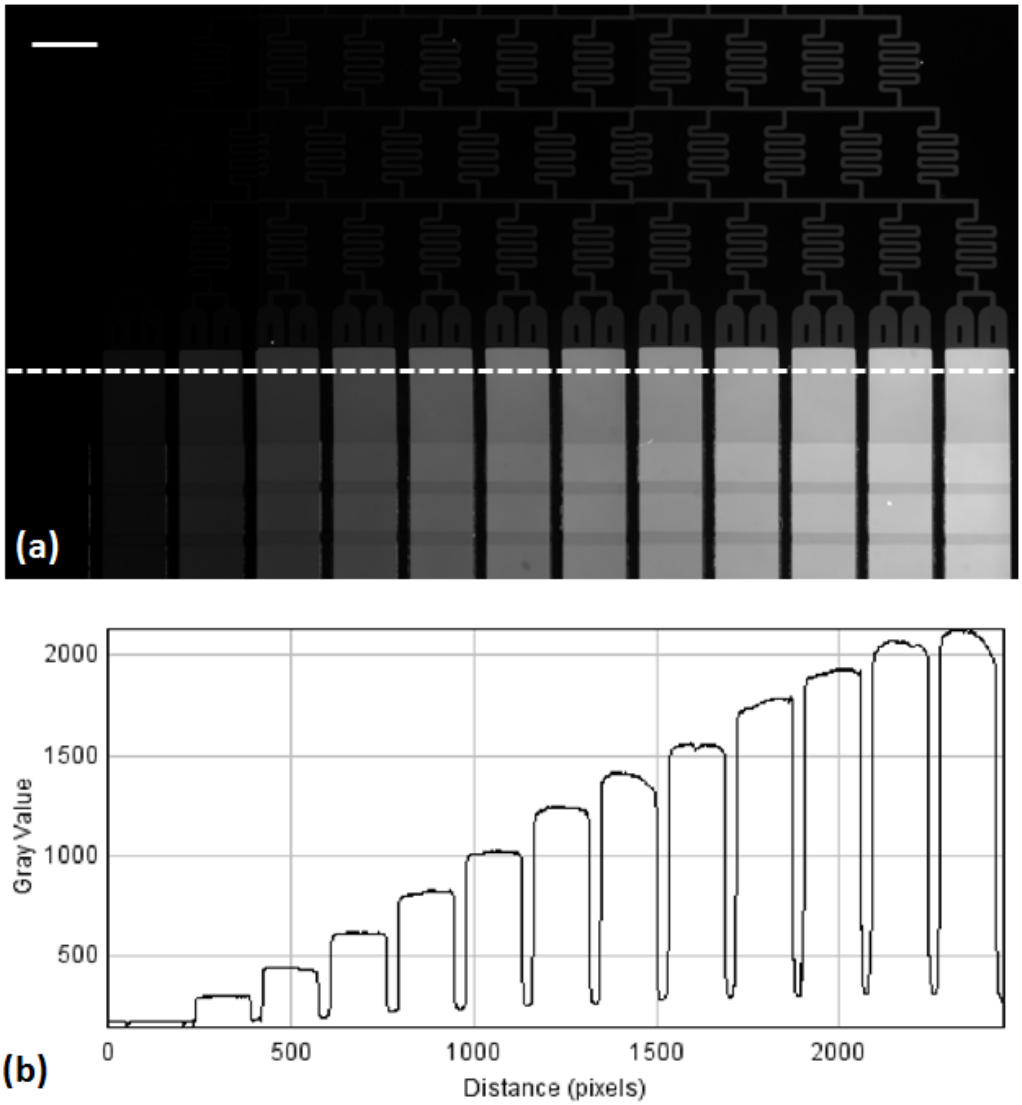


Figure 3.3 (a) Fluorescence images of the 13 levels of NP concentration gradient generation. Extra stages are added to gradient generator to provide more concentration levels. Scale bar: 480um. (b) Fluorescence intensity measurement result along the white dash line, shows the NP concentration changes among different cell culture channels.

There are two key aspects for the gradient generator described here to work properly. One is neat flow dividing and rejoining in the vertical channels, so that the two injected flows with different concentrations can be combined together but not thoroughly mixed into a uniform concentration before entering the next stage's serpentine channel. As we can see from the previous results, the vertical channels are designed short enough to limit the mixing. And the other is the sufficient mixing within the serpentine channel, which provides a uniform concentration flow output for the next stage. In case of microfluidic laminar flows, this kind of mixing is majorly realized by diffusion. The diffusion distance can be estimated with:

$$x \approx \sqrt{4Dt}$$

, in which x is the diffusion distance, D is the diffusion coefficient and t is the diffusion time. With a given channel width, sufficient mixing is affected by the photosensitizer's diffusion coefficient and the flow rate (maximum allowing diffusion time within the serpentine channel). Multiple gradient generation tests with different injection flow rates have been carried out with both FITC and NPs. Fluorescence intensity profiles along the cross section of the serpentine mixing channels are measured. With a uniform concentration distribution resulted from sufficient mixing, the fluorescence profile along the channel cross-section becomes symmetric near the serpentine channel output. As shown in Figure 3.4, under a high injection flow rate of 10ul/min, FITC cannot be sufficiently mixed within the channel; while under a low flow rate of 1ul/min, the fluorescence profile reaches symmetric quickly, implying a sufficient mixing and uniform FITC concentration output. Diffusion coefficient can be estimated through:

$$D = (1/6\pi\eta r)kT$$

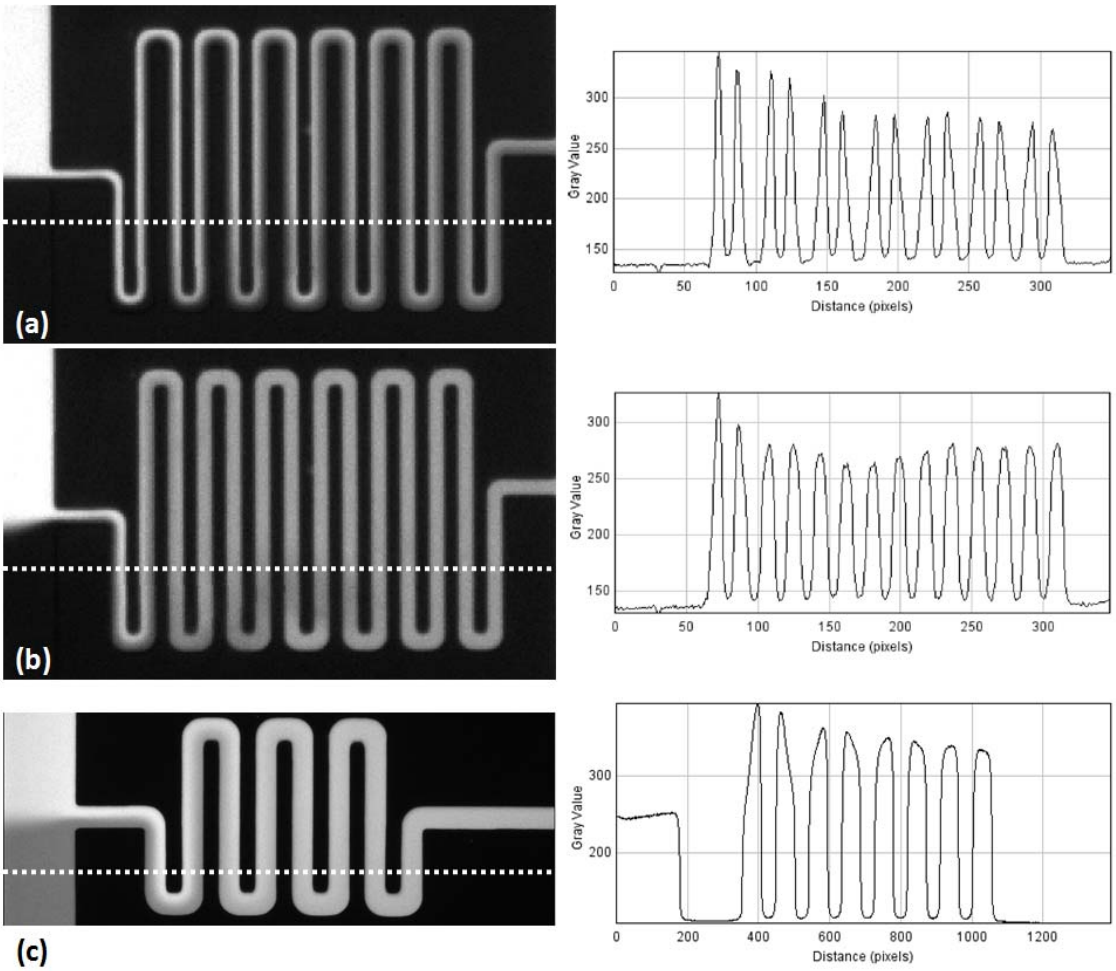


Figure 3.4 (a) Fluorescence image of the FITC solutions mixing in the serpentine channel under a flow rate of 10ul/min. Fluorescence intensity is measured along the white dash line. (b) Fluorescence image of the FITC solutions mixing in the serpentine channel under a flow rate of 1ul/min. Fluorescence intensity is measured along the white dash line. (c) Fluorescence image of the NP solutions mixing in the serpentine channel under a flow rate of 0.06ul/min. Fluorescence intensity is measured along the white dash line.

, where k is the Boltzman constant, T the absolute temperature, η the viscosity and r the radius of sphere. When adopting different kinds of photosensitizers, changes in the photosensitizer size would affect the mixing efficiency. Considering the close molecule mass between FITC (389) and Methylene Blue (320), Methylene Blue can be considered as much or easier to be mixed. However, the functionalized NPs are having a dramatically increased size (~50nm), which means the flow rate need to be reduced to

ensure they would have sufficient time within the serpentine channels to mix. As the results shown in Figure 3.4, under a flow rate as low as 0.06ul/min, NPs could have sufficient mixing and a uniform concentration output.

Two kinds of methods have been adopted for driving solutions flow through the gradient generator. One is the widely used syringe pump and the other is a customized gravity flow setup. Syringe pump is usually considered good at providing constant flow rates, but it is having two limitations considering our application. First, it has a limit of minimum flow rate, which is not small enough to provide a sufficient time for large size photosensitizers mixing, like functionalized NPs. Second, due to the syringe's elasticity, there is a transition time between setting up a new flow rate in panel and the pump actually reaching that rate. In case of PDT tests including both photosensitizer gradient and oxygen gradient, it is necessary to stop the flows in cell layer completely before imposing the oxygen gradient. Using the syringe pump means a long extra time of waiting during this step because it can not realize instant flow stop after it is turned off. Using a gravity flow setup, as shown in Figure 3.1, could help solve these two problems. The pressure difference of the gravity flow setup is estimated as:

$$\Delta p = \rho g \Delta h$$

, in which ρ is the medium density, g the standard gravity and h the height difference between the inlet and outlet. The flow rate in chip is decided by the pressure difference and the flow resistance in chip, which is subjected to design. This setup could provide a flow rate as low as 0.06ul/min, which is sufficient even for mixing the functionalized NPs. Also it can instantly bring the flow rate in chip down to zero, details of which are discussed in the last section of this chapter.

It is important to estimate how long it takes after applying photosensitizer samples to reach a stable photosensitizer distribution over the chip, so that following steps like applying oxygen gradient or PDT illumination can start. In case of the FITC/MB solution refreshing the 9 cell culture channels' chip under a flow rate of 1ul/min, it takes around 1.5min to refresh the whole chip. In case of the NP solution refreshing the 13 cell culture channels' chip using the 200Pa driven gravity flow, it takes around 2hours to refresh the whole chip. The flow rate of NP solution is measured on chip by tracking the NP fluorescence within the chip.

One limitation of this and many other microfluidic gradient generators is that they rely on the continuous flows to maintain the gradient profile. Once inlet flows are stopped, established gradient profile would gradually disappear due to diffusion. However in some PDT tests, like those including oxygen level control, it is essential to keep the flows stopped to impose the oxygen gradient on the testing area. Thus it is necessary to make sure that after stopping the flow and until completing PDT illumination, photosensitizer concentration profile in the active testing area is maintained constant. To verify that, time lapse fluorescence changes within the cell culture channels after stopping gradient generation flows are recorded to estimate how vulnerable they are to diffusion. As shown in Figure 3.5, high concentration FITC started diffusing into the other cell culture channels after the flows stopped, through the gradient generator or the outlet reservoir. But so long the gap between the PDT test area and the gradient generator or output reservoir is large enough (around 3mm here), constant photosensitizer concentrations can be maintained for more than 40mins within the PDT test area (including 10mins for imposing oxygen gradient and 30mins for PDT illumination). The

gap size can be further increased if necessary. Another final alternative design solution would be adding microfluidic valves at both ends of the active test area, which although might make the chip and test protocol more complex [3].

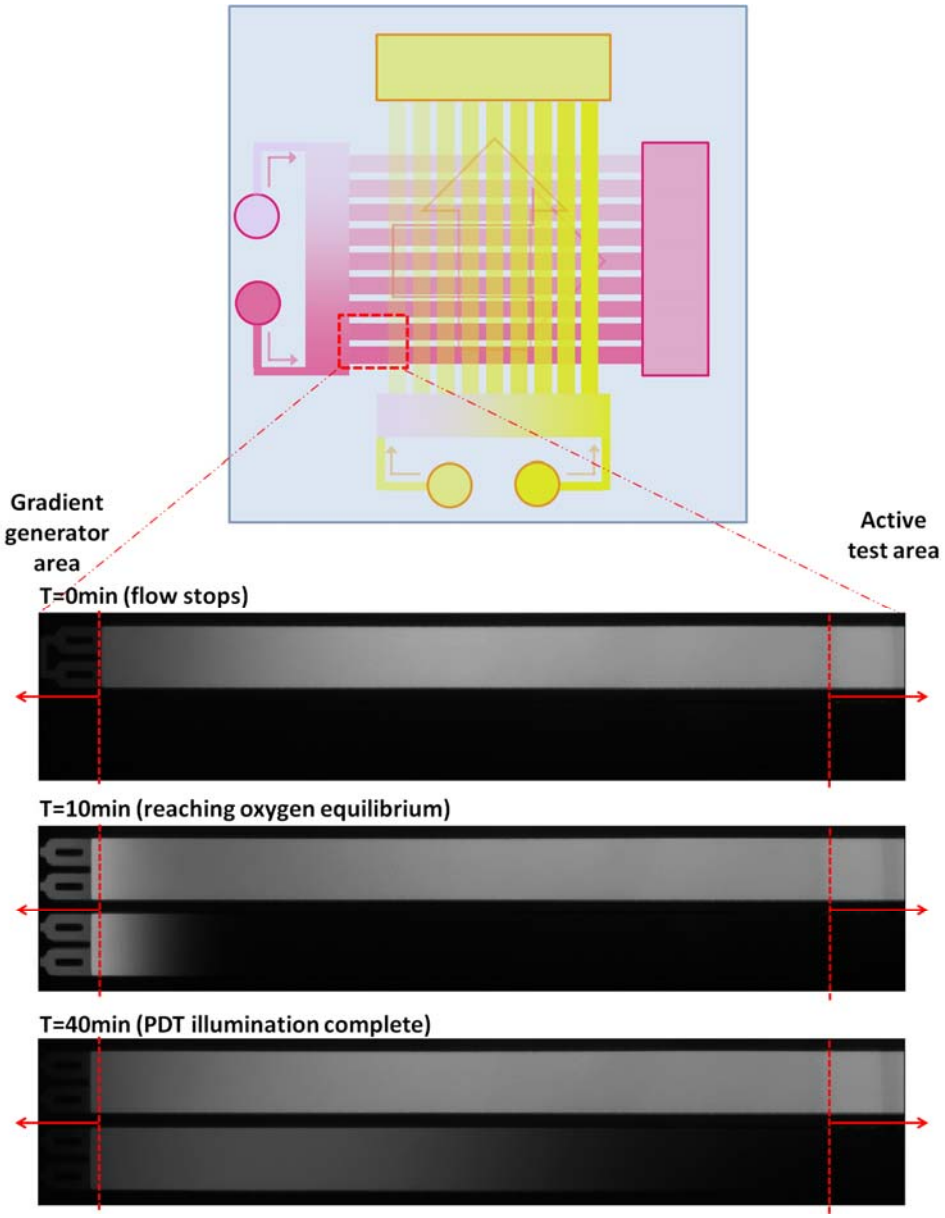


Figure 3.5 Time lapse recording of the diffusion phenomenon among cell culture channels after stopping the gradient generation flows. Low FITC concentration channel is gradually "invaded" by high FITC concentration solution, but the concentration at the active PDT test area remains constant during the whole test period (40mins).

### 3.2 Oxygen gradient generation and measurement

As we mentioned earlier, oxygen gradient generation is realized in chip using a similar gradient generator for photosensitizer gradient generation. The gas flows are driven by a pressure difference between the inlets and outlet. Figure 3.6 shows the scheme of gas supply setup. To provide a single oxygen level (either oxygen depletion or 21% oxygen as in atmosphere) throughout the whole chip, either nitrogen or compressed air is supplied to chip. To provide an oxygen gradient, both of them are supplied to chip with a same supply pressure (5psi) at chip inlets. To estimate the gas pressure distribution through the whole system, flow resistance of each segment is calculated by either:

$$R = \frac{8\eta L}{\pi a^4}$$

or:

$$R = \frac{12\eta L}{H^3(W - 0.6H)}$$

, where $\eta$ is viscosity, L is channel length, a is cylindrical channel radius, W and H are rectangle channel width and height [4-6]. As the calculation result shows, $R_g$ is around 5000 times larger than $R_t$ and $R_c$. As a result, the overall pressure drop of 5 psi would be almost all over the oxygen gradient generator. Pressure drop over Tygon tubing is neglected and the read out values of $P_r$ from the gas regulator are directly adopted as the boundary conditions at gas layer inlets in the following simulation. As another result of that, the pressure drop over gas diffusion channels is also negligible and the microfluidic dimension changes of this active PDT test area would not likely affect the oxygen gradient generation, which makes further platform expansions including oxygen level controls simpler in design.

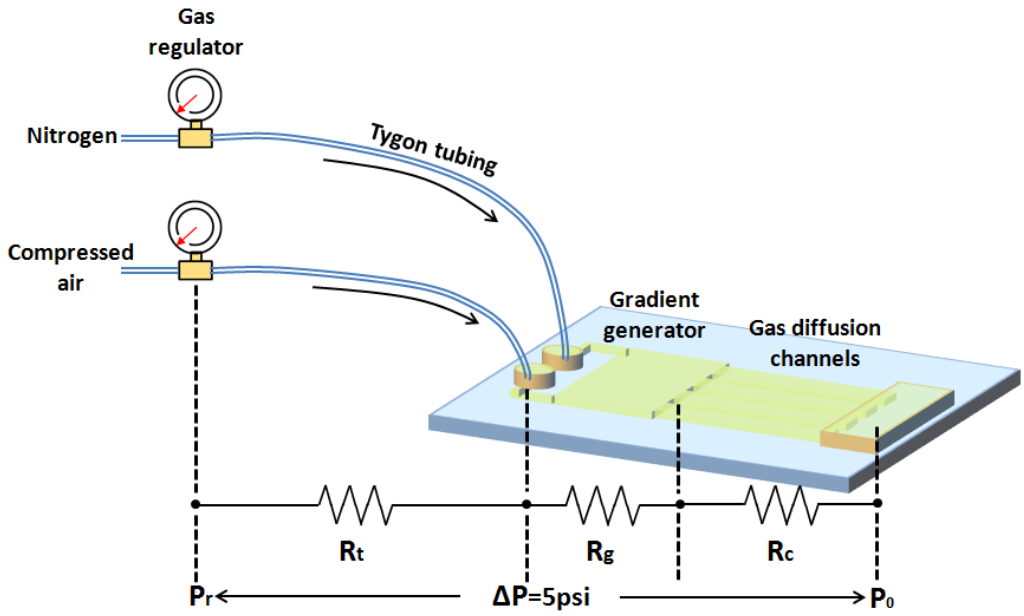


Figure 3.6 Schematic of the oxygen gradient generation setup. Regulated gas supplies of nitrogen and compressed air are connected to gas layer inlets via 0.02inch ID Tygon tubing. Gas layer outlet is open to atmosphere. Rt, Rg and Rc represent the flow resistance of in serial segments of Tygon tubing, gradient generator and gas diffusion channels.

Similar with the photosensitizer gradient generation, successful oxygen gradient generation requires neat gas flow splitting/rejoining and sufficient mixing within the serpentine channels. A 2D FEM is developed in COMSOL Multiphysics software, using the imported mask file of gas layer geometry, to help simulate the gas behavior in the gradient generator as shown in Figure 3.7. Gas velocity vector field is calculated in the incompressible Navier-Stokes subdomain, with an initial dynamic viscosity value of 1.8e-$^{5}$Pa·s as reported previously [7]. No-slip boundary conditions are applied at the channel surfaces. Convection and diffusion subdomain is then added for calculating oxygen concentration, assuming an isotropic diffusion coefficient of 2.19e-5m$^2$/s. Considering the different viscosities of oxygen and nitrogen, dynamic viscosity is modified as 1.8e-5(1+0.16[$O_2$]/9.69e-6), where [$O_2$] is the local oxygen concentration in mol/m$^3$. Both sub

domains are coupled together to calculate the final oxygen distribution under different input gas pressures. As the results shown in Figure 3.7, an optimized input pressure of 5psi is enough for generating discrete oxygen concentrations feeding into different gas diffusion channels, with a maximum value like atmosphere ($9.69\times10^{-6}$mol/m$^3$) and a

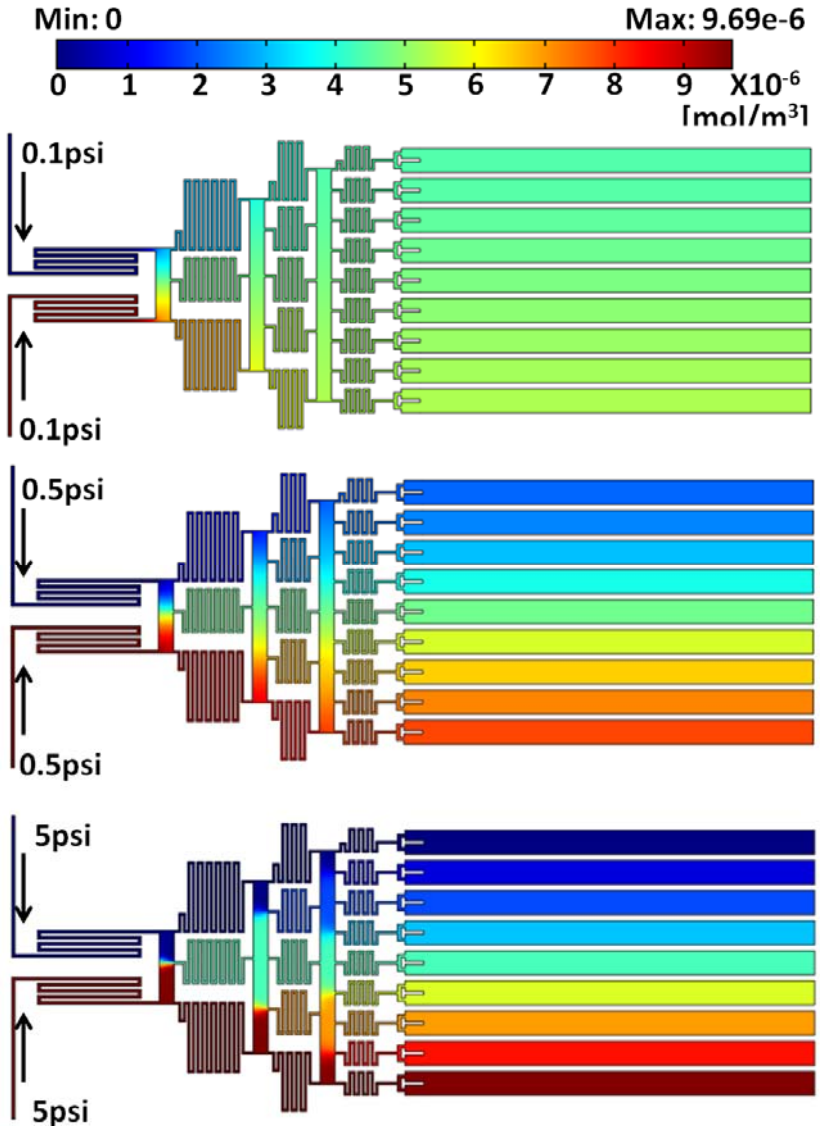


Figure 3.7 FEM simulation results of oxygen gradient generation and distribution. (a) Simulation result shows color coded oxygen gradient generation within gas layer under different input gas pressures.

minimum value like pure nitrogen (0mol/$m^3$).

As mentioned previous, oxygen concentration in the cell layer is decided by the concentration in the same position of gas layer, which is imposed onto the cell layer and the gas could diffuse through the PDMS membrane dividing these two layers. Another 2D FEM is developed simulating such oxygen diffusion through PDMS membrane and reaching equilibrium in cell layer, as shown in Figure 3.8. The whole model is set up following the actual dimensions of the chip. The chip bottom and top boundary conditions are set as insulation since glass is not gas permeable. The chip side boundaries of oxygen concentration are set as 9.69e-6mol/$m^3$, corresponding to the atmosphere air condition with [$O_2$] =21%. The gas channels are numbered from 1 to 9 and oxygen concentrations within them are preset in 9 levels with a linear increase from 0 to 9.69e-6mol/$m^3$, following the results of previous single gas layer simulation. Gas channels are 33um deep, 320um wide and having an 80um gap between each other. The cell culture channel beneath them is 150um deep and the PDMS membrane between two layers is 70um thick. The total thickness of the chip is set as 3mm. Oxygen concentration is calculated in convection and diffusion domain, with diffusion coefficients of 1.3e-9$m^2$/s in PDMS and 2e-9$m^2$/s in media as reported [8, 9]. The simulation result in Figure 3.8 shows the oxygen distribution after it reaches equilibrium within the chip, with color-coded concentration. Oxygen concentration values along the dash line at the bottom of the cell culture channel, where the cultured cells are supposed to be, are measured to estimate the actual oxygen stress on cells during PDT efficacy tests. Two dimensions are playing important roles here for successfully imposing generated oxygen gradient onto the cells. One is the distance between gas channels and the cells, which is also the vertical

oxygen diffusion distance. The other is the width of gas channel, which decides the maximum tolerable diffusion distance in the horizontal direction.

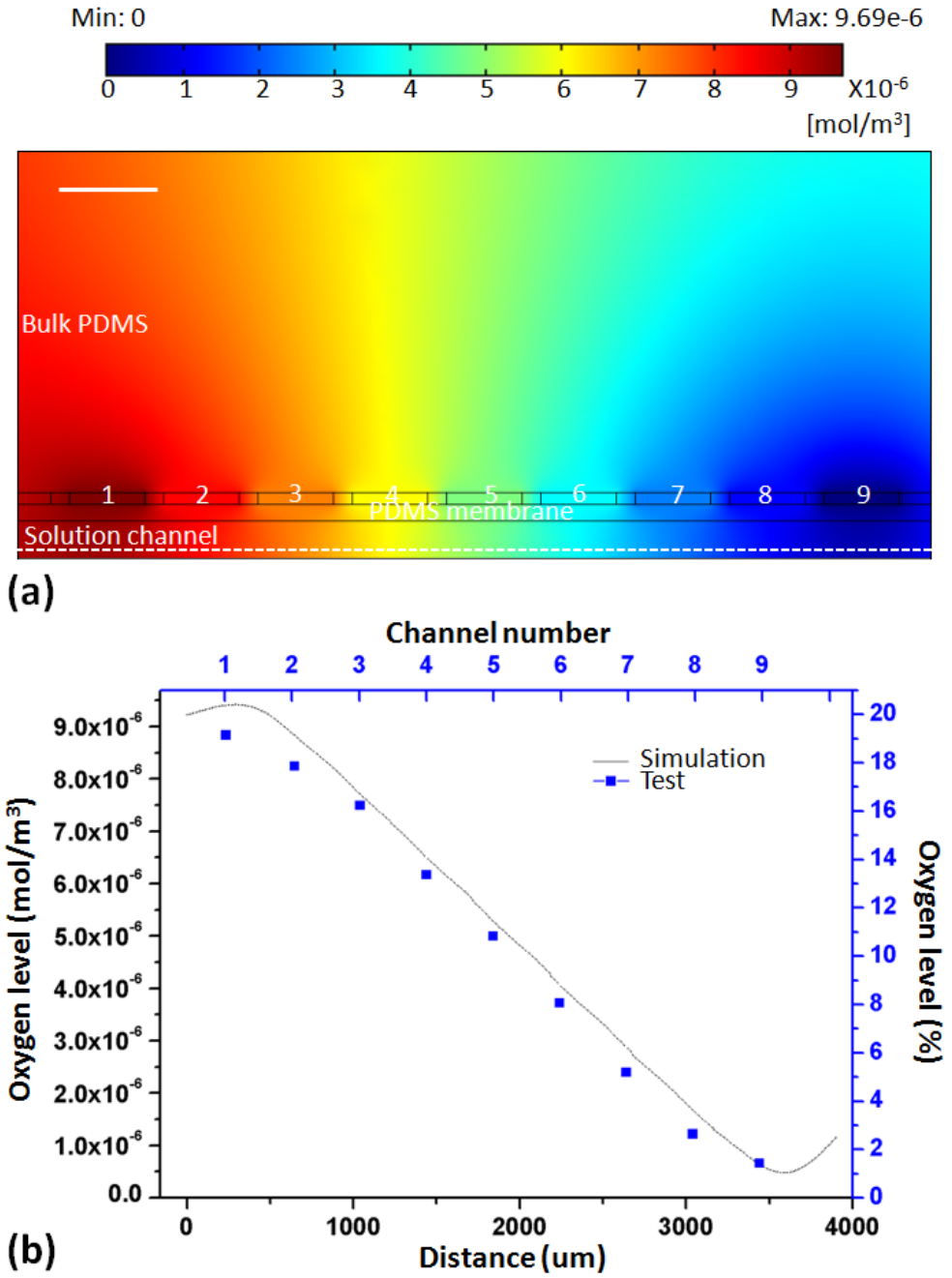


Figure 3.8 (a) Simulation results demonstrating the oxygen concentration distribution surrounding the active test area, using color coding. (b) Comparative plot of the simulation result and the measured result of the oxygen concentration distribution along the cell culture channel. Scale bar: 400um.

Oxygen gradient is measured on chip and compared with the results in simulation. So far various technologies for measuring oxygen levels in aqueous media have been reported, of which the optical method is determined to be most suitable for our application considering the micron scale resolution, quick response, compatibility with microfluidic chips and other therapeutic factor measurements [10-12]. Ruthenium tris(2,2'-bipyridil) dichloride hexahydrate (RTDP) is a fluorescent dye sensitive to the oxygen concentration in solution. Its fluorescence can be quenched by oxygen molecules so that its intensity decreases as the oxygen concentration increases. Based on that, Stern-Volmer equation can be utilized to calculate the actually oxygen concentration:

$$I_0/I=1+Kq[O_2]$$

, where $I_0$ is the intensity without oxygen, I the measured intensity, Kq the quenching constant, and $[O_2]$ is the oxygen concentration. The value of Kq is pre-obtained by comparing the fluorescence intensities of the RTDP solution either under saturation with nitrogen ($[O_2]$ =0) or under the atmosphere condition ($[O_2]$ =21%).

Oxygen gradient generation and measurement test is carried out with a double layer (cell layer and gas layer) chip with nine gas diffusion channels. The cell layer is prepared in a similar way as described in previous section and filled with 1000ppm RTDP (Sigma-Aldrich) in DMEM. The chip top is covered with a thin glass slide avoiding influence of atmosphere from top. Two gas tanks, one with nitrogen and the other with compressed air, are set up as gas supplies. Both of them are regulated at a pressure of 5psi with a pressure regulator (Airgas) and connected to the gas layer inlets. Solenoid valves controlled by a self-written Labview program are used to turn ON/OFF the gas supplies. In other words, when the solenoid valve is turned on, gas layer inlet is connected to the 5psi

nitrogen/compressed air supply; and when it is turned off, the inlet is sealed as a dead end. Fluorescence images are captured and processed in a similar procedure as described in the previous section for FITC fluorescence imaging. The only difference is a special filter set (Chroma Technology Corp, ChlorophyII) fitting the excitation/emission spectrum of RTDP is used. During the test, first the gas layer is supplied only with compressed air or nitrogen for 10mins individually and corresponding fluorescence images are recorded. By comparing the fluorescence intensity changes under this two conditions (maximum oxygen concentration of 21% and minimum oxygen concentration of 0%), Kq the quenching constant is acquired as mentioned earlier. Then both compressed air and nitrogen are supplied under a same 5 psi pressure. After 10mins, oxygen reaches equilibrium in chip and fluorescence images are taken. The fluorescence intensity below each gas channel is sampled from channel's central overlapping area with the cell culture channel, with a dimension of 125um×125um. The average gray value is adopted for calculating the mean oxygen concentration below each gas channel, using Stern-Volmer equation as mentioned earlier. The results are plotted in a corresponding method and demonstrate a close matching with simulation outcomes, as shown in Figure 3.8(b).

In high-throughput PDT efficacy test combining oxygen gradient with photosensitizer concentration gradient, it is important to generate oxygen gradient among different gas channels while maintaining a same oxygen concentration in one gas channel. To verify that, the fluorescence distribution of the whole testing area (overlapping area of gas channels and cell culture channels) is recorded as shown in Figure 3.9. The fluorescence profiles are measured along different directions. While areas beneath different gas

channels are having distinct fluorescence intensities (along x axis), areas beneath a same gas channel are having a constant fluorescence intensity (along y axis).

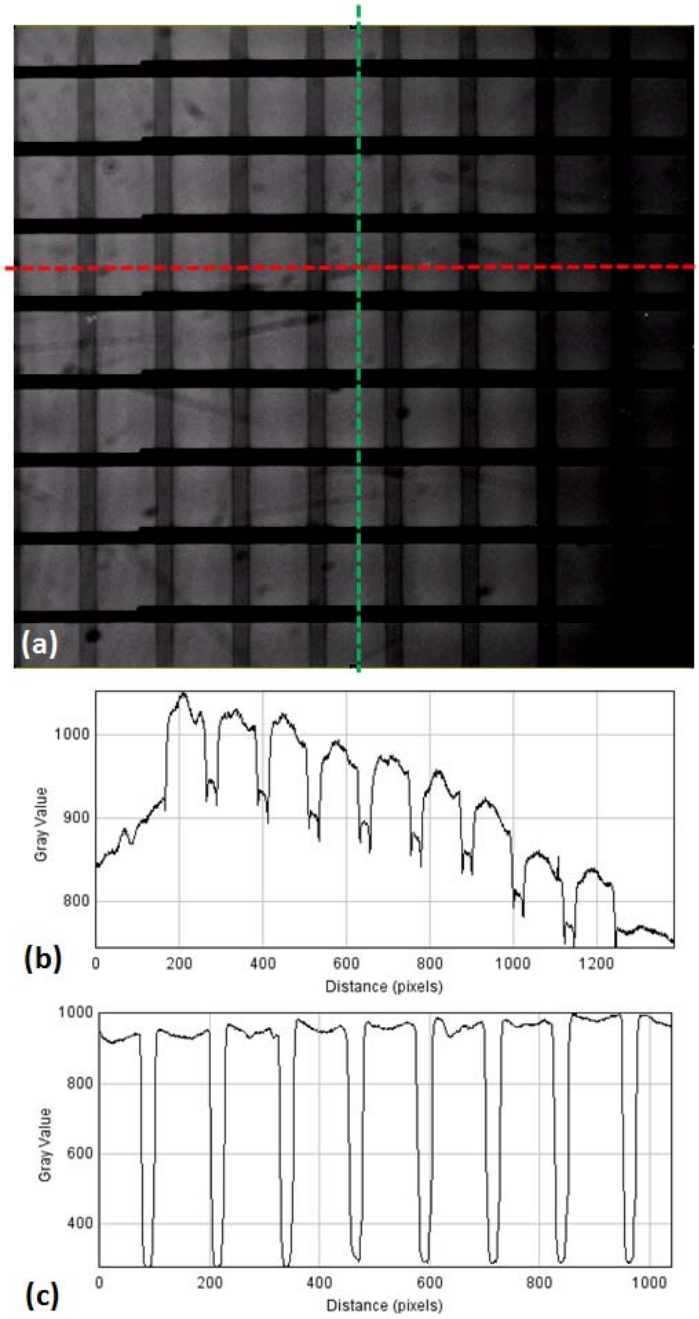


Figure 3.9 (a) Fluorescence image showing the oxygen gradient distribution of the active test area. (b) Fluorescence intensities are measured along the red dash line (along a same cell culture channel, including different gas channels). (c) Fluorescence intensities are measured along the green dash line (along a same gas channel, including different cell culture channels).

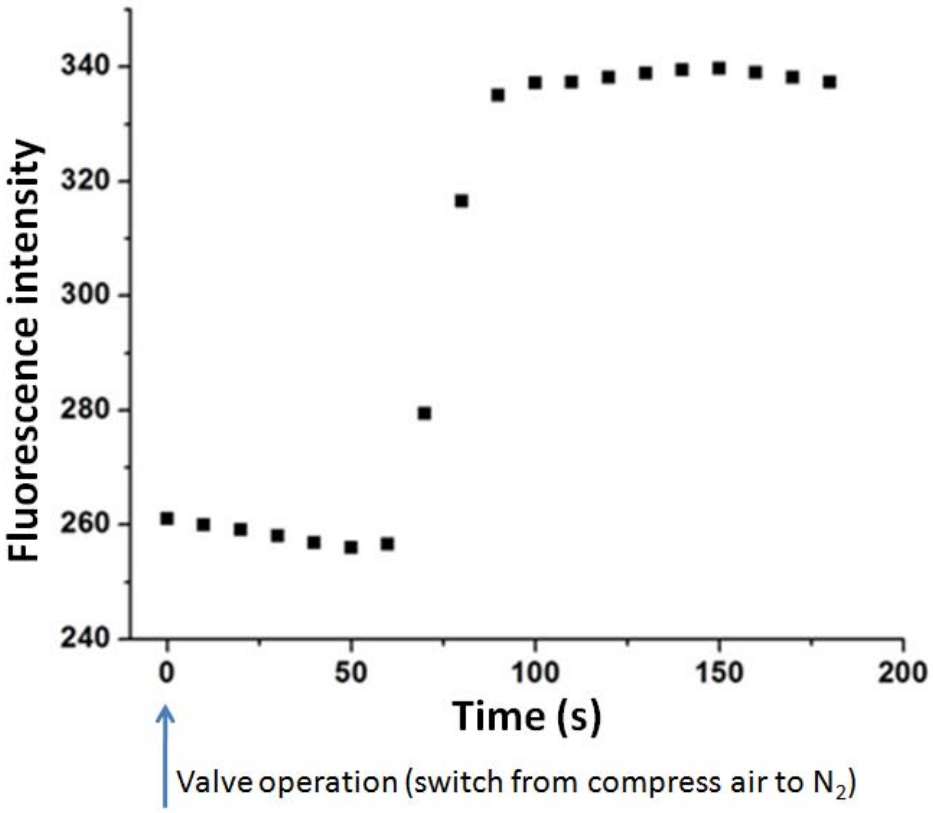


Figure 3.10 Time lapse recording of the RTDP fluorescence intensity changes after the gas supply switched from compress air to nitrogen.

Response time of oxygen gradient generation on chip is an essential parameter for setting up the protocols for PDT efficacy test on chip involving the oxygen level response. In other words, how long it takes after switching the gas supplies on until reaching oxygen equilibrium in the cell layer with a stable concentration profile. This might be affected by the equilibrium all over the system including the gas supply setup, gradient generator, the chip and atmosphere. For that, time lapse changes in RTDP fluorescence intensity in recorded after switching between different modes of gas supplies. As shown in Figure 3.10, fluorescence intensity at a same position of cell culture channel is recorded every 10 second after switching from supplying the whole chip with compressed air to pure nitrogen. It takes around 60s for oxygen concentration in cell layer to start

changing, but the transition time takes only around 30s, which is close to what has been reported in previous publications [7].

### 3.3 Illumination intensity gradient generation and measurement

Illumination is a unique therapeutic factor in PDT, and directly affects PDT efficacy. Effective illumination dose is decided together by light source spectrum (efficiency of photosensitizer on generating radical oxygen species), illumination intensity and illumination time. In this microfluidic platform setup, the whole chip is illuminated by a single LED light source, which provides a same illumination spectrum and identical illumination ON/OFF during the PDT test. Thus the illumination dose is only proportional to the local illumination intensity, of which the gradient can be generated by the gray scale filter layer providing different transparency at different positions.

Two kinds of light sources have been adopted in actual PDT efficacy tests. One is a single LED light source (LUXEON), which provides stronger illumination power suitable for quick PDT assay tests. The other is a self-assembly 46×25 LED array (Digikey), covering a similar large illumination area of a 96-well plate (127mm×85mm) suitable for expanded high-throughput chips with a large cell array size. Both light sources are selected to have an emission spectrum matching the absorption spectrum of target photosensitizer. Two kinds of photosensitizers have been used. One is Methylene Blue free dye which is having a wide range of high absorption from 620nm to 680nm. The other is the Methylene Blue incorporated functionalized NPs which has a similar absorption spectrum with Methylene Blue free dye. Figure 3.11 shows the measured emission spectrum of the single red LED light source. It has an emission peak at 637.73nm and a full width at half maximum (FWHM) of 18nm. The red LED array light

source is having an emission peak at 660nm. Notably, both of them fit well in the absorption spectrum of Methylene Blue (NPs).

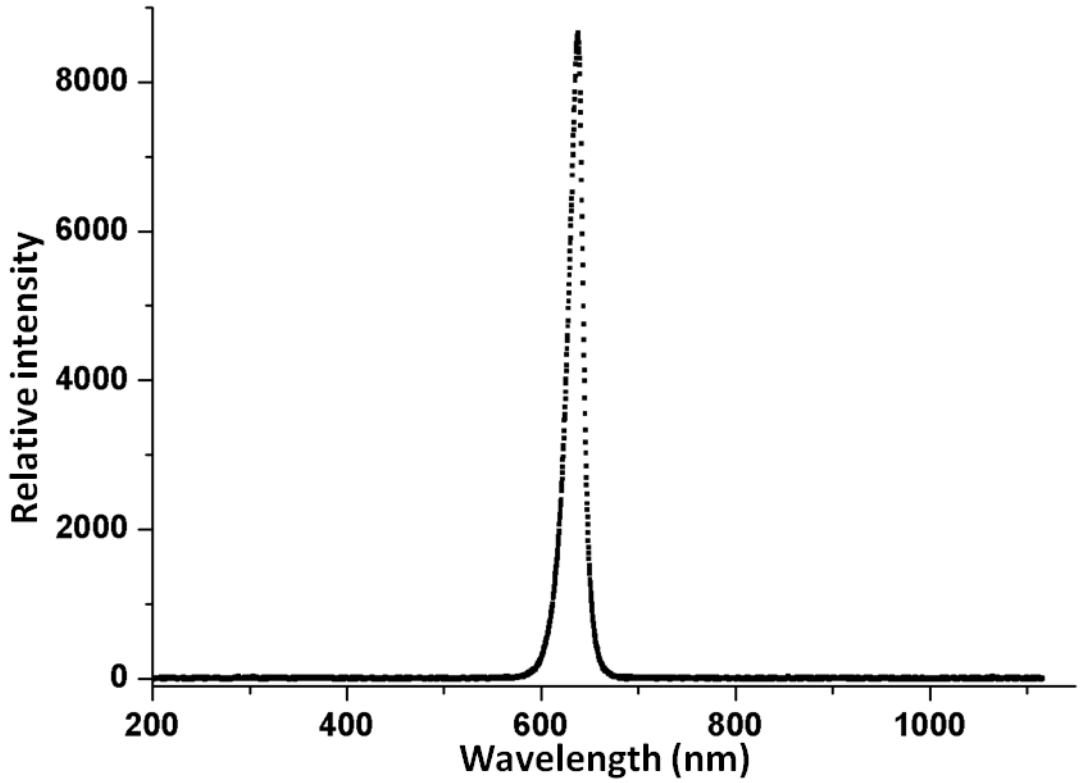


Figure 3.11 Measured emission spectrum of the single red LED light source.

The initial illumination intensity imposed onto the microfluidic chip by the LED light source can be modulated in two independent ways. The first is by modulating the electric current through the light source. For the single LED light source the current is maintained at 250mA; and for the LED array the current through each LED unit is maintained at 20mA. Time lapse images of the illumination intensity profile on the illuminating substrate surface are recorded. For both light sources, a stable illumination output on chip substrate can be maintained. The second is by adjusting the distance between the light source and the microfluidic chip substrate. For the single LED light source, that distance is set at 70mm, and for the LED array light source that distance is 52mm. Such optimized

distances are set based on some trade-offs. On the one hand, the light source should provide a uniform illumination over the whole active PDT test area, which is easier to realize with a long distance. On the other hand, the illumination intensity on chip substrate should be maintained high enough to ensure required illumination dose can be reached in a reasonable time period, which is easier to realize with a short distance. Detailed results about the illumination uniformity and intensity are described in the latter part of this section.

Illumination intensity on the chip substrate surface for cell culturing is measured by two steps, during which previous driven currents and set up distances are adopted.

Step one is to measure the initial illumination intensity provided by the light source. Illumination intensity without the filter layer is measured on a same glass substrate surface using an illuminance meter (Konica Minolta, T-10). The sensing area for the illuminance meter is 6.7mm in diameter, which is larger than the illuminating area of the single LED light source but smaller than that of the LED array light source. So the illumination intensity of the LED array light source can be directly read out from the illuminance meter, which is 16700lx. For the single LED light source, since the sensor covers a larger area than the illuminated area, such direct measurement would also include the surrounding unilluminated area and return an average value including both illuminated and unilluminated areas. To solve that, the sensor is covered with a dark field mask having a 1.5mm diameter aperture in center and an initial value $I_{1.5}$ is recorded. Considering the actual sensor diameter of 6.7mm, the actual illuminance intensity should be proportional higher than $I_{1.5}$ in a same ratio of $(6.7)^2/(1.5)^2$. An assumption here is under uniform illumination, the illuminance meter read out is proportional with the

exposed area of the sensor, which has been verified with a series of dark field masks with different aperture sizes. The final illuminance intensity of the single LED light source is calculated to be 67500lx.

Step two is to measure the transparencies of the filter layer. The transparency profile of gray-scale pattern liquid filter is recorded using microscope imaging. To do that, the LED illumination light source and the microfluidic chip with the filter layer are mounted together onto the microscope stage, set with a same optimized distance between them as mentioned previously. One image focusing on the cell culture substrate is recorded, to demonstrate the illumination intensity distribution after the light passing through the filter layer and reaching the cell culture substrate. Another image taken without the filter layer is recorded as the initial illuminance distribution for later normalization. By combining these two images, we are able to reconstruct the transparency profile of the liquid filter layer.

Based on the measured results of previous two steps, local illuminance intensity at different chip positions can be calculated as $I_n = I_0 * T_n$, where $I_n$ is the actual local illuminance intensity for target cells, $I_0$ the original illuminance intensity from light source and $T_n$ the local transparency of the gray-scale liquid filter.

Illumination intensity gradient generation and measurement are carried out with a single filter layer chip. First, the chip is vacuumed in desiccator for 1h similar as the cell layer preparation process mentioned in previous section. Second, different concentrations of Methylene Blue solutions are fed into the filter layer. The top surface of the filter layer is sealed with another thin glass cover, which helps avoid evaporation and maintains the solution concentrations for at least 24h for test.

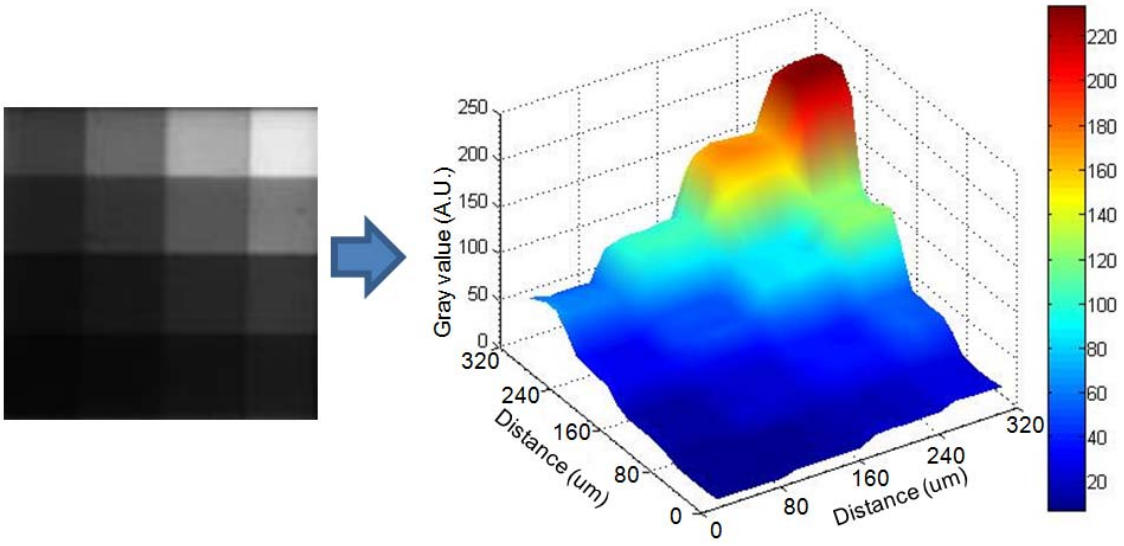


Figure 3.12 Image of the illumination intensity gradient of the 4 by 4 grid array and the 3D plot of corresponding profile.

As mentioned previously, the major gray-scale liquid-filter patterns generated here are 4 by 4 grid arrays, which have 16 levels of illumination intensity. Figure 3.12 shows an example of 4 by 4 grid unit got by feeding the filter layer with two different concentrations of Methylene Blue (50mg/ml and 12.5mg/ml). The profile of illumination intensity can be plotted in a 3D format with color code. Notably, while the 16 levels of illumination intensity are different from each other, illumination intensity within each grid is pretty uniform. Each grid is having a size around 80×80um and directly adjacent with other grids. Considering the PDT generated oxygen singlet's short life time (~20ns) and diffusion distance (~20nm), it is assumed that radical oxygen species generated in one grid with its own specific illumination intensity can only affect the cancer cells within that area [13, 14].

Different kinds of illumination intensity gradient profile can be generated based on the filter layer design and absorption solution changes. Single PDMS layer liquid filter providing 4 levels of transparency has been utilized for high-throughput PDT efficacy

assay with multiple therapeutic factors. Also as shown in Figure 3.13, by feeding different concentration combinations of absorption solutions in the filter layer, the transparency profile changes in both dynamic range and steps between each other. Figure 3.13 shows the 16 levels of transparencies of the 4 by 4 grid array with different feeding Methylene Blue concentrations of (a) 12.5mg/ml and 5mg/ml, (b) 25mg/ml and 5mg/ml, (c) 50mg/ml and 5mg/ml, and (d) 50mg/ml and 25mg/ml. Each bar shows the average transparency sampling from corresponding 80x80um grid.

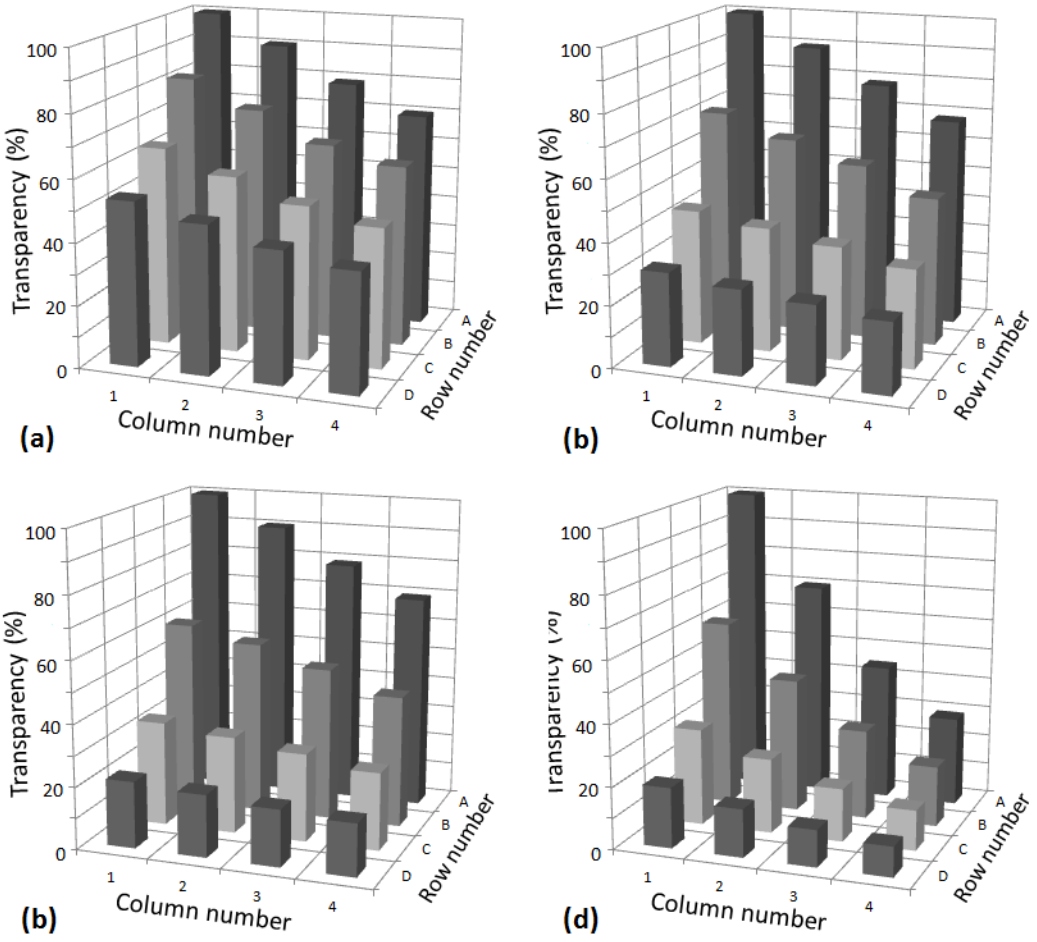


Figure 3.13 Gray-scale transparencies of the 4 by 4 grid array with the feeding Methylene Blue concentrations of (a) 12.5mg/ml and 5mg/ml, (b) 25mg/ml and 5mg/ml, (c) 50mg/ml and 5mg/ml, and (d) 50mg/ml and 25mg/ml.

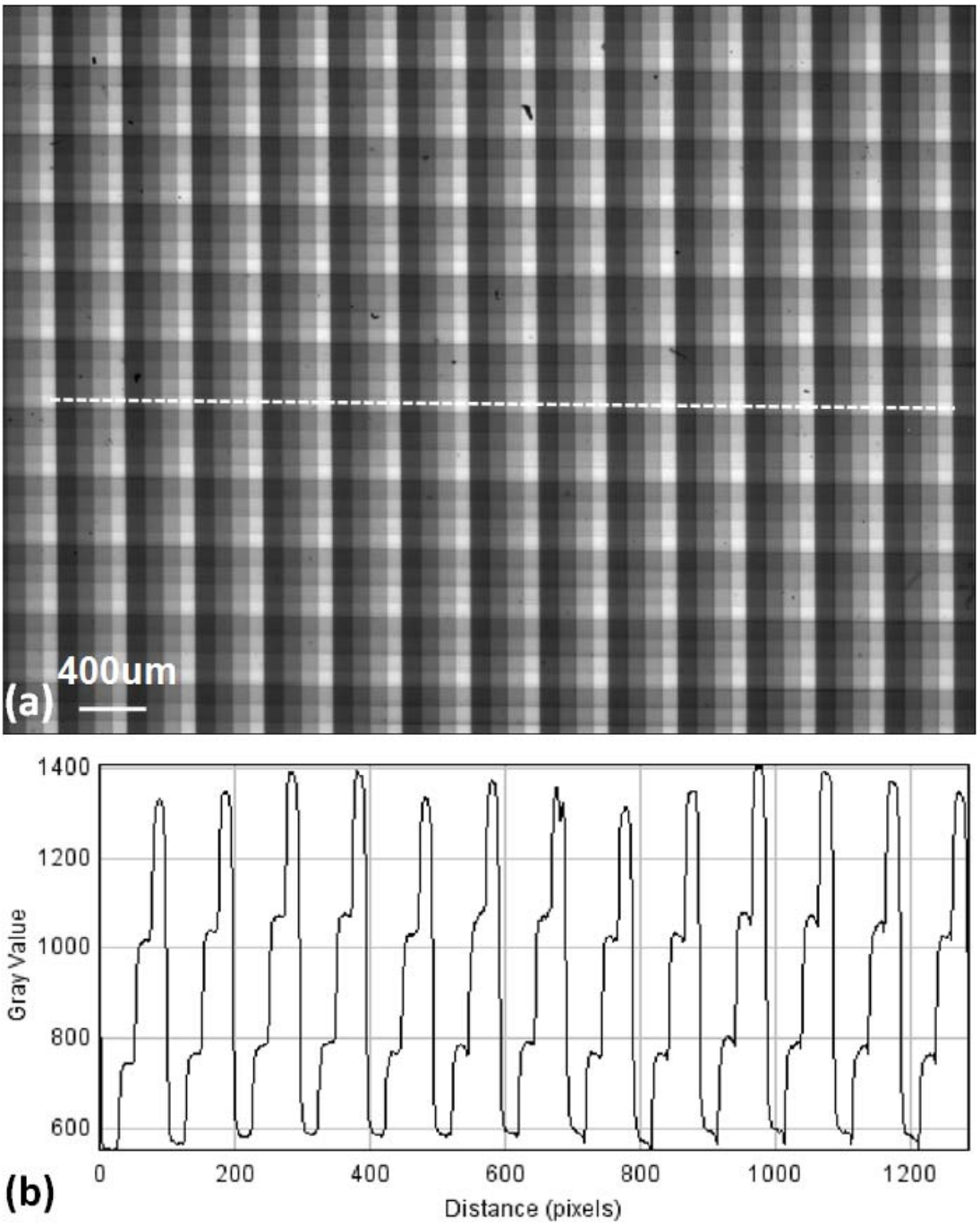


Figure 3.14 (a) Illumination intensity distribution over the whole test area after light passing through the grayscale filter. (b) Illumination intensity profile along the white dash line.

For PDT efficacy tests combining illumination intensity gradient with other therapeutic factor gradients, it is important to make sure the grayscale illumination

patterns are identically repeated throughout the whole active test area. To verify that, the illumination intensity covering the whole test area is recorded by imaging and the gray value profile is measured. Figure 3.14 shows the result from a gray-scale liquid filter, which is large enough to cover all 9 cell culture channels and 9 gas channels. The 4 by 4 grids array demonstrates a good repetition of gray values within the whole area. Based on the measurement along the dash line, these gray values repeat within a deviation of ±5%, excluding some bare defect spots.

Similar with many other dyes, photobleaching could be a potential problem for Methylene Blue. Especially under strong and continuous PDT illumination, it might experience severe molecule destruction and lead to irreversible filter degradation. This kind of filter degrading can be solved by providing a continuous flow of MB solution for our liquid filter. Since PDT illumination is restricted within the chip area, the filter layer can be continuously refreshed with new MB solution which has been free from illumination and maintains a constant absorption capability. We compared the transparency changes of one liquid filter, which is sealed right after the filling of the Methylene Blue solution, with another liquid filter, which is continuously refreshed under a flow rate of 5ul/min using a syringe pump. While illumination intensity through the sealed liquid filter layer gradually increases about 10% after 40mins illumination, the other filter layer with continuous refreshing solution maintains constant illumination intensity, as shown in Figure 3.15. In our PDT test, both sealed and continuously refreshing liquid filters have been used. For the sealed liquid filter, the temporal changes of such illumination intensity are included for properly estimating the total illumination dose at the end.

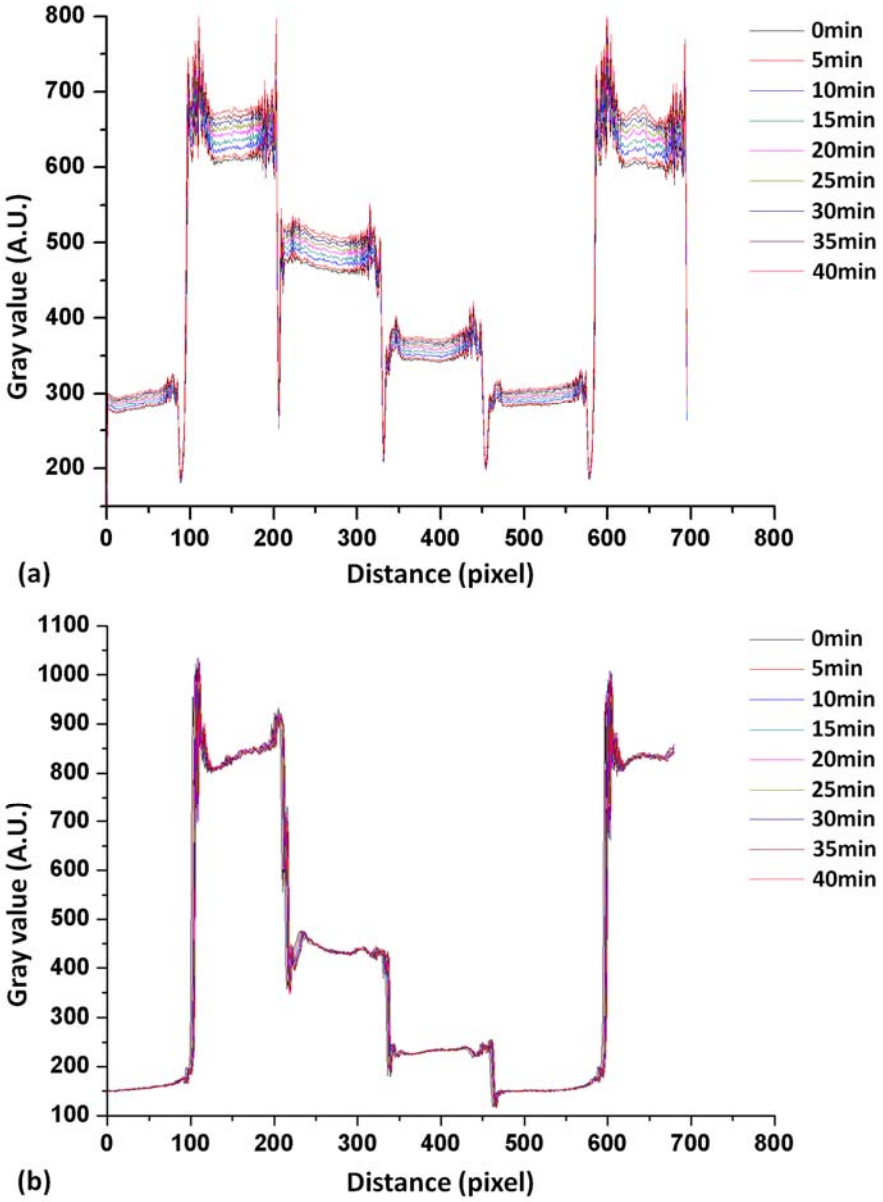


Figure 3.15 Time lapse recording of the illumination intensity changes through (a) a sealed filter layer, and (b) a continuously refreshing filter layer. Gray values are measured along the filter layer grid patterns using the ImageJ software.

### 3.4 Incubation time gradient generation and measurement

Two kinds of photosensitizers have been tested in this platform, one of which is Methylene Blue free dye and the other is functionalized NPs. In vitro PDT efficacy test

procedure is different for these two types of photosensitizers and an extra therapeutic factor of incubation time needs to be considered for the NPs efficacy test. As for Methylene Blue free dye, after the MB solution of a certain concentration is added to the testing cells, the cells are directly exposed to PDT illumination and then have viability evaluated. For the functionalized NPs, after adding the NP solution to the testing cells, the cells are first left in the incubator for a certain time period, like 1hour. During this co-culturing period, the NPs are enabled to be bonded to cell surfaces through the targeting moiety-receptor interaction and then swallowed into the cells through phagocytosis [15]. After that, the NP suspension is removed and a fresh base medium is added to wash away all the remaining unbounded NPs. Then, PDT illumination is applied and only the remaining NPs attaching on or inside the cells are generating oxygen singlets. In brief, incubation time affects how much and how well NP photosensitizers can be attached and taken by the cancer cells. It is intrinsically related with NPs' targeting capability on cancer cells and thus directly affects their PDT efficacy.

The functionalized NPs used here are fabricated in our collaborator's lab (Prof. Raoul Kopelman, Chemistry department, University of Michigan), with the process described in previous publication [16]. While the detailed NP composition is subjected to change depending on the applications, the structure of the PDT NPs have been used in this platform is shown in Figure 3.16. It has a polyacrylamide (PAA) core matrix with Methylene Blue and FITC molecules incorporated inside. Targeting moiety, in this case F3 peptide, is conjugated to the NP surface through a PEG crosslinker. It is provided in the powder format and kept in -20℃ for storage. Before each test, it is dissolved in DMEM based on the desired concentration and vortexed to reach a uniform suspension.

While the NPs are having an average diameter of 20-30nm in dry storage, they swell in solution and could reach an average diameter around 50nm before applying to cells.

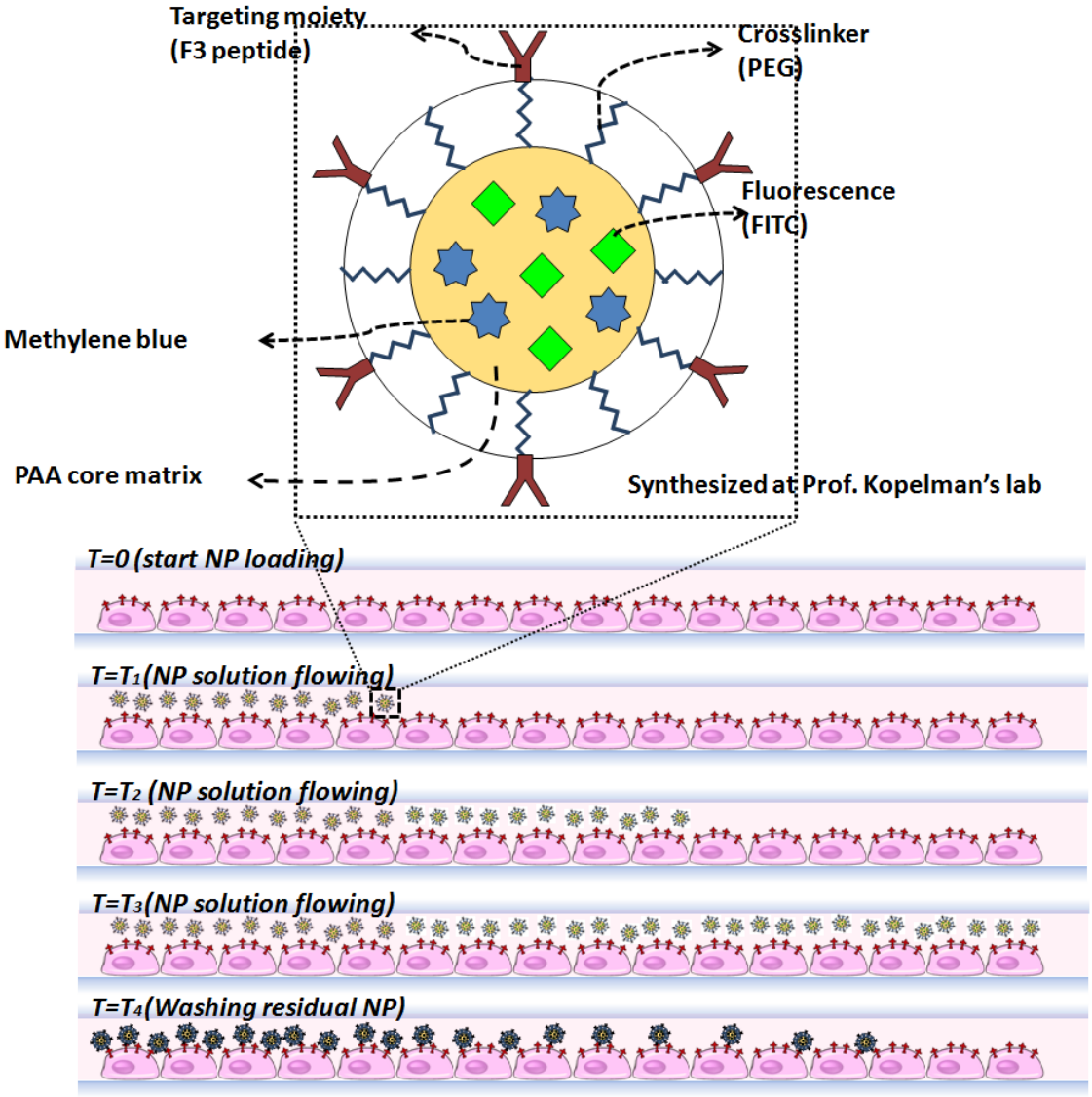


Figure 3.16 Schematic working principle of the incubation time gradient generation utilizing controlled feeding flow rate of the NP solution. Enlarged part shows the diagram of the functionalized NPs that have been adopted for the microfluidic platform test.

To naturally generate an incubation time gradient, we use the method of gradually introducing the NPs into the cell culture channel. As shown in Figure 3.16, the NP solution is fed into the cell culture channel under a slow flow rate from left to right. As a

result, cells closer to the inlet would have the NP solution reaching them first compared to the cells further from the inlet. Or in other words, during the gradual process of NP solution filling the channel, cells at the upstream area keep having a longer incubation time with NPs than the cells at the downstream area. After the whole channel is filled with NP solution ($T=T_3$), a quick washing removes all the unattached NPs and the NPs attachment to the cells can be examined. In brief, to generate an incubation time gradient, it is important to introduce a slow flow rate of the NP solution loading and a quick flow rate of the fresh medium washing. To generate a linear gradient of incubation time along the cell culture channel, it is important to maintain a constant flow rate during the feeding process.

Incubation time gradient generation and measurement are carried out with a single cell layer chip having 13 cell culture channels. It is also having larger channel volumes and flow resistance to help reduce the feeding flow rate. The chip is prefilled with DMEM in a similar way as described in the previous section. One of the inlets is sealed with an extra piece of PDMS membrane, and the other is inserted with a needle for gravity flow setup. The NP solution is prepared in a concentration of 1mg/ml and filled into the inlet needle, and the outlet reservoir is filled with 50ul DMEM, resulting in a pressure difference around 200Pa. Fluorescence images of the cell culture channels are taken every 15mins monitoring the NP solution flowing through the microfluidic channels. And after 90mins' filling, a quick 5mins' washing of DMEM is applied to remove unattached NPs. As shown in Figure 3.17, the cell culture channel is gradually filled with NP solution as the boundary of fluorescence moving to the right under a

constant rate. After washing, all the suspended NPs can be removed showing no more fluorescence in the channel.

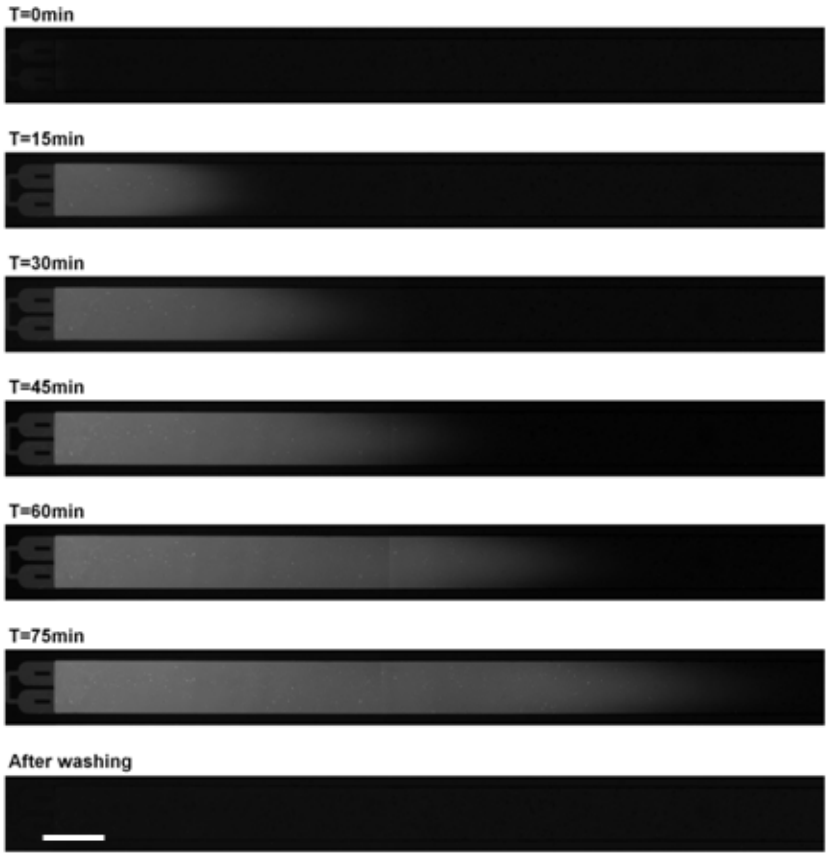


Figure 3.17 Time lapse recording of the fluorescent NP solution gradually filling the cell culture channel and removed with a quick washing at the end. Scale bar:480um.

Incubation time gradient can also be combined with NP concentration gradient within one chip to realize a high-throughput PDT efficacy screening. In this test, a same chip is prepared in the same way as described in previous paragraph, but both inlets are inserted with a needle for gravity flow setup. One of them is filled with the 1mg/ml NP solution and the other is filled with pure DMEM. In this way, NP gradient is generated in the gradient generator and a different concentration slowly fills each cell culture channel. For monitoring the NP gradient and flow rate, fluorescence images covering the whole cell

culture channel area are taken in a time lapse method. Fluorescence images are processed in a similar way to calculate the NP concentrations as mentioned in previous sections. The NP solution flow distance at certain time point is calculated as the distance between the beginning of the cell culture channel and the edge of NP solution flow where the fluorescence intensity drops to the half of its starting value.

As shown in Figure 3.18, after setting up the gravity flow it takes around 4mins for the NP solutions passing through the gradient generator and start entering the cell culture channels. And gradually cell culture channels are filled with different concentrations of NP solutions, indicated by the NP solution fluorescence edges slowly moving towards the outlet. The fluorescence edges in the upper channels might not be as easy to distinguish as those in the bottom channels because of the lower NP concentrations and weaker fluorescence, but still can be plotted out using ImageJ software as shown later. It takes around 120 minutes to fully fill the 20mm long cell culture channels, providing a maximum incubation time gradient range from 0 to 120 minutes. For tests requiring even a longer incubation time, simply elongated cell culture channels can be used with same gravity flow setup since such flow resistance change in cell culture channels is small enough to be neglected. Measured flow rates in each cell culture channel are plotted, as shown in Figure 3.19. Within the 13 channels, the flow rate shows a symmetric distribution as the central channel is having the highest flow rate and the edge channels are having the lowest flow rate. However, this kind of flow rate difference is not affecting the data collection of PDT efficiency tests since the incubation time in each channel is recorded and calculated independently. All channels are able to maintain a constant flow rate within a time frame of 90min, and for longer incubation time applications, inlets can

be refilled and the outlet can be emptied to continuously maintain a constant pressure difference and flow rate.

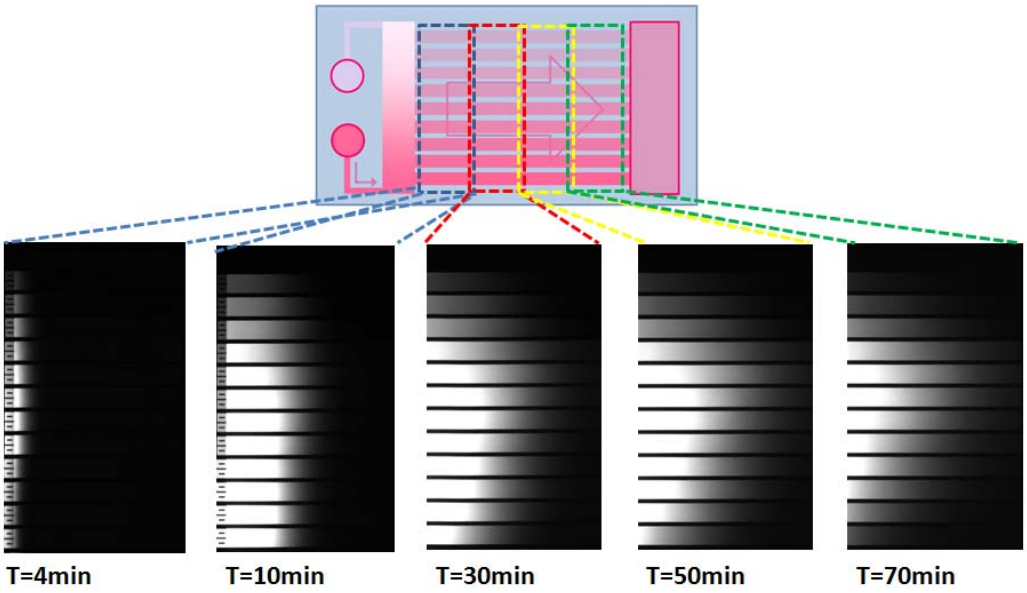


Figure 3.18 Time lapse recording of different concentration NP solutions gradually filling the cell culture channels. Different sections of the cell culture channels are enlarged showing corresponding NP solution edge positions.

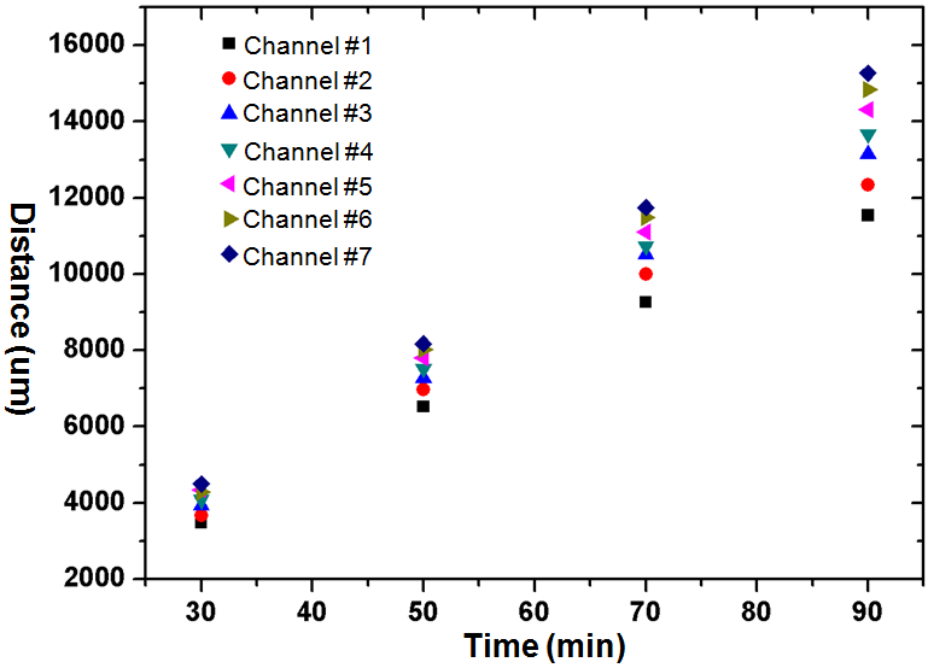


Figure 3.19 Measured results of flow rates in each cell culture channel. Flow distances in each channel at different time point are recorded and plotted.

### 3.5 Flow shear stress gradient generation and characterization

Flow shear stress in a microfluidic device can be intrinsically controlled by dynamically adjusting the inside flow rate, the derivative of which is proportional to the shear stress. To realize a high-throughput analysis, an integratable chamber unit with various channel widths will fit this platform better mimicking different physiological conditions under different shear stress levels [17-21]. A 3D FEM of such a cell culture chamber is developed to simulate the shear stress distribution as shown in Figure 3.20 and Figure 3.21. The whole model is set up following actual dimensions of the device, with a microfluidic channel height of 300um and expanding channel widths from 320um to 3520um. No-slip boundary conditions are applied at the channel surfaces and a pressure difference of 100Pa is applied between the inlet and the outlet driving the flow inside. The flow velocity vector field is calculated in the incompressible Navier-Stokes domain, with a dynamic viscosity value of 8.9e-4Pa•s. As shown in Figure 3.20, there is a gradual pressure drop from the inlet to the outlet and the flow velocity decreases as the channel width increases. Detailed shear stress distribution in each segment of a specific channel width is demonstrated in Figure 3.21. Shear stress imposing on culture cells is estimated by calculating the value 10um above the substrate, based on the flow velocity distribution results and utilizing:

$$\tau(y) = \mu \frac{\partial u}{\partial y}$$

, where μ is the dynamic viscosity of cell culture medium, u the fluid velocity and y the height above the boundary. As the channel width increases, the maximum shear stress in each segment decreases from 14.1 to 0.75dyn/cm$^2$, while the value at the edges could be as low as 0.0084dyn/cm$^2$ fitting in the physiological range of shear stress [22-24]. So

long as the channel width reaches 1120um (much larger than channel height), shear stress distribution becomes uniform over the central channel area and makes it suitable for statistic data collection of cell reactions. For further verifying the shear stress distribution, there is not any reliable method for directly measuring shear stress distribution within a microfluidic device reported yet. However, we consider some technologies are having the potential filling that gap in the future with improved resolution and reliability [25].

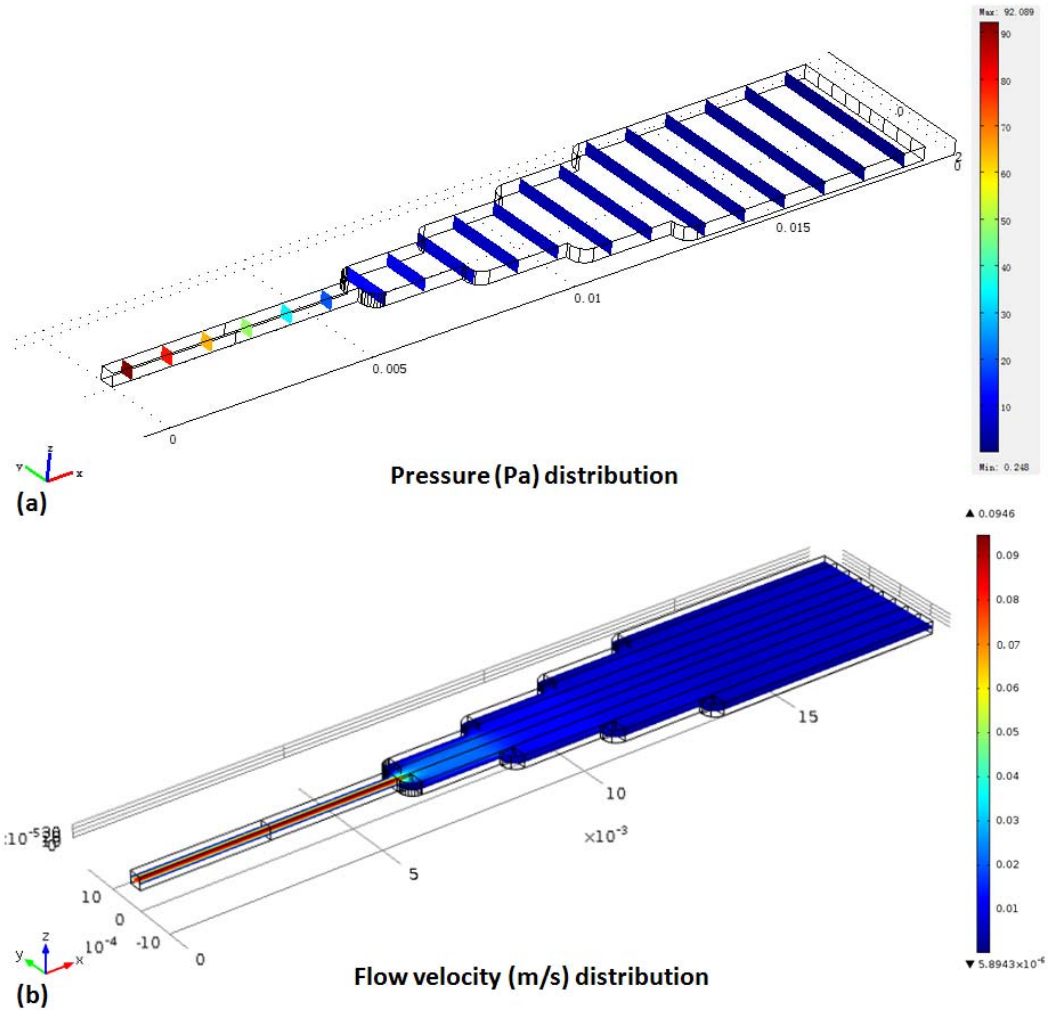


Figure 3.20 FEM simulation results of the cell culture chamber with an expanding channel width. (a) Simulation result shows the pressure drop along the chamber from inlet to outlet, demonstrated in a color scale. (b) Simulation result shows the flow velocity decreases as the channel width increases, demonstrated in a color scale.

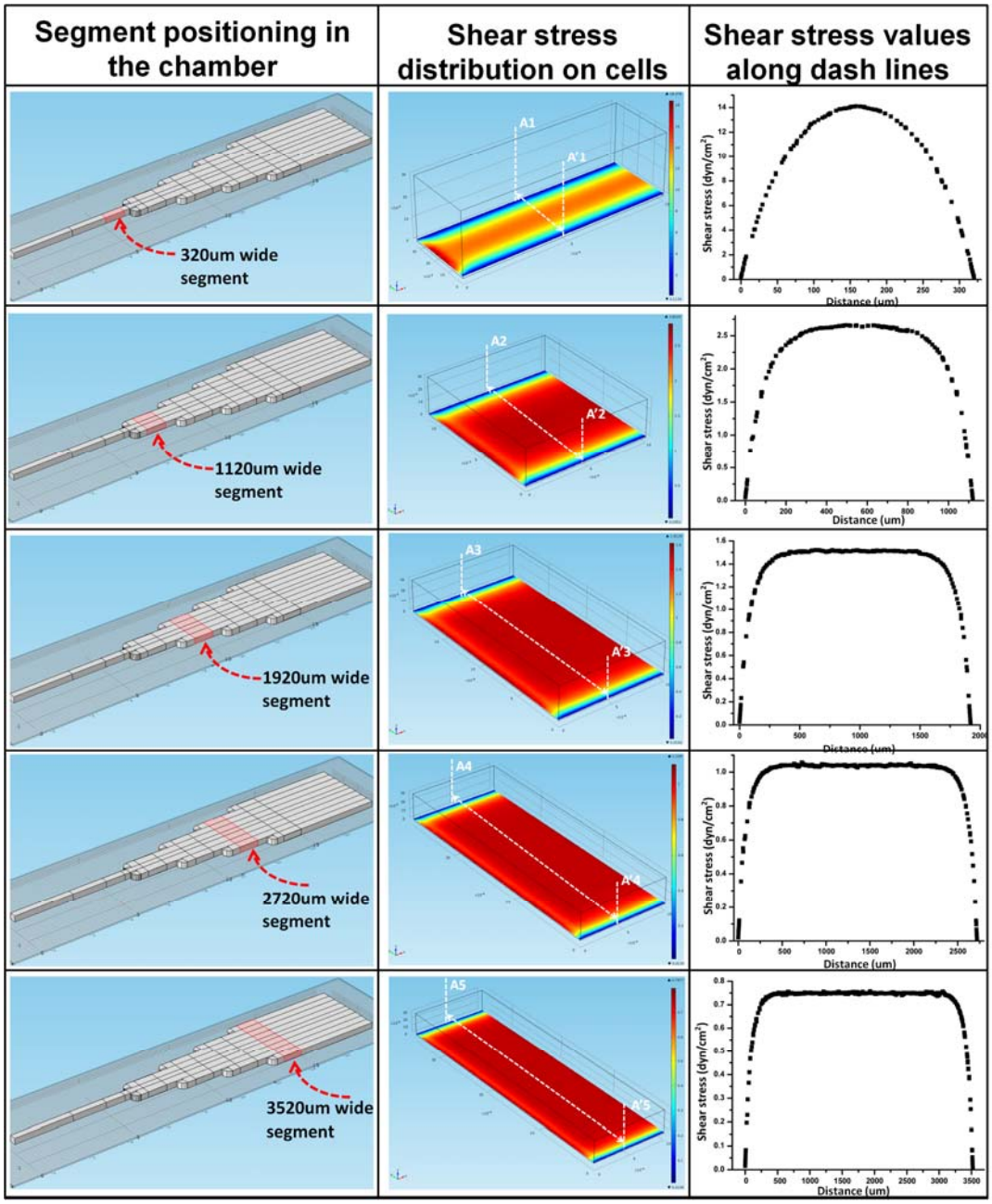


Figure 3.21 FEM simulation results of the shear stress distribution within the chamber. Each selected segment of a specific channel width is highlighted with red in the first column. Second column shows the amplitude of imposing shear stress on culture cells in each segment. Third column plots the shear stress values along the dash line in second column.

## Chapter 3 References


[1] J. R. Lakowicz, *Principles of Fluorescence Spectroscopy*: Springer, 2006.

[2] K. Campbell and A. Groisman, "Generation of complex concentration profiles in microchannels in a logarithmically small number of steps," *Lab on a Chip,* vol. 7, pp. 264-272, 2007.

[3] J. Melin and S. R. Quake, "Microfluidic large-scale integration: the evolution of design rules for biological automation," *Annu Rev Biophys Biomol Struct,* vol. 36, pp. 213-31, 2007.

[4] (2012). *Microfluidics/Hydraulic resistance and capacity*. Available: http://en.wikibooks.org/wiki/Microfluidics/Hydraulic_resistance_and_capacity

[5] A. Brask, *et al.*, "Theoretical analysis of the low-voltage cascade electro-osmotic pump," *Sensors and Actuators B: Chemical,* vol. 92, pp. 127-132, 2003.

[6] S. Zeng, *et al.*, "Electroosmotic flow pumps with polymer frits," *Sensors and Actuators B: Chemical,* vol. 82, pp. 209-212, 2002.

[7] M. Polinkovsky, *et al.*, "Fine temporal control of the medium gas content and acidity and on-chip generation of series of oxygen concentrations for cell cultures," *Lab Chip,* vol. 9, pp. 1073-84, Apr 21 2009.

[8] M. Adler, *et al.*, "Generation of oxygen gradients with arbitrary shapes in a microfluidic device," *Lab Chip,* vol. 10, pp. 388-91, Feb 7 2010.

[9] G. Mehta, *et al.*, "Quantitative measurement and control of oxygen levels in microfluidic poly(dimethylsiloxane) bioreactors during cell culture," *Biomed Microdevices,* vol. 9, pp. 123-34, Apr 2007.

[10] B.-K. Sohn and C.-S. Kim, "A new pH-ISFET based dissolved oxygen sensor by employing electrolysis of oxygen," *Sensors and Actuators B: Chemical,* vol. 34, pp. 435-440, 1996.

[11] Z. Wei, *et al.*, "Imaging fluorescence lifetime modulation of a ruthenium-based dye in living cells: the potential for oxygen sensing," *Journal of Physics D: Applied Physics,* vol. 36, p. 1689, 2003.

[12] C.-C. Wu, *et al.*, "Fabrication of miniature Clark oxygen sensor integrated with microstructure," *Sensors and Actuators B: Chemical,* vol. 110, pp. 342-349, 2005.

[13] M. C. Butler, *et al.*, "A high-throughput biophotonics instrument to screen for novel ocular photosensitizing therapeutic agents," *Invest Ophthalmol Vis Sci,* vol. 51, pp. 2705-20, May 2010.

[14] M. K. Kuimova, *et al.*, "Singlet oxygen in a cell: spatially dependent lifetimes and quenching rate constants," *J Am Chem Soc,* vol. 131, pp. 332-40, Jan 14 2009.

[15] H. J. Hah, *et al.*, "Methylene Blue-Conjugated Hydrogel Nanoparticles and Tumor-Cell Targeted Photodynamic Therapy," *Macromolecular Bioscience,* vol. 11, pp. 90-99, 2011.

[16] X. Lou, *et al.*, "Investigating Photodynamic Efficiency of Tumor Targeted Nanoparticular Photosensitizer Using Microfluidic Chips," *International Conference on Miniaturized Systems for Chemistry and Life Science (uTAS),* pp. 2058-2060, October 2011.

[17] O. C. Farokhzad, *et al.*, "Microfluidic System for Studying the Interaction of Nanoparticles and Microparticles with Cells," *Analytical Chemistry,* vol. 77, pp. 5453-5459, 2005/09/01 2005.

[18] A. D. Meer van der, *et al.*, "A microfluidic device for monitoring siRNA delivery under fluid flow," *Journal of Controlled Release,* vol. 132, pp. e42-e44, 2008.
[19] M. Mellado, *et al.*, "Drug Testing in Cellular Chemotaxis Assays," in *Current Protocols in Pharmacology*, ed: John Wiley & Sons, Inc., 2001.
[20] M. Y. Rotenberg, *et al.*, "A multi-shear perfusion bioreactor for investigating shear stress effects in endothelial cell constructs," *Lab on a Chip,* vol. 12, pp. 2696-2703, 2012.
[21] L. Wang, *et al.*, "Patterning cells and shear flow conditions: convenient observation of endothelial cell remoulding, enhanced production of angiogenesis factors and drug response," *Lab Chip,* vol. 11, pp. 4235-40, Dec 21 2011.
[22] D. Kim, *et al.*, "On-chip evaluation of shear stress effect on cytotoxicity of mesoporous silica nanoparticles," *Anal Chem,* vol. 83, pp. 8377-82, Nov 15 2011.
[23] J. Y. Park, *et al.*, "Cell morphological response to low shear stress in a two-dimensional culture microsystem with magnitudes comparable to interstitial shear stress," *Biorheology,* vol. 47, pp. 165-78, 2010.
[24] J. W. Song, *et al.*, "Microfluidic Endothelium for Studying the Intravascular Adhesion of Metastatic Breast Cancer Cells," *PLoS ONE,* vol. 4, p. e5756, 2009.
[25] J. Lee and J. Kim, "Multiphasic sensory alginate particle having Polydiacetylene Liposome for selective and more sensitive multi targeting detection," *Chemistry of Materials*, vol. 24, pp. 2817, 2012.

# CHAPTER 4 ON-CHIP PDT EFFICACY TEST: PROCEDURE AND RESULTS

As demonstrated in the previous chapter, various therapeutic factors' gradients can be generated on chip and combined together to provide comprehensive microenvironment control on cells. It is necessary to apply this to in vitro cell line models for corresponding PDT efficacy tests. In particular, it is necessary to:

- ✧ Set up on-chip cell test protocols following previous gradient generation and measurement procedures so that they provide identical therapeutic conditions
- ✧ Evaluate cell viability changes under different PDT conditions, especially including the transition zone from low to high cell killing efficiency
- ✧ Develop software programs for automatic data collection and results plotting of PDT efficacy response changes

This chapter describes the details of experiment work, related data collection, and result analysis of on-chip PDT efficacy tests.

## 4.1 Cell culture

Five kinds of cells have been adopted for PDT efficacy screening tests on chip, including C6 glioma cells, 9L glioma cells, MCF-7 breast cancer cells and DI TNC1 cells (astrocyte-derived) for 2D monolayer PDT tests, and Skov3 ovarian cancer cells for 3D spheroid PDT tests. Most of the PDT efficacy tests have been carried out with C6 cells. For testing functionalized NP's selective targeting capability, C6 cells' test results are

compared with DI TNC1, 9L and MCF-7 cells for evaluating the efficacy changes on different cancer cells and non-cancerous cells.

Cell line maintenance and preparation are conducted in a standard method. Take the C6 cell line as an example, the cell culture medium is composed of 500ml DMEM (GIBCO/Invitrogen), 50ml FBS (GIBCO), and 5ml Penicillin Streptomycin (GIBCO). Cells are maintained in a 75mm petri dish with the growth medium in an incubator with atmosphere of 21% oxygen and 5% carbon dioxide at 36.6℃. When the petri dish substrate is fully covered by the cells in monolayer, cells are harvested for passaging or PDT tests. To harvest the cells, cell culture medium is removed and around 1.5ml 0.05% Trypsin-EDTA (GIBCO) is added covering the cells. The dish is left in the incubator for 5mins. Then 3.5ml culture medium is added, and the cells are detached from the substrate and collected in a 15ml Falcon tube through aspiration. The collected cell suspension is centrifuged for 5mins at 1000RPM. Supernatant is removed and the cell pellet is resuspended in fresh culture medium to a specific concentration: either $5.0x10^6$/ml for PDT tests or $1.0x10^4$/ml for cell passaging. The cell number is countered with a haemocytometer. 9L cells, MCF-7 cells, and DI TNC1 cells are maintained in a similar way, while only MCF-7 cells are usually having a higher seeding concentration of around $1.0x10^5$/ml due to its comparatively lower cell dividing rate. DI TNC1 cells share a same culture medium with C6, while 9L, MCF-7 and Skov3 cells are maintained in a medium composed of RPMI (Invitrogen), 10% FBS and 1% Penicillin Streptomycin.

### 4.2 Microfluidic chip preparation for PDT test

Before the PDT efficacy test, the microfluidic chip need to be properly prepared including filling it with corresponding solutions and having target cell lines cultured

inside. In this section, we are describing the chip preparation procedure for a triple layer chip for high-throughput PDT efficacy test on C6 cells regarding the gradient combination of Mathylene Blue concentration, oxygen level and illumination intensity. Although depending on the actual testing therapeutic factors, photosensitizers and cell lines, different chip schemes can be adopted and the chip preparation procedure varies a bit. This example includes almost all the steps could be necessary and exceptions would be brought up in following their own sections.

The fabricated chip is sterilized with 70% isopropyl alcohol (IPA) and then left in a vacuuming desiccator for 1h, which later helps the water based solutions fully fill the cell layer and filter layer. Then the filter layer is filled with Methylene Blue solutions of certain concentrations by suck them in using a syringe. After the residual bubbles vanish, the filter layer is covered with a 100um thick glass cover, which can adhere to PDMS and prevent evaporation from the filter layer during the test. The cell layer is prepared in a similar way by filling it with the cell culture medium. Both inlets and the outlet are covered or filled with the cell culture medium, and a negative pressure is applied using connected syringes at inlets sucking in the medium into the cell layer. After all air bubbles vanish and the cell layer is fully filled with the medium, outlet reservoir is emptied and refilled with prepared C6 cell suspension. Using a same method, C6 cells are sucked into the cell culture channels. By monitoring under the microscope, inlets' negative pressure is removed before the C6 cells could go further into the gradient generator network region, to avoid channel blocking or unpredictable gradient generation during later test steps. Again, remained C6 cell suspension in outlet is removed and replaced with the fresh culture medium. The whole chip is left in the incubator for 1h,

allowing C6 cells attach down to the glass substrate. After that, the gravity flow is set up by inserting needles in the inlets and filling a few media around 50ul in the outlet. It provides a 200Pa pressure difference, which continuously drives the fresh medium through the cell culture channels, allowing for a supply of nutrition and remove of waste. Every 8h, fresh media are added and the outlet waste is removed, until C6 cells within the cell culture channels reach a monolayer and are ready for the PDT test.

### 4.3 Cell Viability assay

Cell viability is evaluated using LIVE/DEAD fluorescence staining after the PDT test. LIVE/DEAD viability kit (Invitrogen) with green fluorescence of Calcein-AM (live cell intracellular esterase activity) and red fluorescence of ethidium homodimer-1 (dead cell losing plasma membrane integrity) is adopted. Calcein-AM and ethidium homodimer-1 are prepared together in DMEM/RPMI with an optimized concentration of 10uM each. Then the solution is introduced into the cell culture channels and the chip is left in the incubator for 10mins (60mins for the Skov3 spheroids staining). After that, cells are imaged using an inverted fluorescence microscope under three conditions: the bright field (for cell positioning within the chip), the green fluorescence channel (live indicator, filter set FITC HYQ), and the red fluorescence channel (dead indicator, filter set TRITC HYQ). Image processing procedure and data collection method are described in the later sections.

### 4.4 Cell test results of PDT efficacy screening

As one important feature of this microfluidic platform, it is adaptable for different kinds of PDT efficacy screening in terms of therapeutic factor combinations. A series of PDT efficacy tests has been carried out with all previous mentioned single therapeutic

factor gradients, and combinations of double or triple therapeutic factor gradients for high-throughput screening. In this section, each kind of test procedure including device operation is described in detail and corresponding PDT efficacy response results are demonstrated.

### 4.4.1 PDT efficacy response tests on a single therapeutic factor

**Photosensitizer concentration**

Photosensitizer concentration response is tested with both Methylene Blue free dye and Methylene Blue incorporated functionalized NPs. For Methylene Blue, a single cell layer chip with nine cell culture channels is used. Pure DMEM and 10uM Methylene blue in DMEM are introduced into the chip using a syringe pump with a flow rate of 1ul/min for both. After 10mins' stabilization of Methylene Blue concentration in each channel, the chip is moved to the single LED light source and illuminated for the PDT treatment. After that, the LIVE/DEAD staining solution is introduced for cell viability evaluation. For functionalized NPs, a single cell layer chip with thirteen cell culture channels is used. Pure DMEM and 1mg/ml NPs in DMEM are fed into the chip using the gravity flow setup. After 1h's feeding, both inlet reservoirs are emptied and refilled with fresh DMEM, which continues the gravity flows for another 2h. In this case, the NP solutions flow through the cell culture channels for 1h, and then the DMEM refreshes the channels. It is noteworthy that instead of generating a culture time gradient along the cell culture channel, cells are experiencing a same culture duration with NPs since the NP solution is introduced and washed away under a same flow rate. After that, the chip is mounted on the red LED array light source and illuminated for 30mins ($42.8J/cm^2$). Then cells are stained for viability assay.

Figure 4.1 shows the results of PDT efficacy changes under different Methylene Blue concentrations. From top to bottom channel, Methylene Blue concentration decreases from 10uM to 0uM. Figure 4.1 (a) shows the cell viability distribution after 10mins' illumination (28.7J/cm$^2$), in which some cells in high Methylene Blue concentration channels are already killed. Figure 4.1 (b) shows the cell viability distribution after another 10mins' illumination (total 57.5 J/cm$^2$), in which cells in top four channels are almost all killed and clearly it shows a transition of PDT efficacy change from high to low at channel 5. Notably, the increase of illumination dose enhances the PDT efficacy in general comparing these two results, and also it demonstrates a threshold concentration, below which PDT efficacy does not improve much even with higher illumination dose.

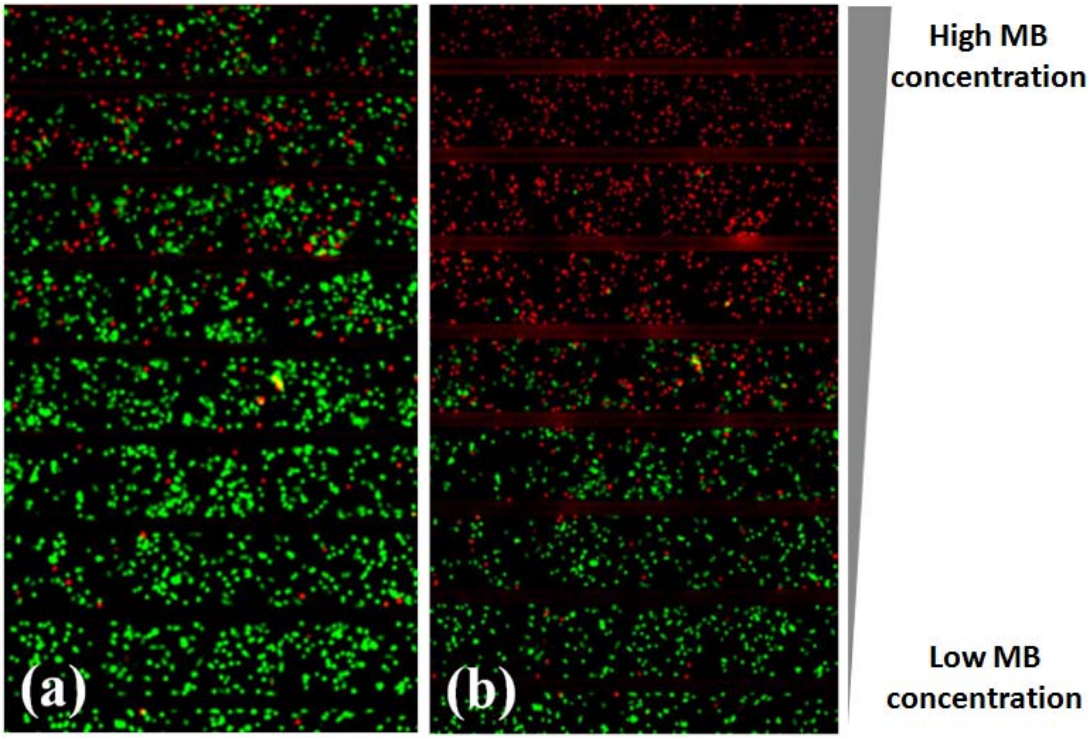


Figure 4.1 C6 cells after live/dead staining showing that viability changes according to the Methylene Blue concentrations from highest (top channel) to lowest (bottom channel) with an illumination of (a) 10mins and (b) 20mins, respectively.

Figure 4.2 shows the results of PDT efficacy changes under different functionalized NPs concentrations. As shown in the enlarged parts, C6 cells incubated with a high NP concentration (1mg/ml) are having more NPs attached and showing brighter FITC fluorescence than the low NP concentration (0mg/ml). After PDT illumination, the cell viability gradually decreases as the incubated NP concentration increases.

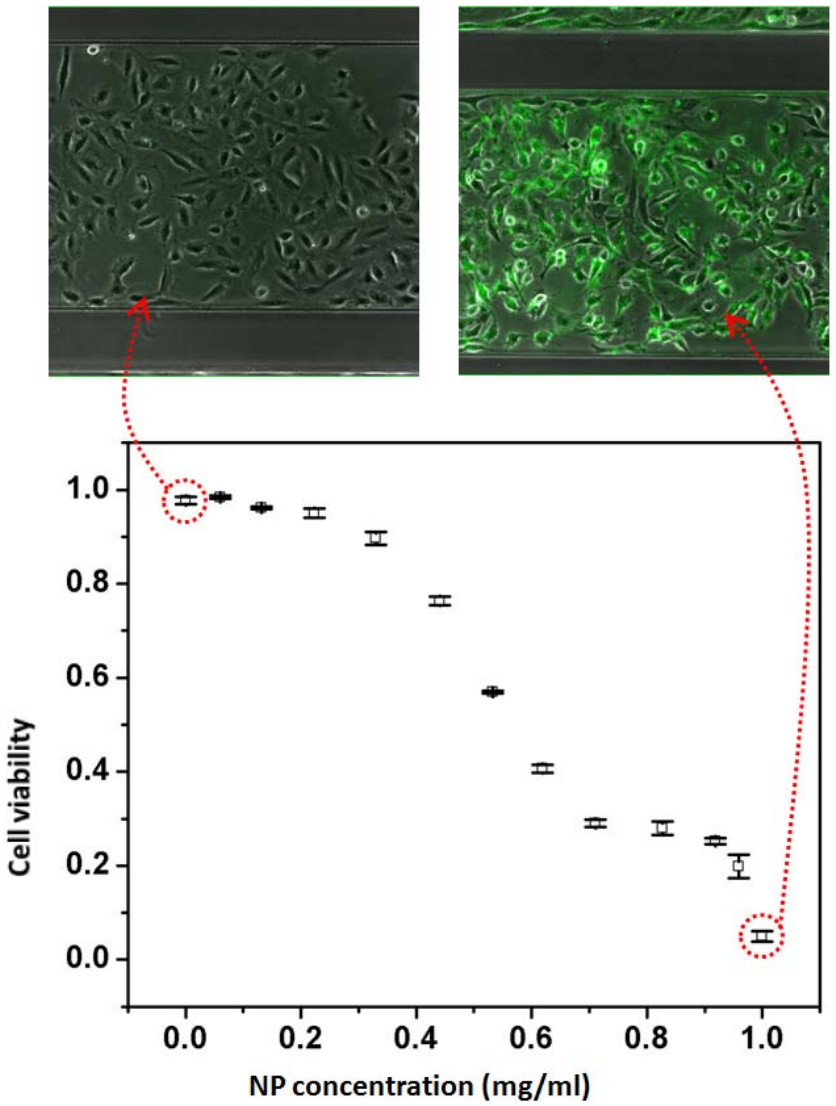


Figure 4.2 C6 cells show a viability decrease after PDT treatment as the incubated NPs concentration increases. The enlarged parts show the cells cultured with a higher concentration of NPs are having more NPs attached on cells, indicated by the NP incorporated FITC fluorescence. Cell viability data is expressed as the mean and standard deviation.

**Oxygen concentration**

The oxygen concentration response is tested with Methylene Blue free dye on C6 cells using a double layer chip composed of the cell layer and the gas layer, which both have nine channels. A same solution of 10uM Methylene Blue in DMEM is introduced into the chip from both inlets using a gravity flow setup providing a pressure difference of $1.0x10^4$Pa. After 10mins, the pressure difference is brought down to zero making the flow halt. Then, compressed air and nitrogen are connected to the gas layer inlets both under a pressure of 5psi. After another 10mins allowing oxygen concentration gradient generation and reaching equilibrium in the cell layer, the chip is moved to the single LED light source and illuminated for 25mins (71.9 J/cm$^2$), during which the gases are continuously supplied. Then the cells are stained for viability assay.

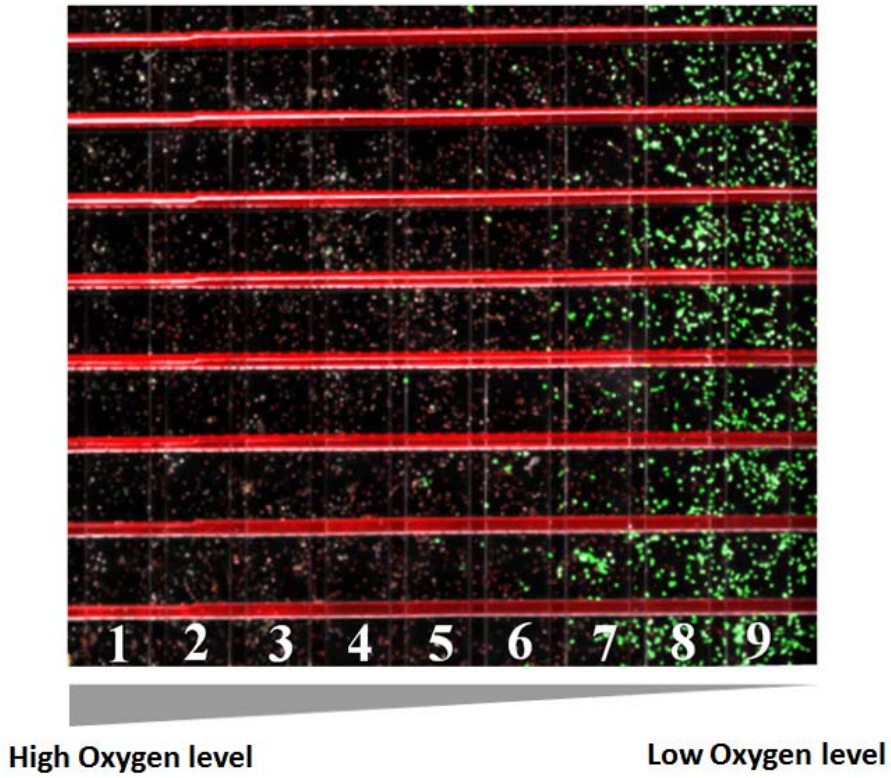


Figure 4.3 C6 cells after live/dead staining show their viability changes according to oxygen concentration gradient from highest (channel 1) to lowest (channel 9).

Figure 4.3 shows the results of PDT efficacy response of oxygen concentration gradient. From left (channel #1) to right channel (channel #9), oxygen concentration decreases from around 19.1% to 1.4%. While comparing the horizontal cell culture channels from top to bottom, C6 cells are showing a similar viability since all channels are filled with a same 10uM Methylene blue solution. But from left to right, C6 cells are showing a viability rate transition from low to high as the oxygen concentration decreases.

**Illumination intensity**

Illumination intensity/dose response is tested with Methylene Blue free dye on C6 cells using a double layer chip, including the filter layer and an open cell culture chamber as the cell layer. The filter layer is prefilled with two different concentrations of Methylene Blue solutions (50mg/ml and 12.5mg/ml). C6 cells are cultured in the open chamber with a starting intensity around $1.0x10^6$/ml. After reaching a monolayer, 10uM Methylene Blue in DMEM is added to the chamber and the chip is moved to the single LED light source and illuminated for 25mins (71.9 J/$cm^2$). Then the cells are stained for viability assay.

Figure 4.4 shows the results of PDT efficacy response of illumination intensity gradient. As mentioned previously, the filter layer is generating repeated grayscale patterns of illumination. As the result of the overall area shows, the cell viability distribution is showing corresponding repeated patterns changing from low viability (red fluorescence dominant) to high viability (green fluorescence dominant). The enlarged part shows the cell viability of the corresponding area of 4x4 grayscale pattern grids. The

C6 cells are showing a gradually viability increase from the highest illumination intensity area (1D) to the lowest illumination intensity area (4A).

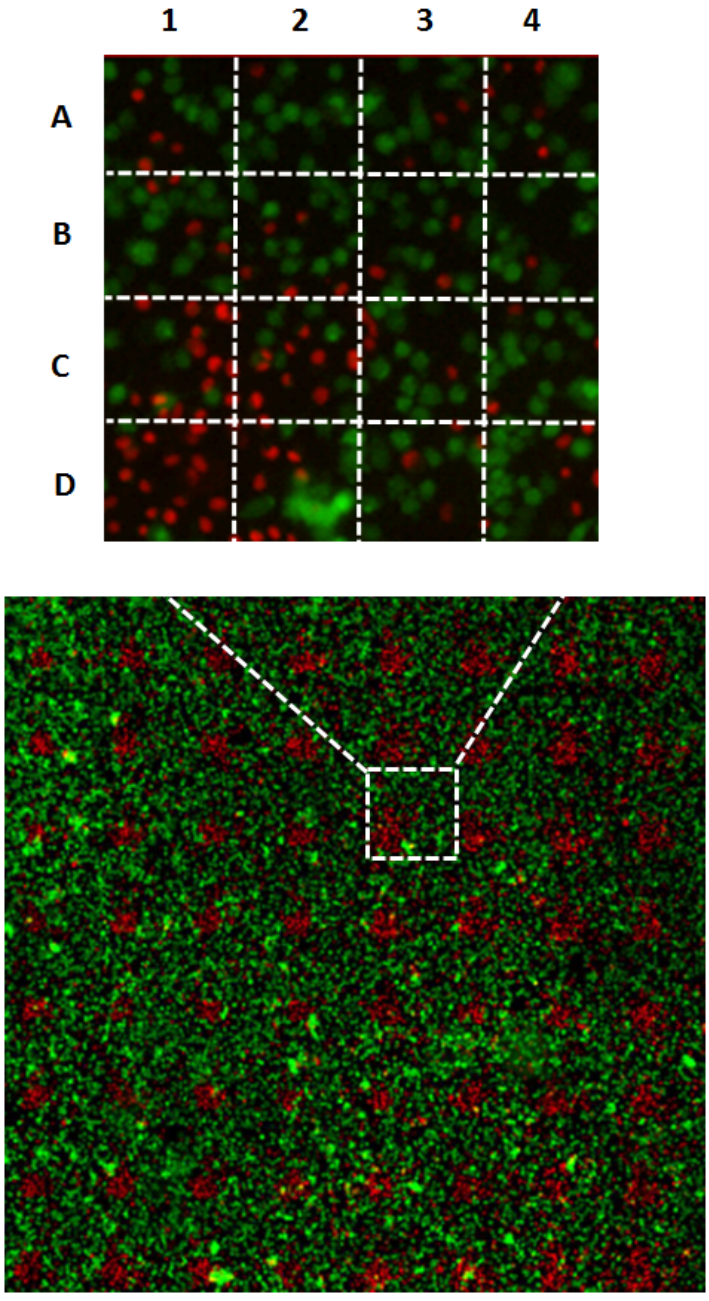


Figure 4.4 C6 cells after live/dead staining show that the viability rate changes according to the transparency of integrated liquid filter. The enlarged part shows the result from a corresponding 4 by 4 grids gray scale pattern, with highest transparency at 1D and lowest transparency at 4A.

**Incubation time**

Incubation time response is tested with Methylene Blue incorporated NPs on C6 cells using a single cell layer chip. 1mg/ml NPs in DMEM are fed into the chip through both inlets with a gravity flow driven by 200Pa pressure difference. After 90mins' loading, outlet reservoir is emptied and refilled with fresh DMEM. A negative pressure is applied at the inlets sucking in the fresh DMEM and washing away unattached NPs. After 5mins' washing, the chip is mounted on the red LED array light source and illuminated 30mins ($42.8J/cm^2$). Then the cells are stained for viability assay.

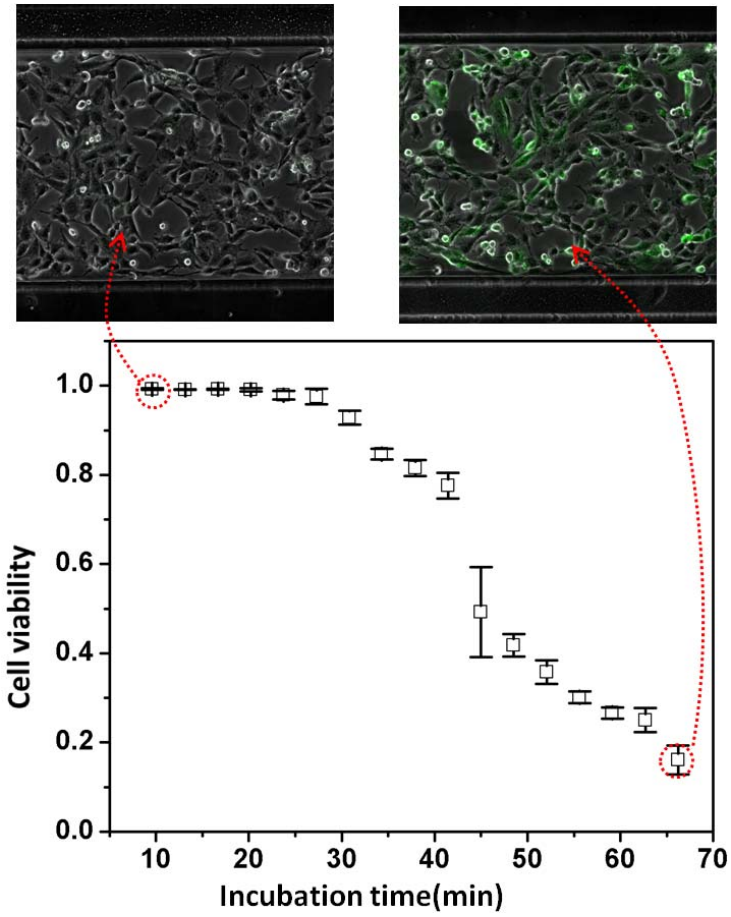


Figure 4.5 C6 cells shows a viability decrease after PDT treatment as the incubated time with NPs increases. The enlarged parts display the cells cultured with longer time are having more NPs attached on them. Cell viability data is expressed as the mean and standard deviation.

Figure 4.5 shows the results of the PDT efficacy response of NP incubation time gradient. As shown in the enlarged parts, with a same NP concentration (1mg/ml) C6 cells incubated with a longer duration (66mins) are having more NPs attached and showing brighter FITC fluorescence than shorter incubation duration (10mins). And after same PDT illumination, the cell viability shows a gradual decrease as the previous incubation time increases.

### 4.4.2 PDT efficacy response test on double therapeutic factors

The capability of PDT efficacy screening with the combination of two therapeutic factors is demonstrated by combining the photosensitizer concentration and oxygen concentration gradients. A double layer chip, including both cell layer and gas layer with nine channels is used in this test. Pure DMEM and 10uM Methylene Blue in DMEM are introduced into the chip from the two inlets using a gravity flow setup with a pressure difference of $1.0x10^4$Pa. After 10mins, the pressure difference is brought down to zero making the flow halt and maintaining the Methylene Blue gradient within the cell culture channels. Then, compressed air and nitrogen are connected to gas layer inlets both under a pressure of 5psi. After another 10mins allowing the oxygen concentration gradient generation and reaching equilibrium, the chip is moved to the single LED light source and illuminated for 15mins (43.1 J/cm$^2$). Then the cells are stained for viability assay.

Figure 4.6 shows the result of cell viability distribution after the PDT treatment. In general it shows a cell viability decrease from the right bottom corner (low photosensitizer concentration + low oxygen concentration) to the left up corner (high photosensitizer concentration + high oxygen concentration). This kind of cell viability rate transition suggests it is essential to provide both sufficient level of photosensitizer

and oxygen to make the PDT treatment effective under a given illumination dose. Comparing to the previous test results of single therapeutic factors, it shows similar efficacy changes under overlapping PDT conditions.

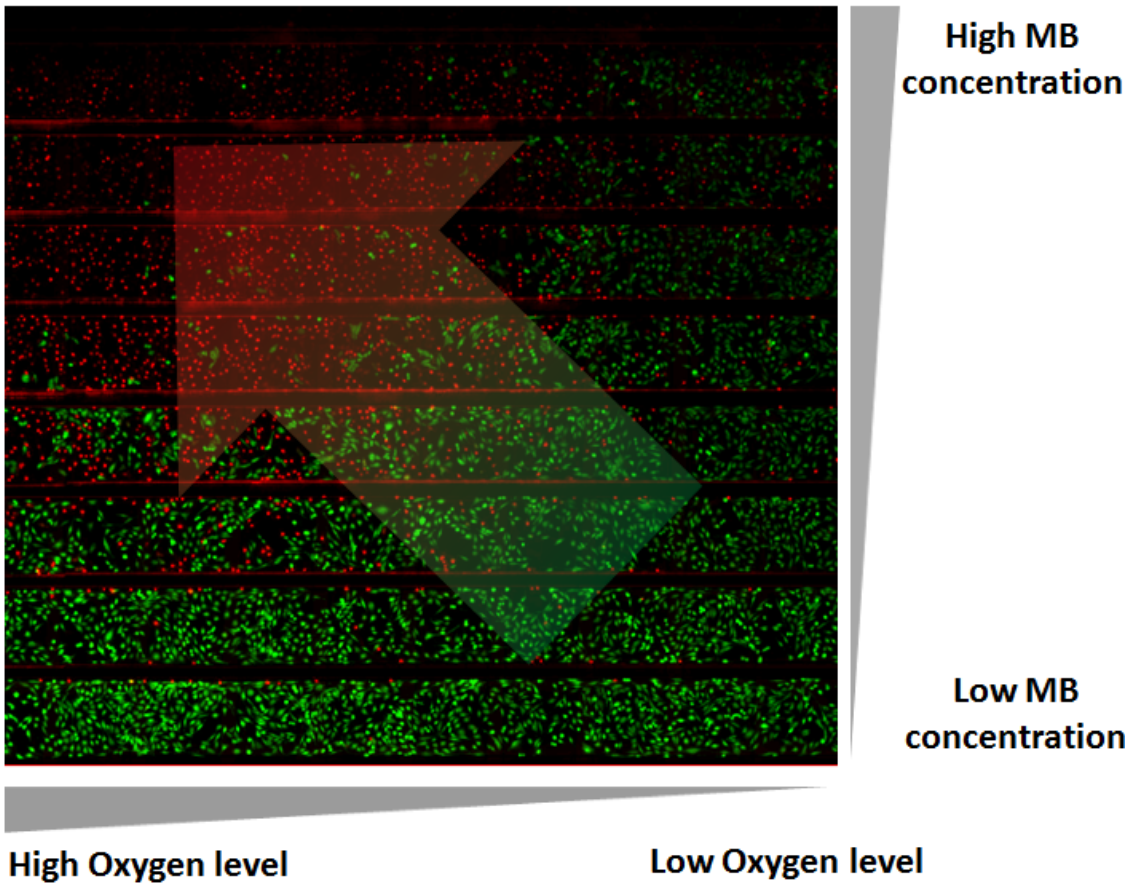


Figure 4.6 C6 cells after live/dead staining show that the viability changes depending on both the oxygen level gradient from highest (left) to lowest (right) and the MB concentration from highest (top channel) to lowest (bottom channel).

### 4.4.3 PDT efficacy response test on triple therapeutic factors

The capability of PDT efficacy screening with the combination of three therapeutic factors is demonstrated by combining the photosensitizer concentration, oxygen concentration and illumination intensity gradients. A triple layer chip including the filter, cell and gas layers is used in this test. The filter layer is composed of a single PDMS layer, which is prefilled with 50mg/ml Methylene Blue. The cell and gas layers are same

as the previous section. Mathylene Blue and oxygen gradient are also generated and maintained in a same procedure. After that the chip is moved to the single LED light source and illuminated for 30mins (86.2 J/cm$^2$). Then cells are stained for viability assay.

Figure 4.7 shows the result of cell viability distribution after PDT treatment. In general it shows the cell viability decreases following the increase of all three factors: photosensitizer, oxygen and illumination. The enlarged part shows the 4 levels of transparency/illumination intensity generated by the filter layer, and a same grayscale pattern is repeatedly arranged all over the active test area. This kind of test straightforwardly demonstrates how the three key elements in PDT mechanism are affecting its efficacy and could provide guidance in later animal or in vivo trials.

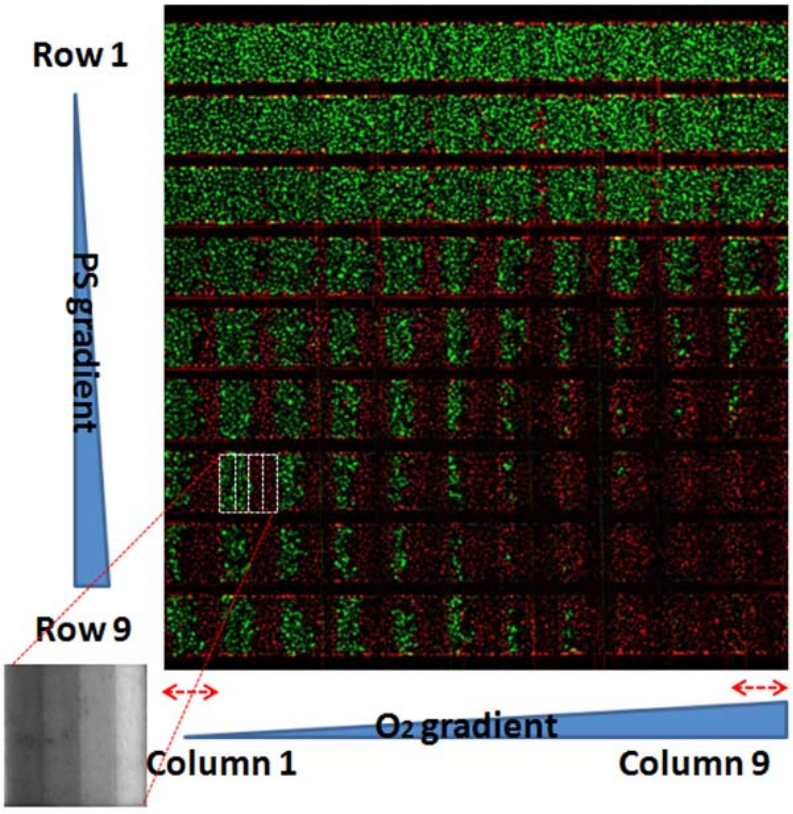


Figure 4.7 Image of the C6 cell viability distribution of high-throughput PDT efficacy test combining the gradients of Methylene Blue (photosensitizer), oxygen and illumination intensity. 9 horizontal channels are filled with 9 different

concentrations of Methylene Blue (from lowest in top to highest in bottom). 9 oxygen levels are applied in 9 vertical columns (from lowest in left to highest in right). Within each overlapped area of a horizontal and a vertical channel, the gray scale filter provides 4 levels of illumination intensity during the PDT exposure, as shown in the enlarged part.

### 4.4.4 Nanoparticular photosensitizer's specific targeting on cancer cell lines

As mentioned previously, four different cell lines including C6, DI TNC1, 9L and MCF-7 have been adopted for the screening test of functionalized NPs' selective targeting in PDT treatment and resulted efficacy changes. In this test, a single cell layer chip having individual inlet and outlet for each cell line is used. All cell culture channels are prefilled with culture media. Considering the difference of dividing rate, MCF-7 cells are introduced into its cell culture channel earlier than other cells. After MCF-7 cells have covered more than 80% of the substrate area, the rest three cell lines are introduced into their own culture channels. All cell lines are cultured until reaching a similar monolayer within the cell culture channels. During the test, a same 1mg/ml concentration NPs in DMEM/RPMI is introduced to each cell line and the cells are cultured with NPs for 1h. After that, fresh DMEM/RPMI is introduced washing away residual NPs and the chip is mounted on the red LED array light source for PDT illuminated. Then the cells are stained for viability assay.

Figure 4.8 shows the test procedure and the results comparing PDT efficacy responses of C6 and DI TNC1 cells. After filling with a same concentration NP solution, both cell culture channels are showing a similar FITC fluorescence (pseudo-colored with blue) from the NPs. After 1h's culture and the washing step, only the C6 cell side channel is having the fluorescence remaining there, verifying that NPs are selectively attached to the C6 cells. As a result of that, C6 cells can be "selectively" killed during the following PDT treatment, while DI TNC1 cells remain alive. As shown in Figure 4.8(c) and (d), C6

cells are gradually killed as the PDT illumination dose increases from 21.4J/cm$^2$ (15mins illumination) to 42.8 J/cm$^2$ (30mins illumination) but DI TNC1 cells survive to the end.

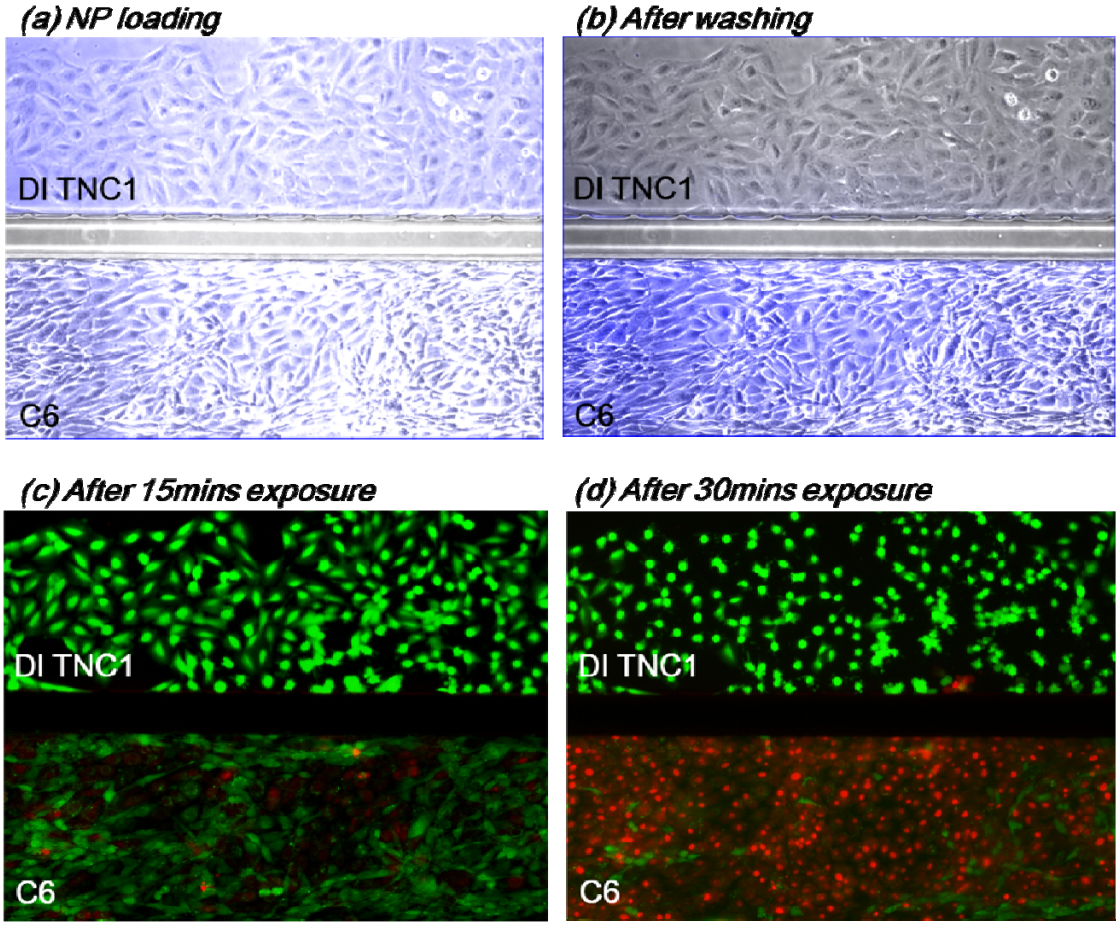


Figure 4.8 (a) DI TNC1 cells (upper) and C6 cells (bottom) after incubation with the same NPs (fluorescence pseudo-colored with blue) solution. (b) Cell images after the NP solution is washed away. Cell viability results after (c) 21.4 J/cm$^2$ and (d) 42.8mJ/cm$^2$ PDT illumination. (Green: live cells, red: dead cells).

Figure 4.9 shows the comparing results of PDT efficacy responses of 9L and MCF-7 cells. Green color shows the FITC fluorescence of NPs. For the cell viability assay, only ethidium homodimer-1 (red) is included for staining dead cells and unstained cells are considered being alive. As the result shows, both 9L and MCF-7 cells could have NPs attached and making the following PDT illumination effective on them. Comparatively,

9L cells are having more NPs attached and showing stronger FITC fluorescence, which results in higher PDT efficacy for 9L cells than MCF-7 cells.

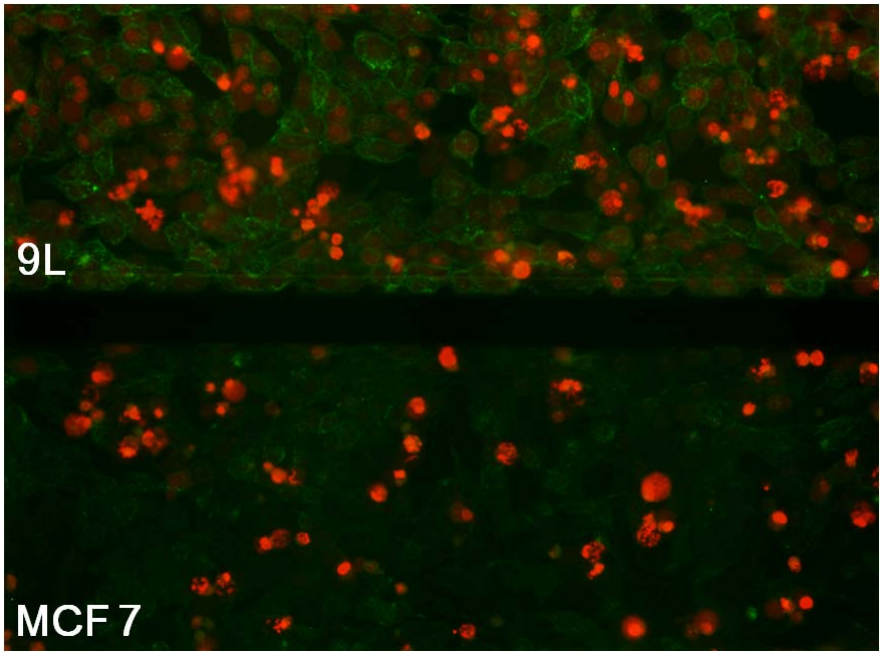


Figure 4.9 The fluorescence image comparing the NP efficacy on 9L and MCF-7 cells after PDT treatment. The green fluorescence shows the attached NPs with FITC incorporated inside and the red fluorescence staining shows the cells killed during the PDT illumination.

### 4.4.5 Shear stress's effects on nanoparticular photosensitizer delivery

Effects of shear stress on nanoparticular photosensitizer delivery to cancer cells are evaluated with a single cell layer chip. The microfluidic channel dimensions are same with the FEM demonstrated in the previous chapter: a uniform channel height of 300um, step-increasing channel widths of 320um, 1120um, 1920um, 2720um and 3520um in serial segments, and each segment has a length of 1920um or above. After C6 cells are cultured into a monolayer, the NP solution is introduced into the chip utilizing a gravity flow set up providing a pressure difference around 100Pa. The NP solution is prepared with concentration of 0.1mg/ml in DMEM and the introductory flow is maintained for 10 minutes allowing NPs attaching to the cells. After that, fresh DMEM is introduced to

wash away unattached NPs, for another 10 minutes. Finally, the cells are imaged under the fluorescence microscope to determine the NPs attachment and distribution.

NP attachments under different shear stress are compared. The result shows that a lower shear stress level makes it easier for the NPs to attach on cells. Besides that, the size of NPs is also having an important impact on attachment. Two types of NPs have been tested separately here, one of which is have an average size of 64nm and the other is 145nm. As shown in Figure 4.10, for small NPs, attachment on cells under different shear stress is similar, while for the large NPs delivery, there is obviously more attachment on cells under low shear stress conditions than high shear stress conditions.

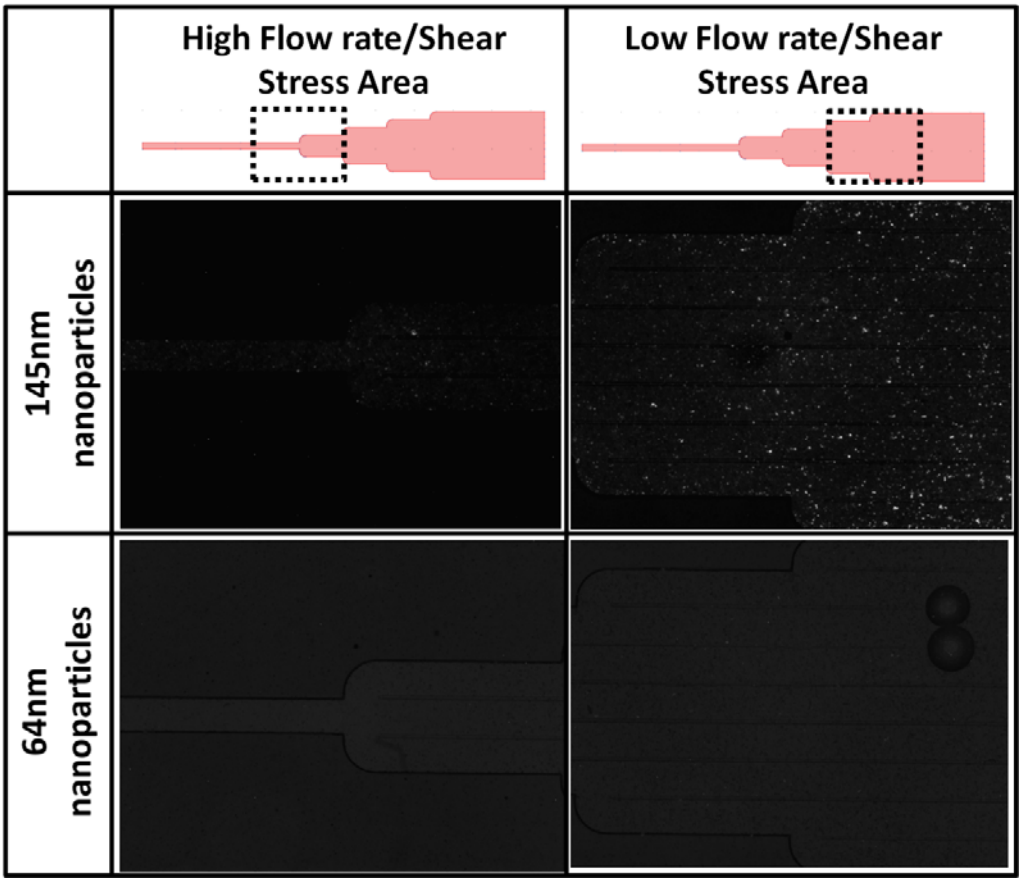


Figure 4.10 Different NP attachment distributions under different shear stress.

Figure 4.10 provides an enlarged view of different size NPs' attachment on C6 cells. Both NPs show attachment to the cells under either low or high shear stress conditions. But only the large NPs are showing an obvious difference of more attachment under low shear stress, especially in the form of large NP aggregates. Another thing worth noticing here is that even under high shear stress, there is still NP attachment to the cells for the large NP sample. One possible reason for that is the NP sample is never perfect in terms of size distribution. Even for the large NP sample, there is always a small portion of small NPs included having a diameter below 30nm, which could attach under even high shear stress (Appendix A). A general understanding is that smaller size particles or molecules are easier to deliver and attach to the cells, as implied in previous research [1].

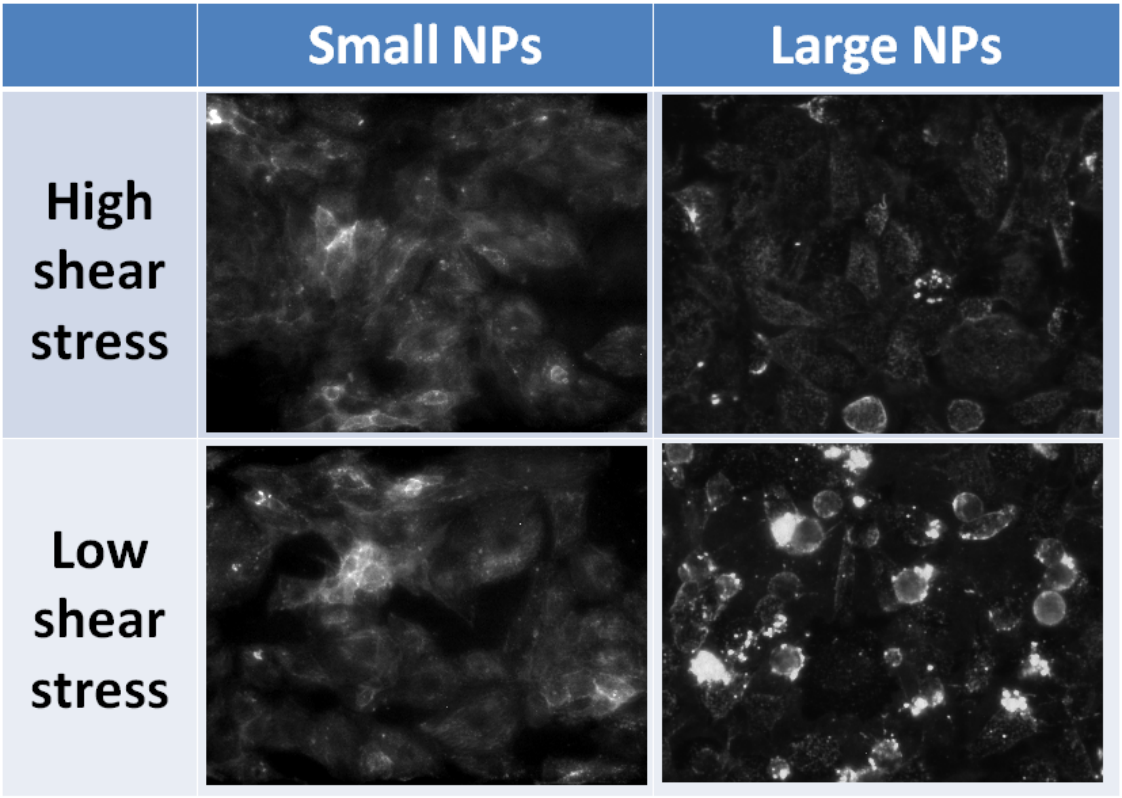


Figure 4.11 Enlarged view of different NPs' attachment distribution under different shear stress. Large NPs are more tending to form aggregates and displays an obvious attachment difference between high and low shear stress conditions.

Another phenomenon confirming the effect of shear stress on large NP delivery is the "edge effect" as shown in Figure 4.12 . As shown by previous FEM simulation, shear stress at the edge area of the microfluidic channel is having a sharp drop to around zero, which makes a low shear stress area ideal for large NP aggregation.

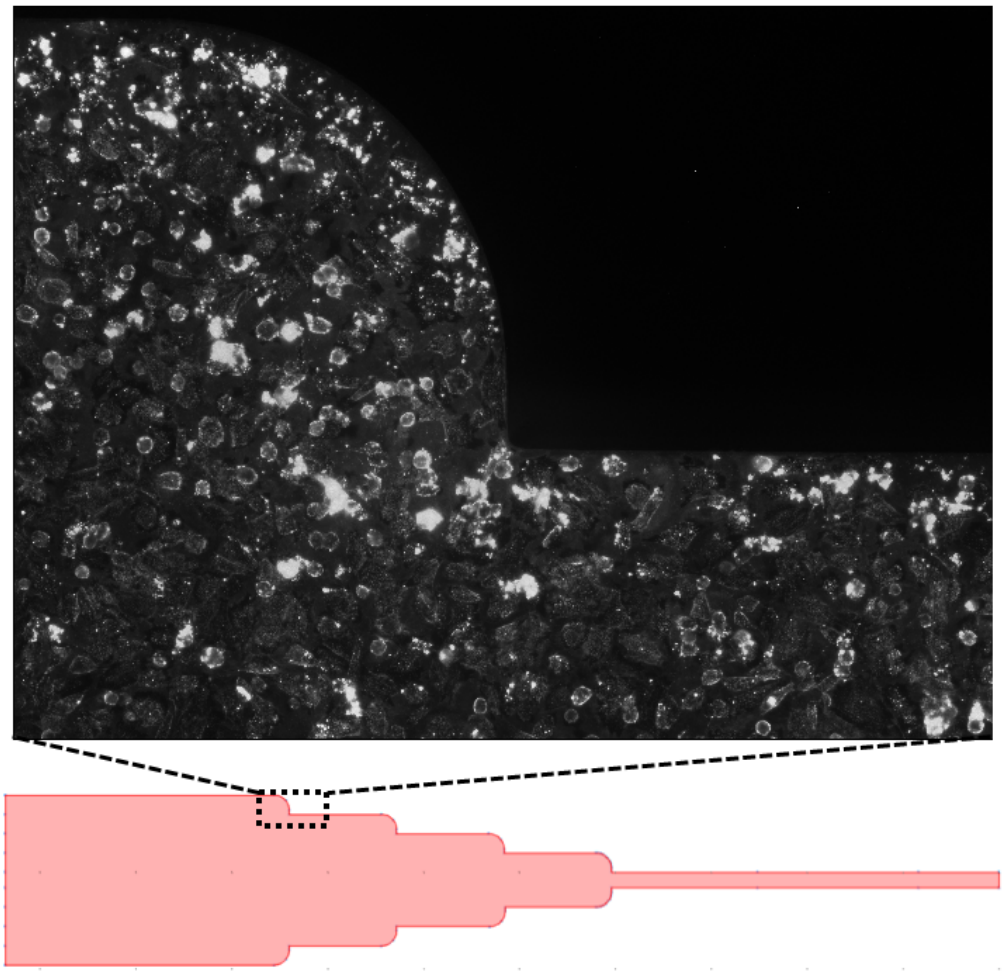

Figure 4.12 Large NPs (average at 145nm) distribution at the edge area of microfluidic channel, where there is a great shear stress drop allowing easier NP attaching to cells.

### 4.4.6 3D spheroid model for PDT efficacy test

The Skov3 ovarian cancer cell line is used as the example of 3D spheroid formation and PDT efficacy test. Not all cancer cell lines are capable of forming in vitro spheroids themselves and the morphology of spheroids is affected by a bunch of different factors

including the culture medium and possible supports from additional cell types [2, 3]. C6, Skov3 and 9L cells have been tested form spheroid formation in this platform with the same culture media for maintenance. While both C6 and Skov3 cells form compact spheroids, 9L cells remain in the form of dispersed aggregates after 1d culture. Details of the chip preparation and test procedure are described in this section. As a new in vitro model for PDT efficacy test in chip, results of 3D spheroids are compared with those of 2D monolayers, and the effects of spheroid size on PDT efficacy are also discussed.

**3D spheroid formation**

One major extra preparation step for 3D spheroid chips is the surface coating of F108 on PDMS to prevent cell attachment [4, 5]. After vacuumed in desiccator for 1h, the chip is filled with 1% (w/v) Pluronic F108 (BASF) and left in the incubator for 1h, allowing the residual bubbles to vanish and the F108 to coat on PDMS. Then the cell culture medium is introduced into the chip washing away the F108 solution. The washing is driven by a 35Pa pressure difference, repeated for 3 times, and lasts 10minutes each time. After the final washing, the chip is filled with the medium and ready for cell loading.

As mentioned previous, besides the chip design, cell loading protocol also affects how many cells can be delivered into each microwell and the final size distribution of spheroids [5-7]. Basically two cell loading protocols, which are called protocol A and B, have been tested and resulted in pretty different spheroid size distributions. As shown in Figure 4.13, protocol A makes comparatively more uniform-sized spheroids, regardless of the difference in microwell size (a), while protocol B makes more distinctive spheroids, of which the smallest ones are composed of only several cells and the largest ones are having hundreds of cells (b).

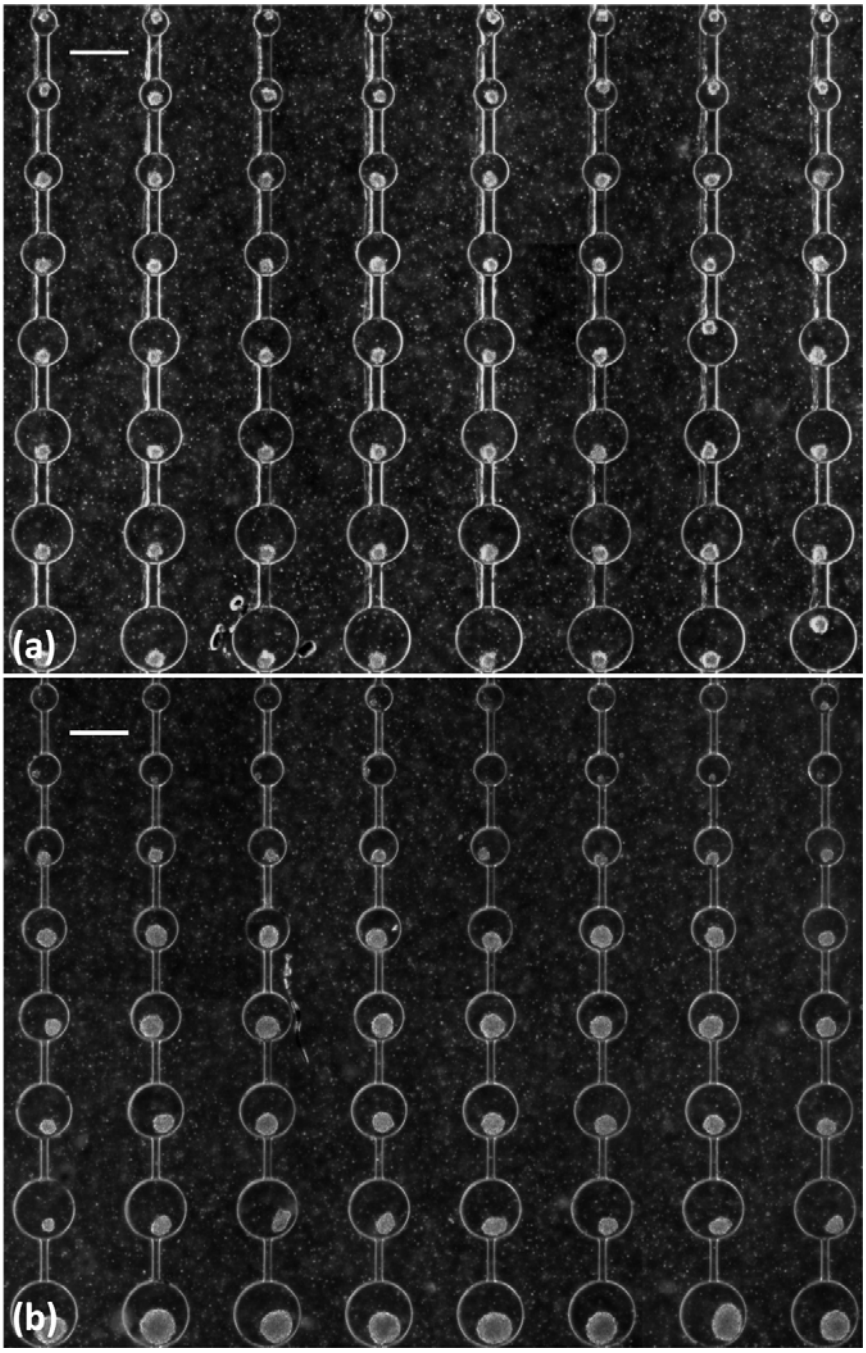


Figure 4.13 3D spheroids formation in the microfluidic microwell array chip utilizing cell loading protocol A (a) and protocol B (b), Scale bar: 400um.

For both protocols, Skov3 cell suspension with a concentration of $5x10^6$/ml is prepared for cell loading. In protocol A, the inlet is added with 100ul cell suspension and the outlet is added with 60ul culture medium, which generates a pressure difference

around 14Pa driving a feeding flow directing from the small microwells towards the large microwells. During this loading process, some of the cells would naturally settle down in the microwell while the others would pass through it. After 15minutes loading, both inlet and outlet are emptied and refilled with fresh culture medium, which has a volume of 100ul in the inlet and 60ul in the outlet. The fresh medium flow helps remove any residual cells in the microfluidic channels and continuously provides nutrition during the following over-night culture. In protocol B, cell loading is composed of two steps. In step one, the inlet is added with 150ul cell suspension and outlet is added with 50ul culture medium, which provides a 35Pa pressure difference driving a feeding flow directing from small microwells to large microwells. This step continues for 5minutes. In step two, inlet is added with 50ul medium and outlet is added with 150ul cell suspension, which drives a reversed feeding flow from large microwells to small microwells. This step continues for 8minutes. After that, both inlet and outlet are filled with fresh medium similar with protocol A, washing away residual cells and providing nutrition supply for cell culture.

During the culturing process, gradually cells within the same microwell aggregate together and form a single compact spheroid within 10hours, as shown in Figure 4.14. Also it is shown here that the difference in spheroid size pretty much reflects the difference in initial cell numbers in each microwell. Several factors are considered contributing to the different results between protocol A and B. The first is the feeding flow rate, under high flow rate (protocol B) cells are more likely to pass by the smallest microwells than under low flow rate (protocol A), while those cells would still be able to settle down in the larger size microwells. As a result of that, in protocol A, tens of cells can settle down in the smallest wells while in protocol B only several cells are there. A

second factor is the feeding duration, which in combination with flow rate contributes to the overall cells number fed into the chip. Within the first several minutes of protocol A, there are more cells in the small microwells than the large wells. The reason for that is the cells are tending to fill in the upstream microwells first before starting filling the downstream microwells. Only after a long-enough feeding duration, cell numbers in the large wells are going to catch up or even slightly exceed those in small wells, as shown in Figure 4.13. The third factor is the feeding direction. Generally cells are more tending to settle down in the upstream microwells so long as the flow rate allows and the wells have not been full. That explains why in protocol A there is not any large spheroid since the large wells in the downstream never get the chance to receive that many cells. However, in protocol B there is a process of reverse direction loading, which helps fill the large wells in priority and form much larger spheroids.

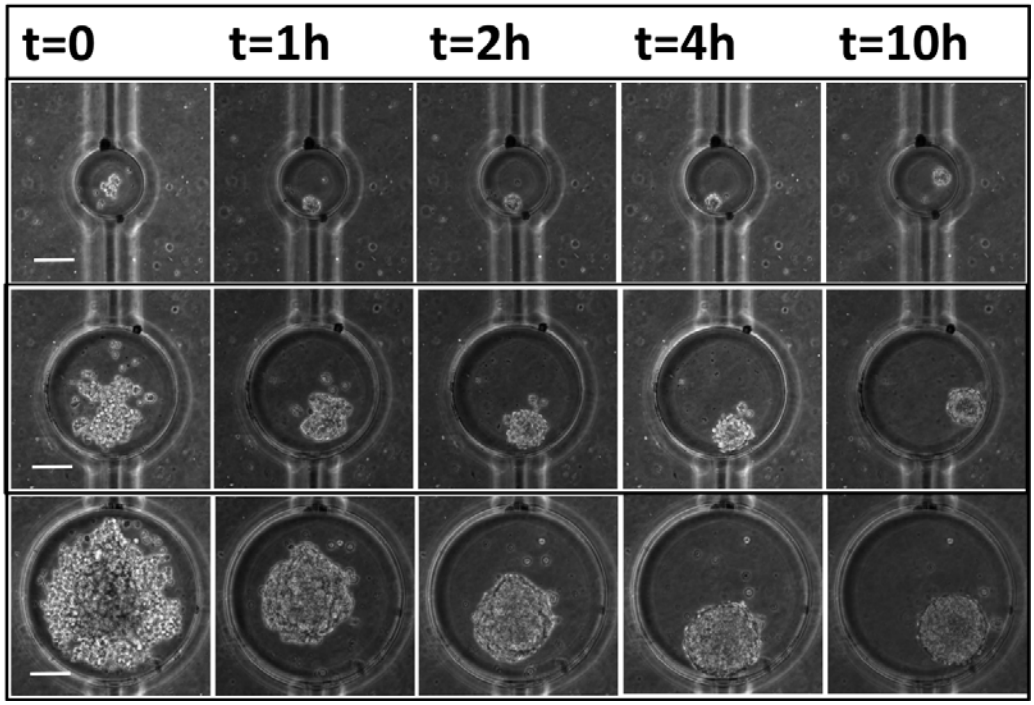


Figure 4.14 Time lapse recording of Skov3 spheroids formation within different size microwells loaded using protocol B. Scale bar: 100um.

During the tests of setting up the protocols, we also optimized the feeding cell concentration to be around $5x10^6$/ml. A too low concentration would take too long time filling the microwells and a too high concentration makes the cells more likely to clog the microfluidic channels.

**PDT efficacy test on spheroids**

First, PDT efficacy is compared between Skov3 cells in a 2D monolayer and a 3D spheroid. Both Methylene Blue free dye and functionalized NPs are tested for their PDT efficacy changes. For the former, 10uM Methylene Blue in RPMI is introduced into the chip and the cells are illuminated for 30minutes (totally 59J/cm2). After another 10minutes wait (allowing the cells to die), live/dead staining solution is added and images are taken after 60minutes' staining. For the latter, 5mg/ml NP solution is added into the chip and the spheroids are incubated with NPs for 1h. After that, residual NPs are washed away with fresh RPMI for 10minutes. Spheroids are illuminated for 1h (totally 118J/cm2) and stained for viability evaluation after a same 10minutes wait. A summative result is demonstrated in Figure 4.15. Generally for both photosensitizers, 3D spheroids display much stronger resistance to PDT treatment than the 2D monolayers. While almost all the cells in monolayer are killed during the PDT process, a significant portion of them within the spheroids are still alive, which is consistent with previous reports of similar comparisons [8, 9]. Another thing worth notice is the difference of live cell distribution in the spheroids treated with Methylene Blue and the functionalized NPs. For the former condition, remained live cells are distributing all across the whole spheroid, while for the latter condition, live cells are mostly restricted within the central space of spheroid. Similar phenomenon is observed in latter tests as shown in Figure 4.16 .

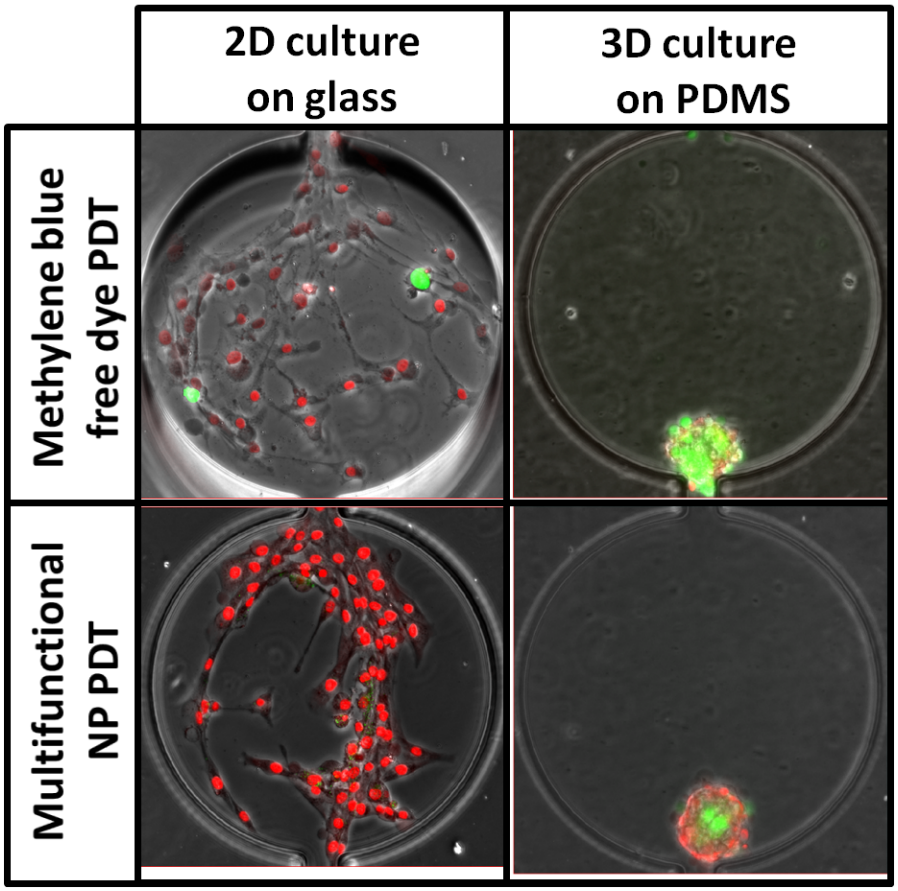


Figure 4.15 Cell viability staining results after PDT test comparing the efficacy under two in vitro models (2D monolayer and 3D spheroid) and two types of photosensitizers (Methylene Blue free dye and functionalized NPs).

Second, relying on the chip's high throughput capability, the influence of spheroid size on PDT efficacy is also examined. Both Methylene Blue and functionalized NPs are tested on various size Skov3 spheroids, following a same protocol as described in the previous paragraph. As shown in Figure 4.16, generally larger size spheroids appear to be more resistant in PDT treatment, which is consistent with related results reported earlier [10, 11]. The smallest spheroids in the smallest microwells can be radically killed during the PDT treatment but as the spheroid size increases, a larger and larger portion of cells in the spheroid survive. Compared to Methylene Blue treated spheroids, NP treated ones are more apparently to have a boundary between killed cells and survived cells. One

reason for that might be the nanoparticles are having a much larger size than Methylene Blue free dye and are more likely to aggregate at the peripheral space of the spheroid, which results in a more focused PDT effect there.

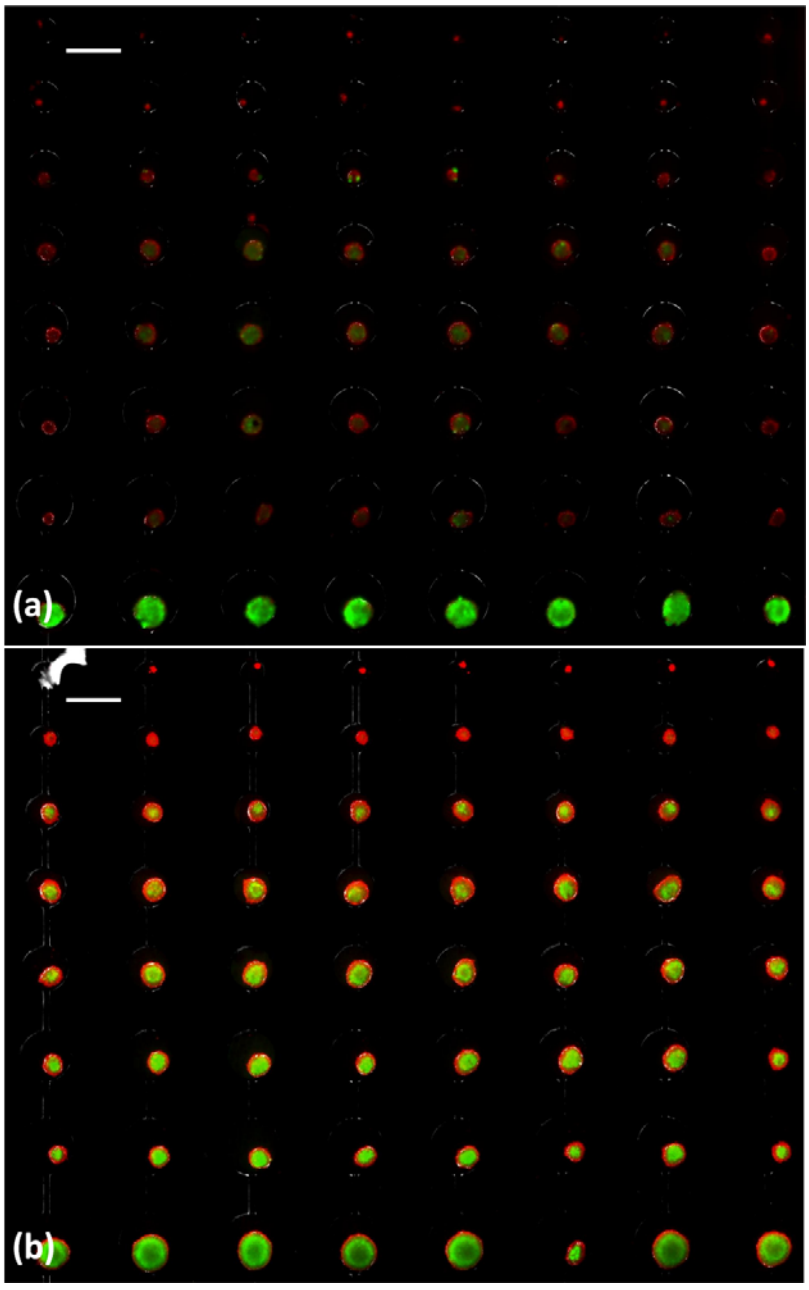


Figure 4.16 Skov3 cell viability distribution within different size spheroids after PDT treatment with (a) 10uM Methylene blue, 30minutes illumination and (b) 5mg/ml NPs, 1hour illumination. Scale bar: 400um.

The cell viability distribution in spheroids is further confirmed utilizing a confocol microscope (Nikon A1R-A1), as shown in Figure 4.17. As the volume view shows, the smallest spheroids turn to be all red throughout while the larger ones are having a green core inside and red dead cells scattering around.

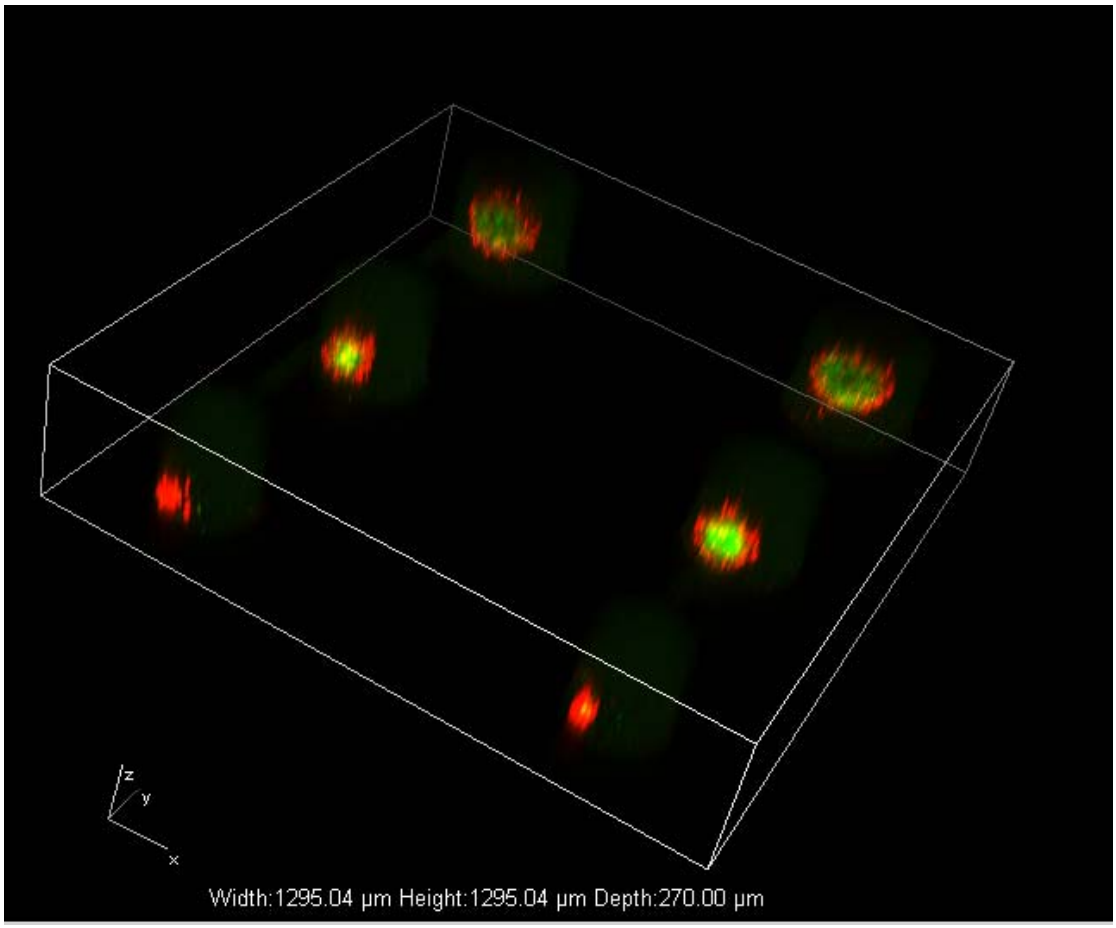


Figure 4.17 Volume view of cell viability distribution within Skov3 spheroids after PDT treatment, taken under a confocal microscope.

### 4.5 Image processing and data collection

For collecting the cell viability data from the chip, images are taken utilizing an inverted fluorescence microscope, processed with the ImageJ software, and the viability rates are calculated using a self-developed Matlab program. Three groups of images are taken during the data collection, including under bright field (recording chip position),

the green fluorescence channel (live cell staining recording), and the red fluorescence channel (dead cell staining recording). The bright field image provides sampling information (starting pixels and ending pixels) for the later Matlab program. Fluorescence images are used for the calculation of cell viability ratio based on the fluorescence intensity ratio. Before being imported into the Matlab program, fluorescence images are preprocessed in two steps with the ImageJ software. First, the background corresponding to no fluorescence emission is subtracted from the image. Second, the image is normalized with a standard image getting from a uniformly fluorescent background. Sampling from the corresponding areas of green and red fluorescence images, cell viability rate is calculated as

$$\%\text{viability} = \frac{\text{I(green)}}{\text{I(green)} + \text{k} \cdot \text{I(red)}} \times 100\%$$

, where I(green) is sum of green fluorescence, I(red) is sum of red fluorescence, and k is the coefficient comparing the fluorescence brightness difference of LIVE/DEAD staining. The detailed Matlab program manuscript is included in the Appendix B.

Figure 4.18 shows the viability data collected from the test result as shown in Figure 4.7. A complete combination of these Methylene Blue, oxygen and illumination gradients contributes to a total number of 9×9×4=324 PDT conditions. Corresponding C6 cell viability rates are calculated and plotted in a 3D bubble chart format. Viability percentage under each condition is displayed by corresponding bubble's color mapping to the color scale on right. This kind of 3D plot including all three basic elements could help provide a higher level view of how the PDT efficacy changes under the dynamic interactions and combined effects of three therapeutic factors than traditional 2D or 3D plots including only one or two factors.

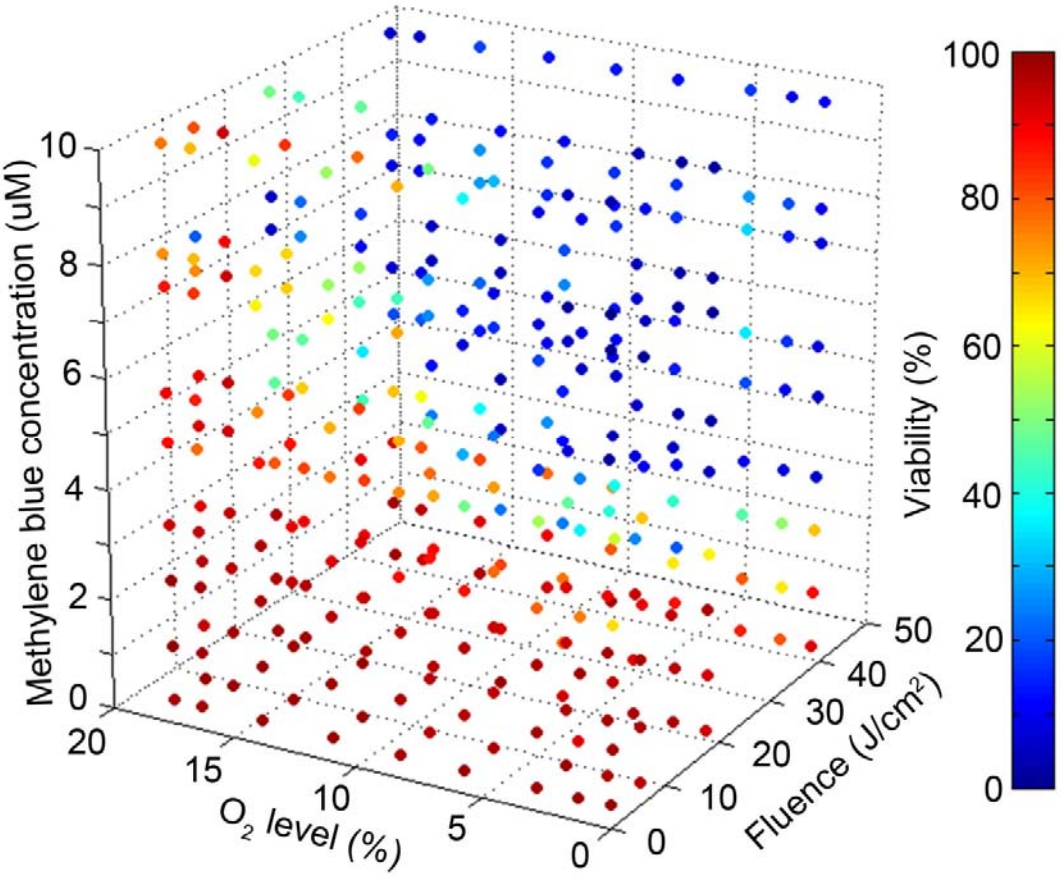


Figure 4.18 3D bubble chart of C6 cell viability percentage calculated by automated fluorescence image analysis program written in Matlab. Viability percentage under each combination of MB, oxygen and exposure gradient is displayed by corresponding bubble's color mapping to the color scale on right.

One straightforward observation in this result is PDT efficiency shows a general increase with all three factors of MB concentration, oxygen level or illumination dose (fluence), which has been frequently reported in previous works [12-14]. However, considering the detailed photosensitizer efficacy evaluation with a maximum number of PDT conditions so far as we know, it could make it much easier to distinguish two photosensitizers based on their efficacy difference. Another phenomenon worth notice here, based on the PDT efficacy changes under different conditions, is always there is one of the three elements playing as the limiting factor of PDT efficacy. That includes the

conditions under 0uM MB treatment cells are having similar high viability no matter what oxygen level and illumination dose is provided, and also some conditions that enhancing one of the factors would more tremendously improve PDT efficacy than the other two factors. This can be explained through PDT's dependence on these factors' interaction for generating reactive oxygen species, the primary effecter of PDT damage, and lacking any of them would limit the resulting therapy efficacy [15-18]. Considering the challenge of such complexity of PDT mechanism and difficulties in predicting its biological effect in clinical treatments, this kind of plot could help the growing number of PDT animal tests or clinical trials in two ways. On the one hand, it is more likely to provide direct empirical guidance for setting up viable protocols with proper light delivery (fluence), corresponding drug delivery method (photosensitizer dose) for the target cancer (local tissue oxygen level). One the other hand, its large amount of information based on the three essential elements could help set up the complex PDT dosimetry, which is a remaining problem for realizing PDT's true potential in cancer treatments [15, 19].

Figure 4.19 shows how much the spheroid size might affect PDT efficacy during a same process of treatment. Skov3 spheroids with different sizes are culture with same 5mg/ml nanoparticular photosensitizer for 1h, washed with culture medium for 10minutes and illuminated for another 1h for PDT treatment. All spheroids are having cells killed during the PDT process. Apparently spheroids with a smaller size are more vulnerable during the process. Spheroids with a diameter around 60um are completely killed during the PDT treatment. Spheroids with a maximum diameter around 300um are having a highest viability around 55%. Overall the Skov3 spheroids demonstrate a

decreasing viability ratio as the diameter feature size decreases. Nanoparticle photosensitzer itself is demonstrating a negligible toxicity and Skov3 spheroids of different size in the control group are all having a viability rate around 95% or above.

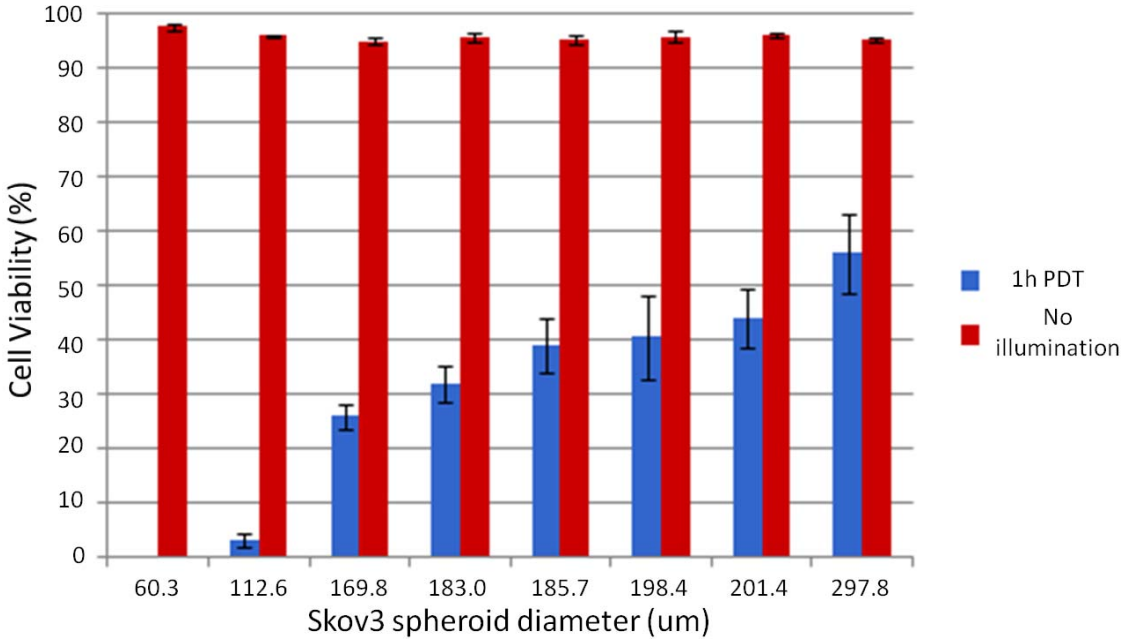


Figure 4.19 Column graph of the cell viability rates of Skov3 spheroids after PDT treatment. Spheroids are either illuminated 1h for PDT treatment or kept in dark as a control group. Final viability are evaluated with LIVE/DEAD fluorescence staining. Data are expressed as the mean and standard deviation.

## Chapter 4 References


[1] O. C. Farokhzad, *et al.*, "Microfluidic System for Studying the Interaction of Nanoparticles and Microparticles with Cells," *Analytical Chemistry,* vol. 77, pp. 5453-5459, 2005/09/01 2005.

[2] J. C. Pease, *et al.*, "Spontaneous spheroid budding from monolayers: a potential contribution to ovarian cancer dissemination," *Biology Open,* May 9, 2012 2012.

[3] M. Vinci, *et al.*, "Advances in establishment and analysis of three-dimensional tumor spheroid-based functional assays for target validation and drug evaluation," *BMC Biol,* vol. 10, p. 29, 2012.

[4] A. Y. Hsiao, *et al.*, "Microfluidic system for formation of PC-3 prostate cancer co-culture spheroids," *Biomaterials,* vol. 30, pp. 3020-3027, 2009.

[5] Y. Xu, *et al.*, "Rapid fabrication of a microdevice with concave microwells and its application in embryoid body formation," *Biomicrofluidics,* vol. 6, pp. 016504-11, 2012.

[6] C. Kim, *et al.*, "3-Dimensional cell culture for on-chip differentiation of stem cells in embryoid body," *Lab Chip,* vol. 11, pp. 874-82, Mar 7 2011.

[7] Y. Markovitz-Bishitz, *et al.*, "A polymer microstructure array for the formation, culturing, and high throughput drug screening of breast cancer spheroids," *Biomaterials,* vol. 31, pp. 8436-44, Nov 2010.

[8] B. Desoize and J.-C. Jardillier, "Multicellular resistance: a paradigm for clinical resistance?," *Critical Reviews in Oncology/Hematology,* vol. 36, pp. 193-207, 2000.

[9] A. I. Minchinton and I. F. Tannock, "Drug penetration in solid tumours," *Nat Rev Cancer,* vol. 6, pp. 583-92, Aug 2006.

[10] C. M. West, "Size-dependent resistance of human tumour spheroids to photodynamic treatment," *Br J Cancer,* vol. 59, pp. 510-514, 1989.

[11] C. M. West and J. V. Moore, "Mechanisms behind the resistance of spheroids to photodynamic treatment: a flow cytometry study," *Photochem Photobiol,* vol. 55, pp. 425-30, Mar 1992.

[12] J. D. Chapman, *et al.*, "Oxygen dependency of tumor cell killing in vitro by light-activated Photofrin II," *Radiat Res,* vol. 126, pp. 73-9, Apr 1991.

[13] R. Z. Renno, *et al.*, "Photodynamic therapy using Lu-Tex induces apoptosis in vitro, and its effect is potentiated by angiostatin in retinal capillary endothelial cells," *Invest Ophthalmol Vis Sci,* vol. 41, pp. 3963-71, Nov 2000.

[14] E. O. Serebrovskaya, *et al.*, "Targeting cancer cells by using an antireceptor antibody-photosensitizer fusion protein," *Proceedings of the National Academy of Sciences,* May 20, 2009 2009.

[15] C. W. Brian and S. P. Michael, "The physics, biophysics and technology of photodynamic therapy," *Physics in Medicine and Biology,* vol. 53, pp. R61-R109, 2008.

[16] M. Seshadri, *et al.*, "Light Delivery over Extended Time Periods Enhances the Effectiveness of Photodynamic Therapy," *Clinical Cancer Research,* vol. 14, pp. 2796-2805, May 1, 2008 2008.

[17] J. D. Vollet-Filho, *et al.*, "Non-homogeneous liver distribution of photosensitizer and its consequence for photodynamic therapy outcome," *Photodiagnosis and Photodynamic Therapy,* vol. 7, pp. 189-200, 2010.
[18] J. H. Woodhams, *et al.*, "The role of oxygen monitoring during photodynamic therapy and its potential for treatment dosimetry," *Photochemical & Photobiological Sciences,* vol. 6, pp. 1246-1256, 2007.
[19] Y. Z. Huang, *et al.*, "Microfluidic chip-based valveless flow injection analysis system with gravity-driven flows," *Analyst,* vol. 133, pp. 1237-41, Sep 2008.

# CHAPTER 5 CONCLUSION AND FUTURE WORK

This thesis presents a microfluidic platform for high-throughput PDT efficacy screening test. It uniquely incorporates microenvironment controls of multiple therapeutic factors, of which corresponding PDT efficacy responses have been demonstrated with various cell lines, photosensitizers and in vitro models. This chapter is a summary of work that has already been completed, and it also outlines the future potential improvement opportunities.

## 5.1 Conclusions and summary of contributions

As a summary, accomplishments of completed work include:

- ✧ Setting up a multi-layer microfluidic platform which is suited for drug screening of photosensitizer, based on the principle that each of the three layers provides microenvironment control on one of the three key PDT elements - drug, oxygen and light;
- ✧ Demonstration of the adaptive platform configuration depending on the selection from therapeutic factors including photosensitizer concentration, oxygen level, illumination intensity, incubation time, shear stress and the combination of multi-factors;
- ✧ Development of the microfluidic chip fabrication;
- ✧ Characterization of therapeutic factor gradients on chip based on FEM simulations and direct measurements;

- ✧ Development of standard operation protocols for PDT efficacy evaluation on chips using different photosensitizers, cell lines and in vitro models;
- ✧ Development of automated data collection and analysis with software programming.

These accomplishments provide the research community with a standardized platform for high-throughput PDT efficacy screening, based on the micro array scheme which has been widely accepted and utilized in drug screening. Compared to the most common method utilizing microwell plates, this platform could increase the throughput capability with a factor of 100 to 1000. Stacks of microwell plates are replaced with glass-slide-sized microfluidic chips. Bulky and expensive automatic robotics instruments and microwell plate readers are also eliminated. Both cell sample and reagent consumptions are greatly reduced due to the chips' microliter inner volumes. This method provides such overall savings owing to the intrinsic benefits of microfluidic technology, the compact system design and limited peripheral accessories. Furthermore, it also overcomes the limitations of many other recently developed high-throughput methods we mentioned in Chapter 1.

In addition, this platform also integrates a variety of therapeutic factors including drug concentration, incubation time, oxygen concentration, illumination intensity and shear stress. The integrated oxygen control and illumination control capabilities make it an especially powerful platform for PDT efficacy test. Even for general chemotherapy drug screening, the platform is capable of providing drug's efficacious response to different combinations of therapeutic factors, which especially facilitates the researches of drug efficacy under hypoxia conditions and drug delivery to targeting cancer cells.

Such drug efficacy profiled comprehensively on multiple factors will provide more predictive guidance for in vivo drug behavior, which in turns provides necessary feedback for development of more powerful but less toxic drugs and optimization of clinical protocols. Distinctive drug groups (free molecules and nanoparticles) and cell models (2D monolayers and 3D spheroids) can be readily adopted on this platform and have principally similar data collection processes for therapy efficacy response tests.

Regarding the microfluidic community, our platform demonstrated a novel microenvironment control methodology (incubation time controlled by the flow rate) and extensive applications of existing technologies that are rarely used (the microfluidic liquid filter) or developed very recently (the oxygen microgradient). Pumping methods of syringe pumps and gravity flows are compared for their advantages and limitations. In addition, it is likely to lead to new development areas besides drug screening, such as microenvironment stimulus on stem cell differentiation, high integrated image systems with switchable filter sets [1], novel 3D cell patterning methods using UV curable hydrogels, selective optical stimulus on neuron, bacterium behaviors under micro environment gradients, etc. [2-5].

## 5.2 Future work

Although this platform has successfully demonstrated its contributions to high-throughput PDT efficacy screening and microenvironment controls, it is not yet explored to utilize its full potential. Following a standardized step-by-step procedure, researchers can develop similar platforms incorporating different therapeutic factors and levels of high-throughput capability. First, as when a new therapeutic factor is brought in, it is verified in its corresponding layer with gradient generation and efficacy response. Second,

it is combined with other factors within the same layer and has a complete combined test. Third, a second layer with additional factors is added and the double layer chip goes through the same kind of test. Forth, a final third layer is added and the triple layer chip also takes the test. Each step emphasizes the characterization of the therapeutic factor's (gradient) control in chip and corresponding sample cell lines' PDT efficiency tests. One example of developing microfluidic platform following this procedure was shown in Figure 2.9 . However, future work should not be limited to only adding new therapeutic factors or trying out different high-throughput combinations, as we will discuss more details in the following subsections.

### 5.2.1 Potential improvement

While the platform has been successfully demonstrated for PDT efficacy tests under various conditions, there are still some aspects, with further exploration and improvements, which can make it more robust and powerful for high-throughput PDT efficacy screening.

First is about the cell culture. Compared with culturing in petri dishes, C6 cells in chips are attaching to the substrate and spreading out more slowly. Sometimes it takes around 24h to form a monolayer ready for PDT test and is currently the most time consuming step during the whole experiment cycle. This phenomenon has also been reported with other platforms and could be improved by providing more favorable micro environments for cell culturing. Current substrate material of glass can be replaced with polystyrene (the material for petri dishes). Or it also helps to coat the glass surface with some extracellular matrix components like collagen, fibronectin or laminin [6, 7]. The gravity flow rate during cell culturing should also be optimized for providing sufficient

nutrition delivery, removing waste in time, and minimizing the side effects of shear stress stimulus.

Second is temperature control. Currently the whole PDT illumination procedure is carried out under room temperature for as long as 30mins. Although based on control group tests all used cell lines could maintain high cell viabilities during this procedure, it could introduce some problem when using more vulnerable samples like primary cells. Commercial environment chambers including temperature control are available for keeping the chips in during the PDT test. Or with proper packaging and sterilization, the whole set up of PDT test could be set within the incubator, maintained at the temperature of 37℃.

Third is automated image acquiring. Currently images are taken under three different channels as we mentioned using manual switching. And also the microscope stage is manually adjusted for focusing on the sampling area. With the size expansion of microfluidic chips, the image acquiring would require much more labor and time. This challenge could be resolved with increased automation, for which microscope upgrades are commercially available including the auto focusing component, electrical rotors for stage moving and filter set switching, and the software for programmed scanning through the whole microfluidic chip.

### 5.2.2 Therapeutic factors

Our platform has included microenvironment controls of most therapeutic factors in photodynamic therapy or general drug development that current researches are focusing on. Their effects on PDT efficacy have also been demonstrated. However, two therapeutic factors, shear stress and illumination dose, can be further explored with more

complicated microfluidic chips and test protocols, providing better physiological relevance and deeper insight into the PDT mechanism as described below.

Human body can be simulated as a series of interconnected microfluidic components, with high flow rates in arteries and low flow rates for interstitial flows. Such a varying flow rate leads to a varying shear stress on the exposed cells. Not only it is affecting the drug delivery efficiency to targeting cells as we have demonstrated, but also it changes cells' behavior in different ways including cell morphology, gene expressions, cell cycle, invasive potential and etc, all of which in turn could change cells' vulnerability to drug treatment [8-12]. As a result, pre cell incubation under a controlled shear stress could be important to prepare the cells in a correct way for drug efficacy test. Although such a capability has not been incorporated into our platform yet, it is not difficult to realize since a microfluidic method intrinsically controls micro flows. A most common method is to include an internal or external pumping unit which can provide continuous flow during the cell culturing process. Also modified versions of gravity flow setups or syringe pumps could be utilized for short-term pre incubations too [13, 14].

Illumination dose directly affects PDT efficacy and is decided by both illumination intensity and illumination time. In real PDT treatments, required illumination intensity is not always reachable due to the biological tissue absorption. Even for cases light absorption is not a problem, too strong illumination intensities might lead to side effects like immunity depression. Also as a unique advantage of PDT, illumination can be applied on a same tumor site repeatedly in an actual treatment to reach an optimized efficiency, in which case the temporal control of illumination is involved. All of these conditions make it necessary to examine the illumination time's effect on PDT efficacy

[15, 16]. While we have demonstrated the gradient generation of illumination intensity and how it affects PDT efficacy, the illumination time has not been examined individually yet. A convenient way of achieving illumination time gradient or dynamic control would be to utilize the flow rate control similar as what we have done with incubation time gradient generation. In larger scale microfluidic platforms where gravity flow might be too slow, syringe pumping or integrated microfluidic valves could also be utilized.

### 5.2.3 High-throughput integration

We have demonstrated the high-throughput PDT efficacy screening with the combination of different Methylene blue concentrations, oxygen concentrations and illumination intensities. However, with the development of new therapeutic factors and specific applications, other high-throughput integrations of different therapeutic factors' combinations are necessary to be examined. One of them is the integrated combination of NPs concentration, incubation time and flow rate, all of which three directly affects the NPs drug delivery to the targeting cells. Another new combination would include the illumination intensity, the temporal pattern of illumination and the total duration, and it helps demonstrate their respective contributions to the PDT efficacy and provides guidance for the light source development which is a major research area nowadays. A third development would be an expanded microfluidic platform, which would include more than three therapeutic factors and 10,000 PDT conditions, as we have demonstrated previously. All these improvements in high-throughput capability are necessary for photosensitizer screening development, which has never make the technology getting so close to the huge demand ever.

### 5.2.4 PDT dosimetry

With the currently developed platform, we have been able to get a complete profile of how PDT efficacy changes depending on various therapeutic factors during the treatment, especially the information about threshold that cancer cells can be completely eliminated. At the same time it is providing a more physiological relevant model to estimate PDT efficacy in animal test or clinical trials. However, to fully utilize the huge amount of information we collect from PDT efficacy test on chips and to make it ready for directing in vivo treatment, we need to introduce the PDT dosimetry as a bridge, like what has been done in chemotherapy and radiotherapy but is lagging behind in PDT [17, 18]. PDT dosimetry quantifies the threshold concentration of oxidizing events that need to take place in a cancer site for cascading tumor elimination. Or in other words it is based on the quantifiable parameters during the actual PDT treatment to estimate corresponding oxygen singlets that can be generated and whether those would be enough for eliminating the cancer cells. Our platform has demonstrated the capability to quantitively measure various therapeutic factors during PDT treatments and resulting PDT efficacies. Combined that with in vivo PDT dosimetry modeling, it is possible to find out what kind of in vivo treatment procedure would be required to realize a similar PDT condition and resulting efficacy [18-21]. Establishing such correlations between our platform and in vivo PDT models, either on an individual therapeutic factor or the final PDT products like oxygen singlets, could greatly expedite the verification of new photosensitizers in animal tests or clinical trials and the optimization of clinical protocols.

### 5.2.5 In vitro cellular model

It has been a long time since people found that the drug screening results from in vitro cell line models are not so predictive for efficacies in actual clinical treatments. Microfluidic technology somewhat addresses this challenge with high-throughput array of 3D cell culturing models, one of which is the 3D cancer spheroid culturing as we have demonstrated, and the concept of body-on-chip which is receiving increasing attention. Both of them provide a better mimic of in vivo tumor microenvironments and drug pharmacokinetics. The "body-on-a-chip" model is characterized by the setup of multi-tissue interactions via near-physiological fluid circulations [22]. Usually multiple compartments are included in the device and each of them is installed holding different engineered human organ samples including liver, kidney, lung, muscle, skin or fat. All compartments are interconnected with a 2D microfluidic channel network and a pump is utilized to allow the functional modeling of culture medium circulation for nutrition delivery, waste removal and stimulus transportation. In this way it provides a realistic in vitro pharmacokinetic model which includes different physiological and metabolic reactions from a variety of organs, as well as the organ responses to testing drugs. Compared to animal models, the "body-on-a-chip" model is considered advantageous to avoid cross-species extrapolation by using human cell lines or even a patient's tissue samples for developing individualized medicines. Due to the modularized design principle and expandability of our current platform, it would not be difficult to incorporate the benefits of body-on-a-chip in a similar microfluidic format that has been demonstrated by other research groups [22-24]. Compartments of various types of targeting cancer cells would still be located in the central testing area, while supplemental elements including other cell culture compartments, microfluidic circulation networks,

and peristaltic pumps would be arranged peripherally. Besides, initial features of the current platform like oxygen level control can be inherited and expanded to the whole system, which is providing future enhancements to current existing body-on-a-chip platforms.

## Chapter 5 References


[1] X. Lou, *et al.*, "Multi-Spectral Fluorescence Microscopy with Embedded Liquid Filters for Poing-of-Care Applications," *International Conference on Miniaturized Systems for Chemistry and Life Science (uTAS),* pp. 598-600, October 2011.

[2] B. H. Chueh, *et al.*, "Patterning alginate hydrogels using light-directed release of caged calcium in a microfluidic device," *Biomed Microdevices,* vol. 12, pp. 145-51, Feb 2010.

[3] B. G. Chung, *et al.*, "Human neural stem cell growth and differentiation in a gradient-generating microfluidic device," *Lab on a Chip,* vol. 5, pp. 401-406, 2005.

[4] G. Nir, *et al.*, "Multi-site optical excitation using ChR2 and micro-LED array," *Journal of Neural Engineering,* vol. 7, p. 016004, 2010.

[5] M. Skolimowski, *et al.*, "Microfluidic dissolved oxygen gradient generator biochip as a useful tool in bacterial biofilm studies," *Lab on a Chip,* vol. 10, pp. 2162-2169, 2010.

[6] (2012). Available: http://www.biochrom.de/en/products/cell-attachment-factors/

[7] M. Cooke, *et al.*, "Enhanced cell attachment using a novel cell culture surface presenting functional domains from extracellular matrix proteins," *Cytotechnology,* vol. 56, pp. 71-79, 2008.

[8] C. L. Avvisato, *et al.*, "Mechanical force modulates global gene expression and beta-catenin signaling in colon cancer cells," *J Cell Sci,* vol. 120, pp. 2672-82, Aug 1 2007.

[9] S.-F. Chang, *et al.*, "Tumor cell cycle arrest induced by shear stress: Roles of integrins and Smad," *Proceedings of the National Academy of Sciences,* vol. 105, pp. 3927-3932, March 11, 2008 2008.

[10] S. Menon and K. A. Beningo, "Cancer Cell Invasion Is Enhanced by Applied Mechanical Stimulation," *PLoS ONE,* vol. 6, p. e17277, 2011.

[11] H. Qazi, *et al.*, "Fluid Shear Stress Regulates the Invasive Potential of Glioma Cells via Modulation of Migratory Activity and Matrix Metalloproteinase Expression," *PLoS ONE,* vol. 6, p. e20348, 2011.

[12] K. Rennier and J. Y. Ji, "Shear stress regulates expression of death-associated protein kinase in suppressing TNFalpha-induced endothelial apoptosis," *J Cell Physiol,* vol. 227, pp. 2398-411, Jun 2012.

[13] M. Y. Rotenberg, *et al.*, "A multi-shear perfusion bioreactor for investigating shear stress effects in endothelial cell constructs," *Lab on a Chip,* vol. 12, pp. 2696-2703, 2012.

[14] P. L. Voyvodic, *et al.*, "A multichannel dampened flow system for studies on shear stress-mediated mechanotransduction," *Lab on a Chip,* 2012.

[15] G. A. Frost, *et al.*, "Photodynamic therapy-induced immunosuppression in humans is prevented by reducing the rate of light delivery," *J Invest Dermatol,* vol. 131, pp. 962-8, Apr 2011.

[16] T. S. Mang, "Lasers and light sources for PDT: past, present and future," *Photodiagnosis and Photodynamic Therapy,* vol. 1, pp. 43-48, 2004.

[17] J. Emami, "In vitro - in vivo correlation: from theory to applications," *J Pharm Pharm Sci,* vol. 9, pp. 169-89, 2006.
[18] F. W. Hetzel*, et al.*, "Photodynamic therapy dosimetry," American Association of Physicists in Medicine, REPORT NO. 88, 2005.
[19] J. Li and T. C. Zhu, "Determination of in vivo light fluence distribution in a heterogeneous prostate during photodynamic therapy," *Phys Med Biol,* vol. 53, pp. 2103-14, Apr 21 2008.
[20] R. L. van Veen*, et al.*, "In vivo fluence rate measurements during Foscan-mediated photodynamic therapy of persistent and recurrent nasopharyngeal carcinomas using a dedicated light applicator," *J Biomed Opt,* vol. 11, p. 041107, Jul-Aug 2006.
[21] T. C. Zhu and J. C. Finlay, "Prostate PDT dosimetry," *Photodiagnosis and Photodynamic Therapy,* vol. 3, pp. 234-246, 2006.
[22] M. B. Esch*, et al.*, "The role of body-on-a-chip devices in drug and toxicity studies," *Annu Rev Biomed Eng,* vol. 13, pp. 55-72, Aug 15 2011.
[23] M. Baker, "Tissue models: A living system on a chip," *Nature,* vol. 471, pp. 661-665, 2011.
[24] C. Zhang*, et al.*, "Towards a human-on-chip: culturing multiple cell types on a chip with compartmentalized microenvironments," *Lab Chip,* vol. 9, pp. 3185-92, Nov 21 2009.

# APPENDICES

# Appendix A

## Multifunctional Nanoparticle Size Distribution

BECKMAN COULTER

**Delsa™ Nano**
Common

**Intensity Distribution** S/N : 118809

| | | | | | |
|---|---|---|---|---|---|
| User | : Common | Group | : | Repetition | : 1/1 |
| Date | : 4/3/2012 | File Name | : HKY1170_0.2mmSF | | |
| Time | : 21:38:16 | Sample Information | : 0.5mg PBS | | |
| SOP Name | : Sizing disposable | | | Security | : No Security |

Version 3.730 / 2.30

Intensity Distribution

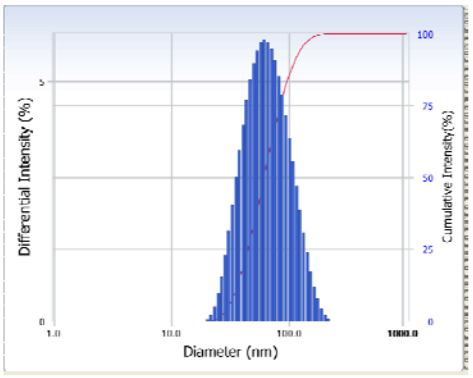


ACF

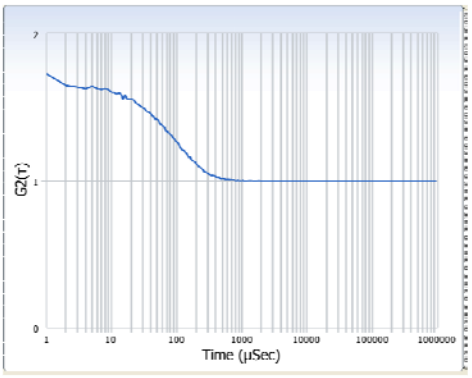


**Distribution Results (Contin)**

| Peak | Diameter (nm) | Std. Dev. |
|---|---|---|
| 1 | 74.2 | 33.9 |
| 2 | 0.0 | 0.0 |
| 3 | 0.0 | 0.0 |
| 4 | 0.0 | 0.0 |
| 5 | 0.0 | 0.0 |
| Average | 74.2 | 33.9 |

Residual : 9.344e-003 (O.K)

**Cumulants Results**

| | | | |
|---|---|---|---|
| Diameter | (d) | : 63.6 | (nm) |
| Polydispersity Index | (P.I.) | : 0.195 | |
| Diffusion Const. | (D) | : 7.740e-008 | (cm²/sec) |

**Measurement Condition**

| | | |
|---|---|---|
| Temperature | : 25.0 | (°C) |
| Diluent Name | : WATER | |
| Refractive Index | : 1.3328 | |
| Viscosity | : 0.8878 | (cP) |
| Scattering Intensity | : 9353 | (cps) |
| Attenuator 1 | : 27.22 | (%) |

BECKMAN COULTER

**Delsa™ Nano**
**Common**

**Intensity Distribution** S/N : 118809

| | | | | | |
|---|---|---|---|---|---|
| User | : Common | Group | : | Repetition | : 1/1 |
| Date | : 5/28/2012 | File Name | : HKY_xia_2xPAA | | |
| Time | : 10:21:03 | Sample Information | : | | |
| SOP Name | : Sizing disposable | | | Security | : No Security |

Version 3.730 / 2.30

Intensity Distribution

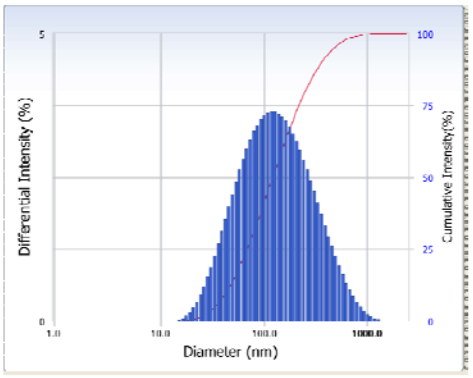


ACF

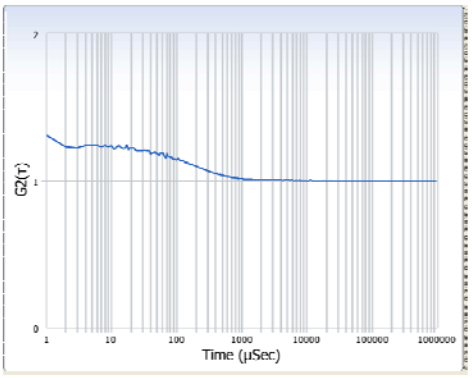


**Distribution Results (Contin)**

| Peak | Diameter (nm) | Std. Dev. |
|---|---|---|
| 1 | 184.6 | 161.8 |
| 2 | 0.0 | 0.0 |
| 3 | 0.0 | 0.0 |
| 4 | 0.0 | 0.0 |
| 5 | 0.0 | 0.0 |
| Average | 184.6 | 161.8 |

Residual : 8.559e-003 (O.K)

**Cumulants Results**

| | | | |
|---|---|---|---|
| Diameter | (d) | : 144.7 | (nm) |
| Polydispersity Index | (P.I.) | : 0.221 | |
| Diffusion Const. | (D) | : 3.399e-008 | ($cm^2$/sec) |

**Measurement Condition**

| | | |
|---|---|---|
| Temperature | : 25.0 | (°C) |
| Diluent Name | : WATER | |
| Refractive Index | : 1.3328 | |
| Viscosity | : 0.8878 | (cP) |
| Scattering Intensity | : 9457 | (cps) |
| Attenuator 1 | : 2.17 | (%) |

# Appendix B

## Matlab Program for Cell Viability Analysis

```
clear all;
close all;

%----------------------------------------
% read input images
%----------------------------------------

szFilename1 = 'green1.tif'
szFilename2 = 'red1.tif'

A_green     = imread(szFilename1);
A_red       = imread(szFilename2);

A_green_d = double(A_green);
A_red_d = double(A_red);

[rr cc] = size(A_green);
zero_image = zeros(rr, cc);

%----------------------------------------
%   bad pixels removal
%----------------------------------------

thBadPixel = 1000;

A_green_med = medfilt2(A_green_d);
indBadPixels = find(A_green_d > thBadPixel);
A_green_d (indBadPixels) = A_green_med (indBadPixels);


A_red_med = medfilt2(A_red_d);
indBadPixels = find(A_red_d > thBadPixel);
A_red_d (indBadPixels) = A_red_med (indBadPixels);

A_green_3ch = cat(3, zero_image,  A_green_d/(max(max(A_green_d))),
zero_image);
A_red_3ch = cat(3, A_red_d/(max(max(A_red_d))), zero_image, zero_image);

subplot(1, 2, 1);
imagesc(A_green_3ch);
title('Green');

subplot(1, 2, 2);
imagesc(A_red_3ch);
title('Red');

max_green = max(max(A_green_d));
max_red = max(max(A_red_d));

%   Windows selection parameters
%       x_start, y_start, x_width, y_height
```

```
%       add x_gap, y_gap

x_start = 782;
y_start = 434;

XW = [17; 19; 22; 20];
YW = [16; 20; 21; 22];

XG = [4; 4; 4];
YG = [5; 5; 5];

numOfX = length(XW);
numOfY = length(YW);

% additional parameters

A_green_d_blend = cat(3, zero_image, A_green_d, zero_image);
A_red_d_blend = cat(3, A_red_d, zero_image, zero_image);

SumGreen = [];
SumRed = [];

nOffsetY = y_start;

for m = 1 : numOfY,

    nOffsetX = x_start;

    for n = 1 : numOfX,

            sumGreen = sum(sum( A_green_d (nOffsetY:nOffsetY+YW(m)-1,
nOffsetX:(nOffsetX+XW(n))-1) ));
            sumRed  = sum(sum( A_red_d (nOffsetY:nOffsetY+YW(m)-1,
nOffsetX:(nOffsetX+XW(n)-1)) ));

         A_green_d_blend (nOffsetY:nOffsetY+YW(m)-1,
nOffsetX:(nOffsetX+XW(n)-1), :) = max_green;
            A_red_d_blend (nOffsetY:nOffsetY+YW(m)-1,
nOffsetX:(nOffsetX+XW(n)-1), :) = max_red;

            SumGreen = [SumGreen; sumGreen];
            SumRed  = [SumRed; sumRed];

            if n < numOfX,
                nOffsetX = nOffsetX + XW(n) + XG(n);
            end
    end
    if m < numOfY,
        nOffsetY = nOffsetY + YW(m) + YG(m);
    end
end

SumGreen = reshape(SumGreen, numOfX, numOfY)';
SumRed  = reshape(SumRed    , numOfX, numOfY)';
```

```
RatioGR = SumGreen ./ (SumRed+SumGreen);

figure;
mesh(RatioGR);
set(gca, 'ydir', 'reverse');
xlabel ('x');
ylabel ('y');
title ('Ratio Green/Red');
colorbar;

csvwrite('ratio_g_r.csv', RatioGR);


%-------------------------------------------------
%   images of selected area
%-------------------------------------------------
A_green_selected    = A_green_d (nOffsetY:nOffsetY+YW(m)-1,
nOffsetX:nOffsetX+XW(n)-1);
A_red_selected  = A_red_d   (nOffsetY:nOffsetY+YW(m)-1,
nOffsetX:nOffsetX+XW(n)-1);

[rr_sel, cc_sel] = size(A_green_selected);
zero_image = zeros(rr_sel, cc_sel);


figure;
subplot(1, 2, 1);
imagesc( cat(3, zero_image, A_green_selected/max(max(A_green_selected)),
zero_image) );
title('selected green');
subplot(1, 2, 2);
imagesc( cat(3, A_red_selected/max(max(A_red_selected)), zero_image,
zero_image) );
title('selected red');


figure;
subplot(1, 2, 1);
imagesc( A_green_d_blend/max(max(max(A_green_d_blend))) );
title('Chosen windows');
subplot(1, 2, 2);
imagesc( A_red_d_blend/max(max(max(A_red_d_blend))) );
title('Chosen windows');
```